DEVELOPMENT AND EVALUATION OF EDGE DEVICES FOR SCOLIOSIS ANALYSIS

ZHENDA XU

PhD

The Hong Kong Polytechnic University

2024

The Hong Kong Polytechnic University
Department of Computing

Development and Evaluation of Edge Devices for Scoliosis Analysis

Zhenda Xu

A thesis submitted in partial fulfillment of the requirements for
the degree of Doctor of Philosophy
June 2024

CERTIFICATE OF ORIGINALITY

I hereby declare that this thesis is my own work and that, to the best of my knowledge and belief, it reproduces no material previously published or written, nor material that has been accepted for the award of any other degree or diploma, except where due acknowledgment has been made in the text.

Signature: _____

Name of Student: Zhenda Xu

Abstract

Adolescent idiopathic scoliosis(AIS) has become a common spinal disorder among teenagers. The traditional evaluation method for scoliosis is mainly using X-ray equipment. However,X-ray equipment produces radiation, which can elevate the risk of cancer with long-term exposure(especially for adolescents), making it unsuitable for long-term follow-up of scoliosis. Additionally, traditional scoliosis screening methods are time-consuming and dependent on experienced personnel, leading to low positive predictive values and potentially unnecessary referrals and radiation exposure. Furthermore, early stage scoliosis is often accompanied by abnormal body posture, making it difficult to distinguish and monitor. To achieve radiation-free early screening and monitoring of scoliosis and abnormal posture, we propose multiple methods for automated screening and monitoring of scoliosis and abnormal posture using edge devices. These edge devices consist of three-dimensional(3D) imaging devices(infrared RGB-D camera) and two-dimensional(2D) imaging device (mobile phone).

However, assessing and screening for scoliosis based on 2D or 3D data of the human back is not straightforward in real life. It requires an understanding of the spine's anatomical structure, the medical anatomical features of the human back, biomechanics, and the correlation between 2D and 3D data of the human back and above features. To build a system for radiation-free assessment and screening of scoliosis based on 2D or 3D data of the human back, we summarize three core challenges in system construction and our main contributions to addressing these challenges in

section 1.3. More precisely, by conducting a comprehensive background review of scoliosis and related analysis system in chapter 2, we intend to build the systems in three aspects: (1) In chapter 3, curvature is calculated from 3D point clouds of the human back to locate anatomical landmarks, and a correlation model integrating spinal anatomy and biomechanics is established to precisely infer the spine's 3D curve. Utilizing the industry-standard for full-spine X-ray imaging, we validated the accuracy of spinal Cobb angle estimation from 3D back point clouds, leading to the development of a commercial system; (2) In chapter 4, a database of 2D back images and 3D point clouds is created, confirming their high correlation on key metric Axial Trunk Rotation(ATR); and (3) In chapter 5, the relationship between 2D postural features and scoliosis X-ray imaging is explored and validated, with a deep learning-based framework for landmark points and topological structures addressing the challenge of accurately screening scoliosis and abnormal posture using 2D images.

In chapter 3, to explore the correlation between the 3D point cloud of the human back and scoliosis and abnormal posture, we established a database of human 3D back point clouds and the corresponding X-ray images. By identifying anatomical landmarks on 3D back point clouds and correlating them with the spine's midline, we derived a 3D model of the spine's midline. The results show that the proposed method can extract anatomic landmark points and evaluate scoliosis accurately (average Root Mean Square Error of anatomic landmark points extraction is around $5mm$ and $Cobb$ angle estimation is around $3°$), which is feasible and promising. In this chapter, we validate the strong correlation between 3D back point clouds and scoliosis, and we proposed a Kinect based low cost, easy to use, non radiation, and high accuracy method to quickly reconstruct the 3D shape of the spine, which can be used to evaluate spinal deformation. This method is effective for scoliosis assessment, but 3D point cloud images require additional RGB-D equipment to accurately evaluate scoliosis and posture, which will limit usage scenarios. If the correlation between 2D human back images and 3D back point cloud images can be verified, then 2D back

images can be used to evaluate scoliosis and abnormal body posture.

In chapter 4, to better explore the correlation of features between 2D back images and corresponding 3D back point cloud images, we develop an efficient deep learning-based framework to allow a large-scale screening for scoliosis using only one 2D unclothed human back image without any X-radiation equipment. We classify the normal individual and abnormal scoliosis using the ATR value as the classification label, calculated from the human back 3D point cloud. Our accuracy in the task of AIS classification reaches 81.3%, far exceeding the accuracy of visual observation by an experienced doctor (65.1%), which can be used as a remote preliminary scoliosis screening method. This chapter verifies that 2D and 3D images of the human back on concave convex features (such as ATR) have strong correlation, which can lay the foundation for inferring the features of 3D point cloud images based on 2D images of the back in the future and it also validates the feasibility of screening for scoliosis using an unclothed back image, thus empowering users. However, while using a single back 2D image can help distinguish whether a person suffers from scoliosis, it is not capable of distinguishing the severity of scoliosis, especially considering that scoliosis often accompanies abnormal posture, yet abnormal posture does not necessarily indicate scoliosis. Furthermore, the inability to quantify mild scoliosis or abnormal posture may hinder regular home monitoring, potentially leading to missed opportunities for optimal intervention.

In chapter 5, to better distinguish the severity of scoliosis and identify the correlation between 2D human body posture features and the 2D curve of scoliosis, we propose a novel approach. we propose a set of back feature points and network topology based on deep learning algorithms. We establish a database with labeled 2D back images and corresponding whole-spine standing posterior-anterior X-ray images and propose a new network topology of the 2D back image to localize the back landmarks. With only an unclothed back image, this system can automatically classify normal and abnormal posture and scoliosis with an overall classification accuracy of 88.1%.

In order to improve the classification rate of scoliosis and posture abnormalities, as well as to better quantify the risk severity of scoliosis and achieve quantifiable risk progression monitoring, we propose the use of three back images for analysis. We have developed an online mini-program where users only need to upload three images to achieve precise screening and monitoring of scoliosis and abnormal posture at home. Simultaneously, we calculate parameters of the human back and the ATR angle for quantifiable daily monitoring. The optimized system has a sensitivity of 96% and a specificity of 89% for scoliosis, far exceeding the accuracy of experienced doctors (sensitivity of 81% and specificity of approximately 86%). The probability of misjudging abnormal posture as scoliosis is 8%, and the probability of misjudging scoliosis as abnormal posture is 5%. In this chapter, we verify that a new set of feature points and network topology based on deep learning algorithms can effectively describe the correlation between 2D body features and scoliosis. Furthermore, based on this structure, we have developed a mobile, cost-effective, accurate, and radiation-free screening and monitoring system for the screening and daily monitoring of scoliosis.

To date, we have successfully deployed and commercialized the aforementioned systems, garnering accolades from numerous international innovation awards. We have catered to over 20 hospitals, rehabilitation institutions, and insurance agencies, facilitating the screening of more than 300,000 adolescents.

Publications Arising from the Thesis

The primary publications covered by this thesis are marked with ★.

- **[ISBI]** ★ **Zhenda Xu***, Yong Zhang, Chunyang Fu, Limin Liu, Cong Chen, Wenchao Xu, and Song Guo. "*Back shape measurement and three-dimensional reconstruction of spinal shape using one kinect sensor*". IEEE International Symposium on Biomedical Imaging, 2020.

- **[ISBRA]** ★ **Zhenda Xu***, Jiazi Ouyang, Qiang Gao, Aiqian Gan, Qihua Zhou, Jiahao Hu, and Song Guo. "*2D Photogrammetry Image of Adolescent Idiopathic Scoliosis Screening Using Deep Learning*". International Symposium on Bioinformatics Research and Applications, 2022.

- **[ICME]** ★ **Zhenda Xu***,Jiahao Hu, Qiang Gao, Donghua Hang, Qihua Zhou, Song Guo and Aiqian Gan. "*Development of Deep Learning Algorithms for Automated Scoliosis and Abnormal Posture Screening Using 2D Back Image*". IEEE International Conference on Multimedia and Expo(**Oral**), 2023.

- **[IOTJ]** Qihua Zhou, Zhihao Qu, Song Guo, Boyuan Luo, Jingcai Guo, **Zhenda Xu** and Rajendra Akerkar. "*On-device learning systems for edge intelligence: A software and hardware synergy perspective*". IEEE Internet of Things Journal, 2021.

- [**USENIX ATC**] Qihua Zhou, Song Guo, Zhihao Qu, Jingcai Guo, **Zhenda Xu**, Jiewei Zhang, Tao Guo, Boyuan Luo and Jingren Zhou. "*Octo:INT8 training with loss-aware compensation and backward quantization for tiny on-device learning*".USENIX Annual Technical Conference, 2021.

- [**NIPS**] Qihua Zhou, Song Guo, Yi Liu, Jie Zhang, Jiewei Zhang, Tao Guo, **Zhenda Xu**, Xun Liu and Zhihao Qu. "*Hierarchical channel-spatial encoding for communication-efficient collaborative learning*". Advances in Neural Information Processing Systems, 2022.

- [**AAAI**] Qihua Zhou, Song Guo, Jun Pan, Jiacheng Liang, **Zhenda Xu** and Jingren Zhou. "*PASS: patch automatic skip scheme for efficient real-time video perception on edge devices*". Proceedings of the AAAI Conference on Artificial Intelligence, 2023.

- [**TPAMI**] Qihua Zhou, Song Guo, Jun Pan, Jiacheng Liang, Jingcai Guo, **Zhenda Xu** and Jingren Zhou. "*PASS: Patch Automatic Skip Scheme for Efficient On-device Video Perception*". IEEE Transactions on Pattern Analysis and Machine Intelligence, 2024.

- [**FRONT PEDIATR**] ★ Runting MA, Qiang Wu, **Zhenda Xu**, Li Zhang, Yixin Wei, Qiang Gao. "*Exercise therapy for adolescent idiopathic scoliosis rehabilitation: a bibliometric analysis (1999-2023)*".Frontiers in Pediatrics, 2024.

Acknowledgments

Completing this thesis has been a journey filled with challenges, yet immensely rewarding. As I reflect on this academic milestone, I find myself deeply grateful to the many individuals who have contributed to pursuing my Ph.D. degree.

First and foremost, I would like to extend my heartfelt gratitude to my supervisors, Professor Song Guo and Professor Yan Liu, for their unwavering guidance and unparalleled support during my Ph.D. studies at Hong Kong Polytechnic University. Their patience, vast knowledge, and inspiring mentorship have nurtured me into a critical thinker and a diligent researcher. Their trust in my abilities and freedom to explore diverse techniques have been crucial in shaping my academic journey. I am profoundly grateful for their mentorship and guidance at every stage, which have been instrumental in my personal and professional growth.

I am also indebted to my collaborators, who have been my partners in this journey. Their diligent work, constructive feedback, and thoughtful discussions have been invaluable in advancing my research. I am particularly thankful to Professor Qiang Gao, Dr. Qihua Zhou, Professor Zhihao Qu, Professor Mengye lv, Professor Yong Zhang, Dr. Jie Zhang, Mr. Zicong Hong and the many other esteemed scholars and researchers who have graciously contributed their time and expertise to my work.

Lastly, I would like to express my profound gratitude to my family. Their unwavering support, unconditional love, and constant encouragement have been my rock throughout this academic journey. They have been my first cheerleaders, my biggest

fans, and my most trusted advisors. Without their steadfast belief in my abilities and their unending support, I would not have been able to achieve this milestone. I am forever grateful for their love and dedication to my success.

As I embark on the next chapter of my career, I carry with me the lessons learned, the experiences gained, and the relationships forged during this transformative period. I am deeply humbled and honored to have had the opportunity to work with such esteemed mentors, collaborators, and family members. Thank you all for making this journey possible.

Table of Contents

List of Figures

List of Tables

Chapter 1

Introduction

1.1 Research Background and Significance

Adolescent idiopathic scoliosis (AIS) is medically defined as a curvature of the spine with greater than 10° of deformity, and the cause of scoliosis is unclear. The *Cobb* angle is generally used to measureandresence of scoliosis in adolescents. *Cobb* angles beyond 10° are defined as scoliosis [55]. Scoliosis is highly insidious and usually occurs in adolescents between 10 and 18 years old. Adolescents who suffer from scoliosis are at significant risk of rapid progression and the development of severe scoliosis if the condition is left untreated before the skeletal maturity stage [117]. Severe cases may impact an individual's appearance and cardiopulmonary function and potentially cause musculoskeletal and neurological pain.

Therefore, to achieve early screening and early intervention for scoliosis and reduce the risk of scoliosis becoming severe in the future, the school scoliosis screening (SSS) program has been advocated [40]. The majority of screening procedures used in SSS are radiation-free. These procedures include appearance evaluation, palpation, *Adam* forward bending test, scoliometer measurements, *Moire*/Infrared topography, ultrasound, and X-ray [122].

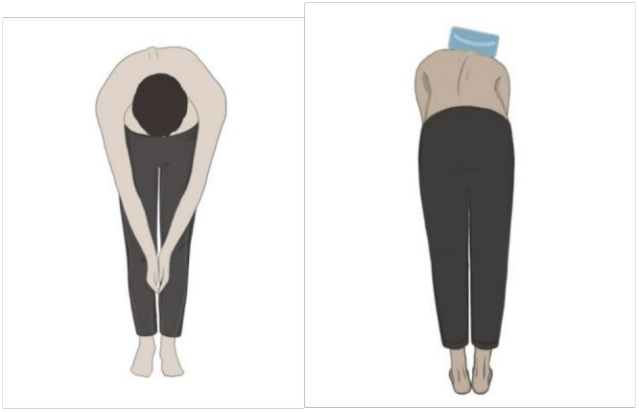

Figure 1.1: Dagrammatic sketch of *Adam* test with scoliometer examination.

At present, the mainstream screening method for abnormal spinal curvature is still the *Adam* test with a scoliometer. The doctor instructed the adolescent to extend their arms and gradually bend them to approximately 90°. The doctor detected whether the subjects had trunk asymmetry by using a scoliometer and calculated the Apical Transverse Rotation (ATR) value. The measurement of schematic diagram of the *Adam* test with scoliometer is shown in Figure 1.1. However, these methods have significant drawbacks, including susceptibility to the subjectivity of screening personnel, a time-consuming nature, and the requirement for unnecessary radiography, owing to their low positive predictive value (PPV) [30][126][60][65].

Early identification of progressive conditions is crucial for effective treatment, necessitating regular monitoring to ascertain potential exacerbation of scoliosis curvatures during growth periods [119]. As early as the 1950s, large-scale school scoliosis screening (SSS) programs were implemented for the early detection of idiopathic scoliosis (IS). However, the implementation of SSS is controversial due to its high false-positive referral rate and substantial costs [45]. In 2004, the United States Preventive Services Task Force recommended not to conduct routine IS screening for asymptomatic adolescents based on comprehensive research recommendations [32][58]. However, a joint position statement from the Society for Scoliosis Research, the American Academy of

Orthopaedic Physicians, the North American Academy of Pediatric Orthopaedics, and the American Academy of Pediatrics underscores the importance of training screening personnel on the judicious use of spinal radiographs. They noted that not all children identified through screening necessitate radiographic evaluation. In cases where radiographs are required, physicians are urged to implement measures to minimize the patient's radiation exposure [46].

From the above background introduction, it can be seen that non-radiation analysis for scoliosis and large-scale screening for scoliosis in adolescents is very necessary. However, according to existing solutions, there are still the following pain points in practice:

1. Although using X-rays for scoliosis screening or analysis has high accuracy, it can expose many teenagers to unnecessary radiation, which is not conducive to physical development;

2. The accuracy of using *Adam* test and scoliometer depends heavily on the experience of screening personnel, resulting in low overall accuracy. In addition, the cost of manual screening in schools is high, which is not conducive to large-scale promotion;

3. It is hard to distinguish mild scoliosis and abnormal posture in adolescents. Even if scoliosis is detected, not every teenager will progress, and only about 20% - 30% of adolescents are at risk of developing scoliosis. However, if there is a lack of adequate follow-up methods, even if it is screened, continuous monitoring cannot be carried out, which can easily miss the optimal intervention period and only exacerbate the anxiety of parents and children.

1.2 Related Work and Challenge

From the above content, it can be inferred that the traditional manual detection method has the following problems: low efficiency, need to touch the back of the

human body, low accuracy, radiation, and no follow-up. Many teams have proposed many solutions in recent years to solve the above problems. In the realm of scoliosis assessment, the most fundamental approach is the clinical examination, specifically *Adam*'s forward bending test, which utilizes a scoliometer for quantitative analysis [39][56]; Additionally, 3D ultrasound (US) imaging has emerged as a promising technique, offering the advantage of employing nonionizing radiation [128]. Despite the high sensitivity (83.3%) and specificity (86.8%) demonstrated by Adam's forward bending test, as well as the moderate linear correlation ($y = 1.1797$, $R^2 > 0.76$) with Cobb's x-ray methods for US imaging [129],the manual placement and measurement of the scoliometer or US imaging probe by the examiner remains a significant limitation. This process is not only time-consuming but also imposes a significant burden on healthcare professionals, such as doctors or school nurses, who are tasked with screening a large number of individuals within limited timeframes. Other teams have proposed 3D reconstruction of the back or the whole trunk using optical non-invasive surface measurement system [80]. They mainly model the anatomical features of the back, represented in section 3.3.3, and then use the physical model to represent the spine's shape in three dimensions. This method can achieve a non-radiation, non-contact, and relatively accurate 3D evaluation of scoliosis. Still, its system needs to be used in scenarios without light interference and is based on highly accurate surface measuring devices, which are generally expensive.

A group proposed using the low-cost RGB-D camera to locate the anatomical landmarks on the back of the human body [13]. Still, their methods have low back anatomical landmarks positioning accuracy and thus lack robustness. In addition, to address the labor cost and education issues of large-scale SSS, some research teams have proposed the idea of home scoliosis screening, based on a single unclothed 2D human back image, using image processing and AI algorithms. A research team has proposed the classification of scoliosis based on a 2D unclothed back image, which divides patients into Lenke type 1 and other categories using conventional image pro-

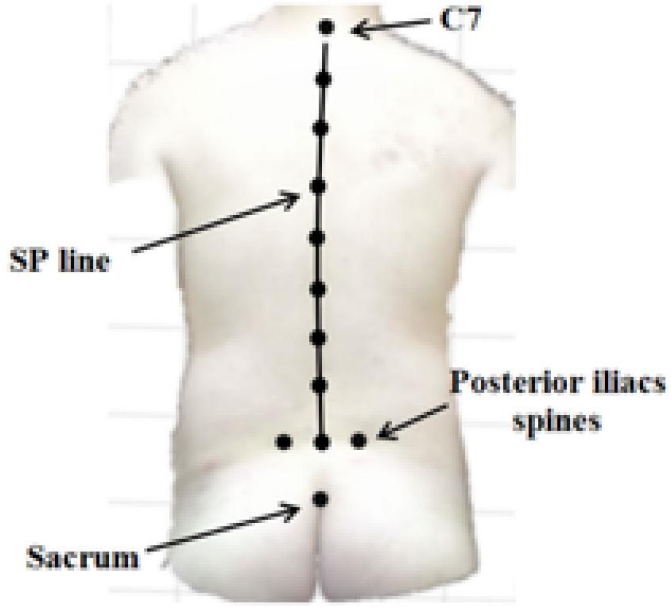

Figure 1.2: Anatomical landmarks of human back.

cessing methods. However, this method has poor robustness and detection accuracy [90]. Recently, a research team has used deep learning algorithms to construct correlation models of unclothed back images and corresponding X-rays to classify scoliosis severity using one back image. The method works well for scoliosis over 20°. However, it performs poorly and cannot classify abnormal posture and scoliosis between 10 and 20° [124].

From this, we can derive the following research challenges:

1. The absence of a comprehensive dataset that includes 2D, 3D human back images, and their corresponding X-ray images.

2. Accurately reconstructing 3D spinal curves from low-resolution 3D back point clouds presents significant challenges.

3. Analyzing scoliosis and abnormal posture accurately using 2D back images is challenging.

1.3 Contributions

By establishing databases of 2D and 3D human back point clouds along with corresponding full-spine X-ray image, we explore and validate the correlations among them based on spinal anatomy, biomechanics, and deep learning technologies, constructing a comprehensive radiation-free closed-loop solution for scoliosis screening and assessment, as can be seen in Figure 1.3.

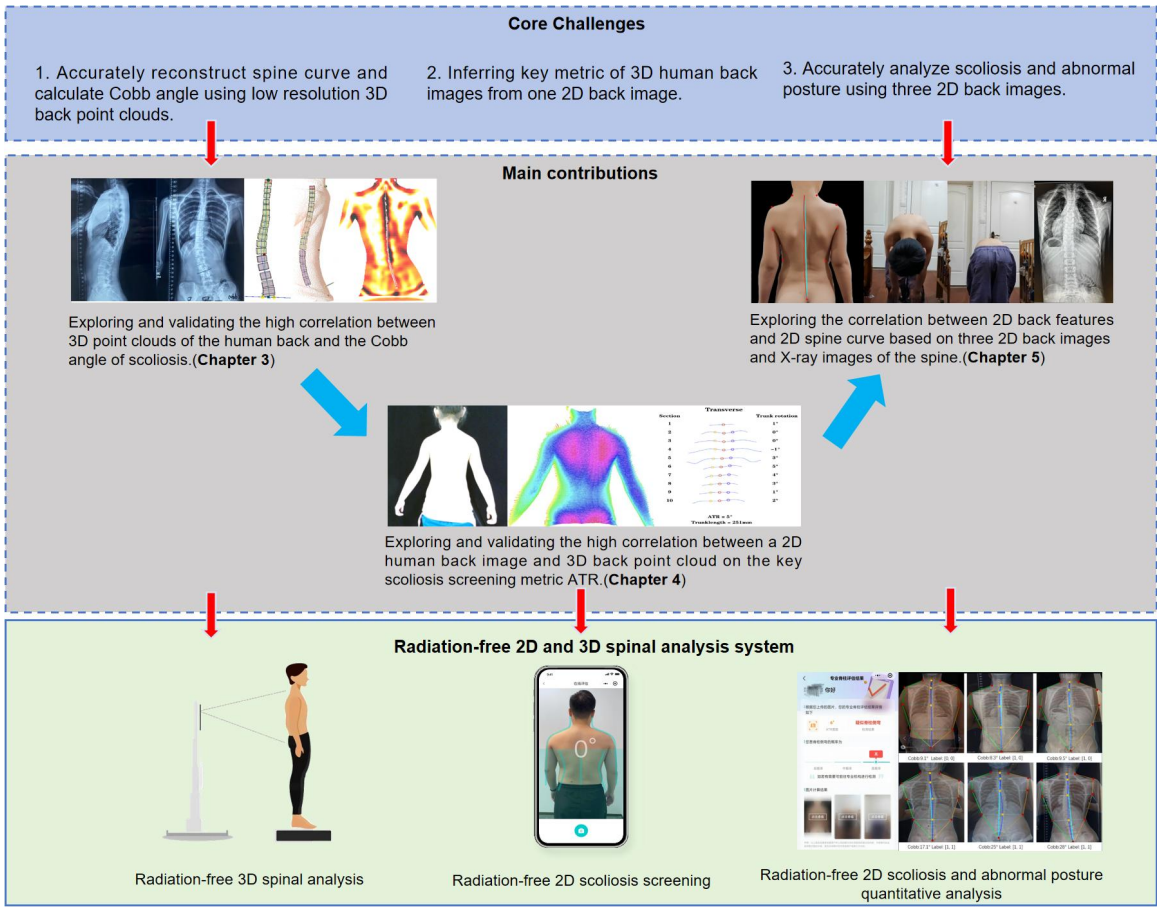

Figure 1.3: The framework for my thesis.

First, as will be discussed in chapter 3. We explore the correlation between the 3D point cloud of the human back and scoliosis and abnormal posture. Also we propose a low-cost, easy-to-use, radiation-free, and high-accuracy method to quickly reconstruct the 3D shape of the spine, which can be used to evaluate spinal deformation.

Firstly, the depth images collected by the low-cost *Kinect* sensor are transformed into 3D point clouds. Then, the features of anatomic landmark points and spinous processes(SP) line are classified and extracted. Finally, the correlation model of the SP line and spine midline is established to reconstruct the spine. The results show that the proposed method can extract anatomic landmark points and evaluate scoliosis accurately (average root mean square error of $5mm$ and around 3°), which is feasible and promising. Concurrently, we have engineered an infrared 3D spinal and posture evaluation system(ITSPES) based on the algorithms. This system has been introduced to the market to cater to the needs of rehabilitation centers, hospitals, fitness institutions, public welfare organizations, and traditional Chinese medicine clinics. This groundbreaking system heralds a significant advance in medical technology, providing comprehensive and precise assessment of spinal health and posture.

While this method allows for a non-radiative, 3D, precise, and objective evaluation of the spine and posture, enhancing the accuracy of mass screenings and reducing overall costs, it may lead to unnecessary privacy breaches and time delays due to the need for undressing. Therefore, we recommend its use as a follow-up measure post-initial scoliosis screening and monitoring method for scoliosis. To achieve a more cost-effective and easily disseminated initial screening strategy, we explore using portable edge devices, such as smartphones, for home-based scoliosis screening in the following chapter.

Second, as will be discussed in chapter 4. We explore the correlation of features between 2D back images and corresponding 3D back point cloud images. Since there is a high correlation between the 2D human back image of AIS patients and ATR(which can be calculated by 3D back cloud point), and ATR is also the standard for the primary screening of scoliosis, we use deep learning technology to predict scoliosis based on the unclothed human back 2D image and ATR value. This system takes one single 2D image of the unclothed human back and uses ATR value as an indicator to classify whether adolescents have scoliosis. First, we collect the 2D back image of

the same sample and its corresponding 3D back point cloud data, and based on the point cloud data, we calculate the ATR value of the back of the human body and mark whether there is scoliosis according to the size of the ATR value. At the same time, an experienced doctor will judge whether the sample has scoliosis through the naked eye. Then, we use the $UNET$ model [89] and the $Yolo$ mode [86] to train the human back segmentation model to segment the human back region on the 2D image to achieve preprocessing. After that, we train the $EFFICIENTNET-B4$ network [106] to classify images using the 2D image of the human back and the corresponding label calculated using ATR values and 3D human back. The experimental results reveal a high correlation between 2D human back image and ATR values. Using the result of classifying scoliosis by ATR value as a label can well realize the classification of scoliosis based on one single 2D human back image. Our accuracy in the task of AIS classification reaches 81.3%, far exceeding the accuracy of visual observation by an experienced doctor (65%), which can be used as a remote preliminary scoliosis screening method.

In this chapter, we have validated the use of mobile phones with 2D image for large-scale, low-cost, and precise home-based scoliosis screening. However, we found that many adolescents with mild scoliosis also exhibit poor posture, which is often overlooked and fails to raise parental concern. Early and frequent home-based screening and intervention for adolescent scoliosis and poor posture can effectively curb scoliosis incidence and mitigate progression risk. Thus, in the following chapter, we explore the use of edge devices for home-based screening and monitoring of scoliosis and postural abnormalities.

Third, as will be discussed in chapter 5. We describe the correlation between 2D human body posture features and scoliosis. Recent developments reveal that deep convolutional neural networks have achieved state-of-the-art performance in human pose estimation [104]. Besides, there is a high correlation between abnormal back pose and spinal abnormality [108]. We propose a mobile-based scoliosis and abnor-

mal posture screening and monitoring system based on the unclothed back image to more effectively screen for scoliosis and categorize postural abnormalities. The system uses deep learning algorithms and a specialized network topology based on human biomechanics to locate and compute the parameters of human back landmarks automatically, and it then classifies the results using correlation analysis. The system correctly detects mild scoliosis and categorizes issues with only postural anomalies (Only postural abnormalities, such as high and low shoulders, but without scoliosis). Furthermore, we have devised an optimized system, leveraging the proposed algorithm, to aid users in home-based scoliosis and posture abnormality screening and monitoring. The optimized system has a sensitivity of 96% and a specificity of 89% for scoliosis, far exceeding the accuracy of experienced screening doctors (sensitivity of 81% and specificity of approximately 86%). The probability of misjudging abnormal posture as scoliosis is 8%, and the probability of misjudging scoliosis as abnormal posture is 5%. This work provides a solid foundation for the quantitative analysis of *Cobb* angle measurements in scoliosis through the utilization of 2D back images.

1.4 Thesis Outline

The sections of this thesis are structured as follows: We dedicate three chapters to exploring scoliosis and abnormal posture analysis via 2D and 3D back images from mobile devices. In chapter 3,We validate the strong correlation between 3D back point clouds and scoliosis, proposing a cost-effective, user-friendly, radiation-free, and highly accurate method for rapid 3D spine reconstruction. In chapter 4, we verify that 2D and 3D images of the human back on concave convex features (such as ATR) have strong correlation and we use deep learning technology to predict scoliosis based on the unclothed human back 2D image and ATR value. In chapter 5, we verify that a new set of feature points and network topology based on deep learning algorithms can effectively describe the correlation between 2D body features and

scoliosis. Also we propose a mobile-based scoliosis screening system based on the unclothed back images to more effectively screen for mild scoliosis and categorize postural abnormalities, thereby laying the research foundation for the quantitative analysis of scoliosis angle measurements using 2D back images. In conclusion, this thesis explores future research prospects and highlights the societal impact of our work through product translation in chapter 6.

Chapter 2

Background Review

To facilitate understanding of scoliosis screening and monitoring, this chapter offers a concise overview of spinal anatomy, types of spinal deformities, prevalent scoliosis and posture assessment tools/methods, and international progress in scoliosis screening.

2.1 Spinal Anatomy

Understanding spinal anatomy, encompassing normal posture, curvature, and functionality, is imperative for evaluating backs, body shapes, and postures of patients with lower back pain and spinal disorders. The human spine, a complex structure comprising 33 distinct vertebrae extending from the skull base to the pelvis, can be segmented into five regions: cervical spine, thoracic spine, lumbar spine, sacrum, and coccyx (as depicted in Figure 2.1). Specifically, the cervical spine, denoted as the "C" spine, comprises 7 cervical vertebrae ($C1$ to $C7$). The thoracic vertebrae, referred to as the "T" vertebrae, encompass 12 vertebrae ($T1$ to $T12$) and are considered a quasi-rigid segment compared to the lumbar and cervical vertebrae. Lastly, the lumbar spine, composed of five vertebrae ($L1$ to $L5$), primarily supports the entire weight of the upper torso [71].

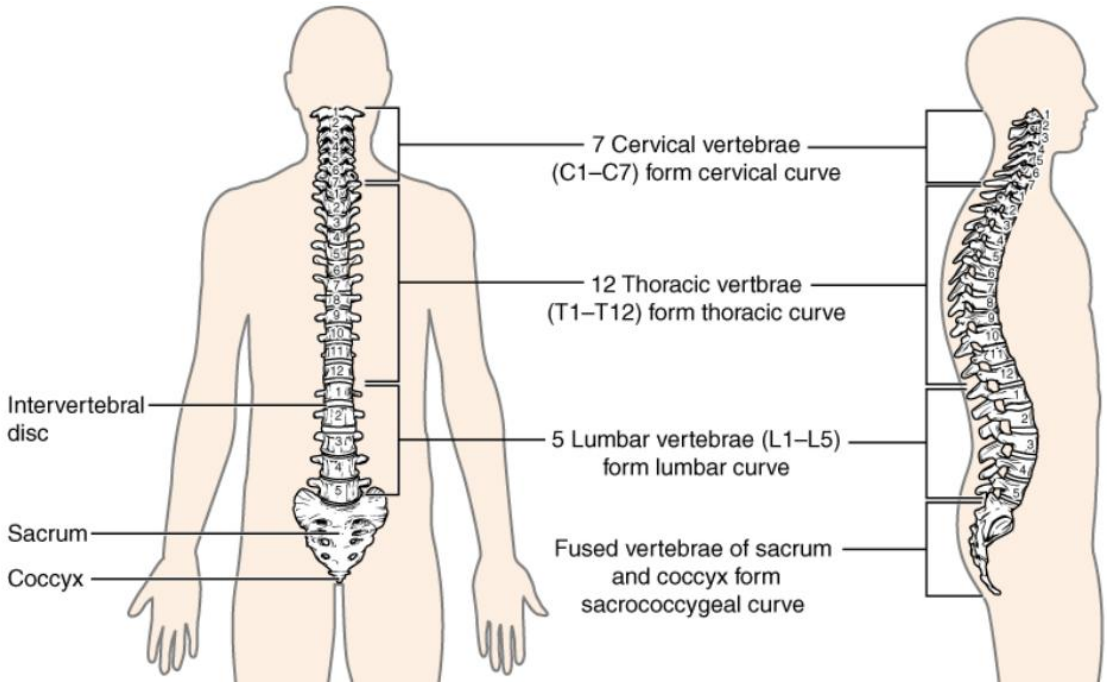

Figure 2.1: Anterior (left) and lateral (right) perspectives of the human vertebral column.

2.1.1 Anatomical Plane Definition

In the human body, three fundamental anatomical planes intersect, serving as reference points for determining the position or direction of anatomical structures' movement, as shown in Figure 2.2.

The sagittal plane, serving as a longitudinal divider, splits the body into distinct left and right sections. In contrast, the coronal plane acts horizontally, segregating the body into anterior and posterior segments. Moreover, the transverse plane, colloquially known as the horizontal plane, divides the body vertically, distinguishing between superior and inferior portions.[84].

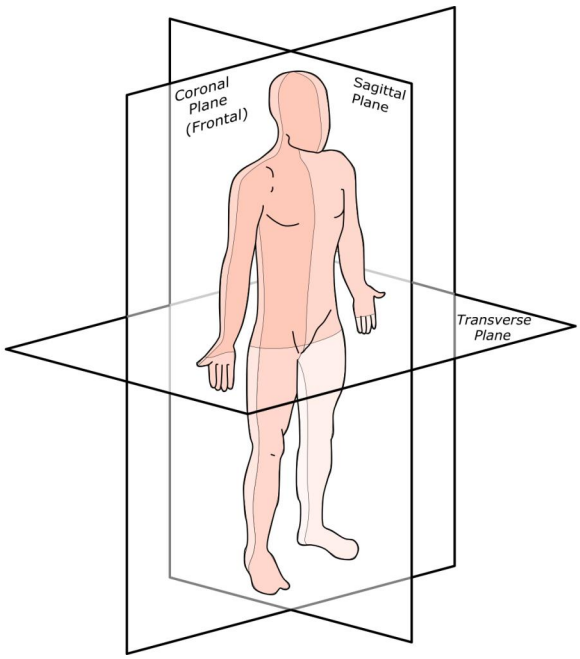

Figure 2.2: Planes of the Human Body: Sagittal, Coronal, and Transverse [76].

2.1.2 Curvatures of Spine

The typical architecture of the spine is characterized by the presence of distinct curves, as shown in Figure 2.3. Conventionally, it is understood that when viewed from the coronal plane, the spine's curvature appears as a straight alignment [9]. A study reported that the right shoulder of right-handed young people is lower than the left shoulder. The changes in shoulder joint level offer an indirect means of assessing modifications in the coronal plane alignment of the spine [68].

When viewed from the sagittal perspective, the vertebral column is characterized by four distinct curvatures. The $S-$*shaped* curvature is characterized by two posterior convexities (thoracic and sacral), referred to as posterior convexity or primary curvature. The cervical and lumbar segments' two anterior convexities are termed anterior convexity or secondary curvature.

The average thoracic kyphosis angle of asymptomatic young people and the average

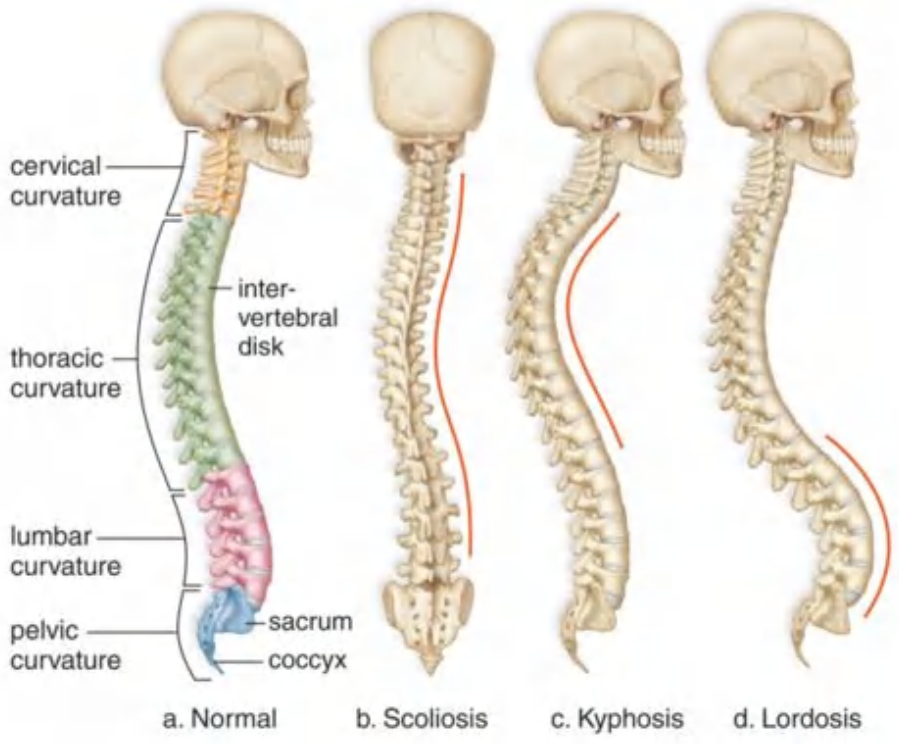

Figure 2.3: The curvatures of spine [74].

lumbar lordosis angle is $29.37 \pm 3.94°$ and $-37.7°$ respectively. These values are closely with those specified by the Society for Scoliosis Research (2017), which states that the standard range for chest kyphosis in X-ray measurements falls between $20°$ and $40°$. Similarly, the standard range of lumbar lordosis on radiographic images falls between $-20°$ and $-60°$ whereas the average thoracic kyphosis angle in adults ranges from $30°$ to $50°$, and the mean lumbar lordosis angle is approximated at $-55°$. The variations in these reported angles can be attributed to discrepancies in measurement techniques and spinal curvature assessment tools. For instance, radiological methods for spinal curvature measurement differ from those based on surface topography. Specifically, X-rays assess spinal curvature through skeletal components, whereas surface topography incorporates body surface characteristics, encompassing bones, muscles, adipose tissue, and skin [102][11].

2.1.3 Evaluation of Spinal and Postural Alignment

Posture, defined as the interrelation of body segments at any given moment, and back shape, which characterizes the asymmetry between bilateral sides, are critical in assessing spinal alignment [51]. Alterations in spinal curvature can induce changes in back shape,such as the development of asymmetrical rib protrusions stemming from axial rotation of the thoracic spine [7]. Distinct anatomical landmarks on the posterior surface of the human back, including the $C7$ vertebral prominence, sacral point, acromion point, suprascapular point, subscapular point, posterior superior iliac, and iliac crest point, are readily visible and palpable [80], as depicted in Figure 2.4. The augmentation in the depth of the median sulcus is attributed to the two longitudinal erector spinae muscle bundles [88]. Three pivotal investigations have documented the typicality and symmetry of back morphology in a standing posture. One such study employed the Integrated Spinal Imaging System (ISIS1) to evaluate the standard back contour in young individuals. This optical computer system enables the measurement of the 3D back surface morphology, allowing the creation of representative scan images to illustrate the the back morphology for all subjects involved in the study. The study reported an average thoracic kyphosis of $24.9mm$ [28][115].

Researchers propose that the categorization of back morphology/posture types can be streamlined by identifying specific back shapes, evaluating posture, analyzing back surface characteristics, and identifying key skeletal landmarks. This approach has the potential to yield a diverse array of back surface parameters that are valuable for research purposes, evidence-based practices, and clinical decision-making.

2.2 Spinal Deformity

Spinal deformities include kyphosis, scoliosis, and lordosis, which may lead to changes in posture alignment and affect lung function [95] According to the literature, these

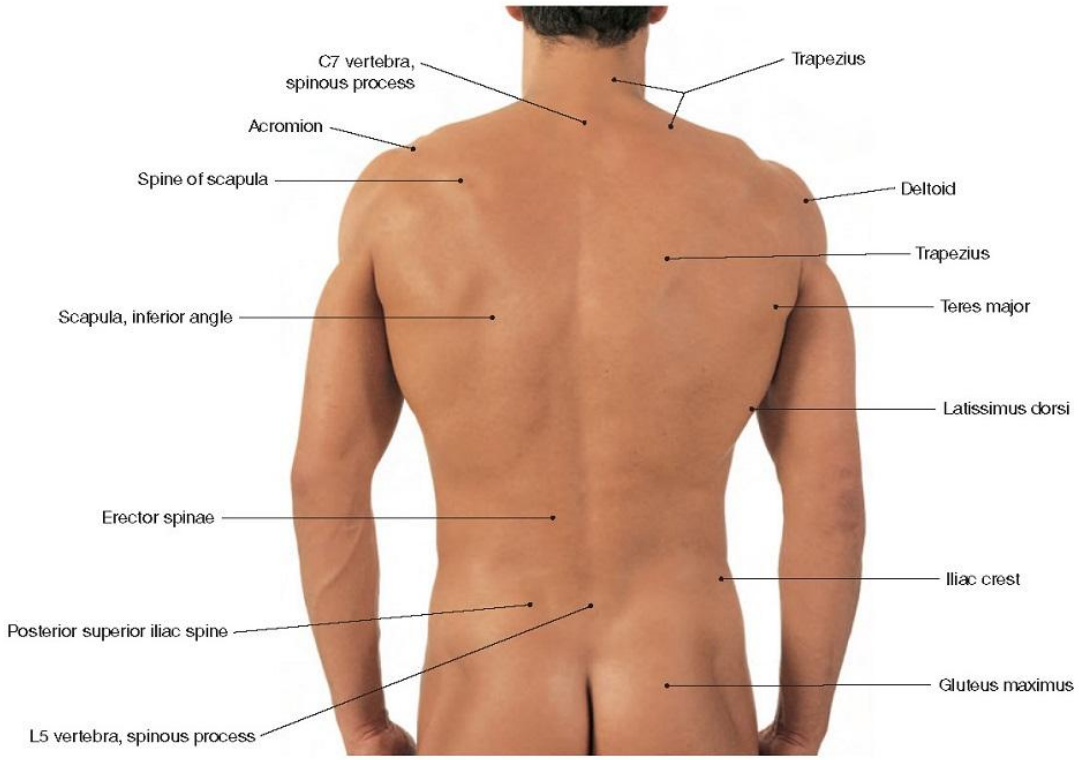

Figure 2.4: Posterior view of back surface anatomic landmarks [75].

deformities are related to various factors, including intervertebral disc and/or vertebral degeneration, vertebral development problems, neuromuscular problems, and hip joint problems. Spinal pain often arises from various factors, and one of the prevalent contributors is idiopathic scoliosis [2].

Spinal kyphosis is a characteristic of sagittal curvature of the chest, resulting in a hunchback posture. Scoliosis refers to the lateral deviation of the vertebral body line from the midsagittal plane, which is often accompanied by kyphosis and can potentially progress into a kyphotic deformity. Spinal lordosis is the result of abnormal sagittal plane of the lumbar spine, characterized by inward curvature. These deformities may be caused by various reasons, such as intervertebral disc and/or vertebral degeneration, vertebral development problems, poor posture, neuromuscular problems, or hip joint problems [59].

These spinal deformities have the potential to induce alterations in posture alignment, thereby exerting adverse effects on the functionality of the musculoskeletal system. In addition, spinal deformities may also lead to limited lung function and may be associated with spinal pain. Therefore, prevention and early correction of spinal deformities are very important.

2.3 Scoliosis and Posture Analysis Tools

A range of techniques exist for assessing posture and back morphology, including tactile, non-tactile, two-dimensional, and three-dimensional approaches. Tactile measurement methods involve the assessment of posture or back shape through direct skin contact, for instance, by measuring flexion angles. Conversely, non-tactile measurement methods, including X-ray and photogrammetric techniques, evaluate back shape and posture without the need for direct skin contact [17].

In clinical practice, a variety of tools is utilized to evaluate posture and back morphology, ranging from traditional to advanced methodologies. Nonetheless, the more advanced technologies, including ultrasound, radiology, and inertial sensors, remain inaccessible to many clinicians due to their high costs, the necessity for specialized training, or their complex and challenging procedures. As a result, simpler and more traditional approaches, such as photography and the use of plumb lines, continue to be prevalently utilized [22].

Reliability and effectiveness are key factors to consider when selecting appropriate posture and back shape assessment methods. [34]. In addition, when selecting the appropriate method, factors such as cost, safety, ease of use, and measurement time need to be considered [7].

2.3.1 Two-Dimensional Analysis of Scoliosis and Posture

Tactile Methods of Measurement

Inclinometers and goniometers are commonly used for posture assessment owing to their cost-effectiveness and user-friendliness. However, these tools have limitations that need to be considered when assessing posture. One limitation of using inclinometers is that the measurements are limited to two-dimensional planes, which means they cannot fully assess posture in both the frontal and transverse planes. Furthermore, maintaining a consistent posture for patients during data collection can be demanding, potentially introducing inaccuracies in the measurements. [33].

Similarly, goniometers have their own limitations. While they can directly measure body posture variables, they are typically limited to individual measurements and may not be suitable for assessing the entire body or posture. Furthermore, using goniometers for posture assessment involves a lengthy evaluation process, which can be time-consuming [83].

Additional research endeavors are imperative to overcome the existing limitations and improve the accuracy and reliability of posture assessment methodologie. One potential avenue is the development of automated tools that can recognize markers and calculate angles automatically. This approach would decrease measurement discrepancies and expedite the process of data collection and analysis.

Additionally, exploring non-tactile measurement methods, such as visual observation methods, could provide a more comprehensive evaluation of posture. Visual observation methods are commonly used in clinical practice and involve observing the patient from multiple angles. By utilizing predetermined guides for ideal alignment, therapists can analyze any visible deviations or asymmetries in posture.

In conclusion, while inclinometers and goniometers have advantages in posture assessment, they also have limitations that must be addressed. Further research and

the development of automated tools can help overcome these limitations and improve the accuracy and reliability of posture assessment. Additionally, incorporating visual observation methods can provide a more comprehensive evaluation of posture [49].

Non-tactile Methods of Measurement

In clinical practice, the visual observation method is frequently adopted for posture assessment, owing to its practicality and minimal requirements for specialized equipment or designated space. any noticeable deviations or imbalances in posture, employing a predefined framework for optimal alignment as a reference. However, studies have shown that the inter-rater reliability of visual observation methods is poor compared to photography measurement methods, making it challenging to assess posture variables [96][100].

On the other hand, the photography measurement method has gained widespread use in posture assessment. This method involves capturing digital images of the patient in their optimal anatomical positions, specifically in the sagittal and frontal planes, and subsequently determining posture angles through the delineation of lines connecting distinct anatomical landmarks. Photography measurement has the advantages of low cost, quantitative assessment, and reduced radiation exposure, making it more feasible in clinical practice. Research has demonstrated reliability in quantifying and measuring posture variables using photography measurement methods [4].

However, there are limitations to the photography measurement method as well. Some studies have observed inconsistencies in the separation between the participant and the camera during data collection, leading to data inconsistency. Moreover, The two-dimensional nature of photography, specifically in the sagittal plane, poses challenges in accurately analyzing deformities with rotational components and precisely assessing genuine spinal curvature. Additionally, the presence of muscle mass in this plane can obscure the midline groove of the back surface, further hindering the study of true

spinal curvature [36][112].

In summary, while the visual observation method is convenient and widely used, it has limitations in assessing posture variables and achieving inter-rater reliability. The photography measurement method offers advantages such as quantification and reliability. Still, it also has limitations in terms of data consistency and difficulties in studying certain types of spinal deformities and rotational components.

Radiographic techniques, notably X-ray imaging, have traditionally been regarded as the benchmark method for evaluating and screening individuals with spinal deformities. X-ray imagery serves as a crucial source of data regarding spinal bone structure, facilitating the detailed examination of individual vertebrae as well as the comprehensive contour of the spine.. This methodology offers precise diagnosis of spinal anomalies and provides an accurate assessment of the extent and severity of the condition [36].

However, radiological methods also have limitations. One major limitation is the increased risk of radiation exposure, especially in adolescents and patients with scoliosis who require long-term rehabilitation and monitoring. As evidenced by numerous studies, accumulated exposure to X-ray radiation has been consistently associated with an increased risk of breast cancer development. Additionally, radiological examinations are expensive, have strict requirements on the site, and require a technician to operate the equipment. These factors have limited the usage of X-ray systems, especially in home settings, where patients may not be able to receive timely screening and miss the best chance for effective therapy [111].

In summary, while radiological methods provide valuable information on spinal deformities, they have limitations, such as increased radiation exposure and cost. Non-invasive methods like photogrammetry offer some advantages, but they also have limitations in data consistency and accurately capturing 3D aspects of spinal deformities.In recent years, various 3D measurement systems have been introduced to

procure a comprehensive 3D characterization of spinal deformities as well as back surface. These systems aim to provide a more comprehensive assessment of spinal deformities.

2.3.2 Three-Dimensional Analysis of Scoliosis and Posture

In the past decade, there have been significant advancements in the 3D analysis of posture and back morphology. These developments have expanded their applications in spinal research and clinical settings, utilizing tactile and non-tactile tools.

Measurement of Spinal Curvature Using Tactile Tools

The *Posturometer* − *S* is a unique electronic device designed for objective, non-invasive measurement of body posture. It incorporates three interconnected components: a mechanical pointer to designate the position of the measured point, an electronic unit to calculate the pointer's three-dimensional spatial position, and a software interface for analyzing the obtained results. This system grants practitioners the ability to visually assess spinal curvature in all three planes and provides a quantitative representation of postural parameters. Nevertheless, a significant limitation noted in the study is the lack of user-friendliness, the substantial space requirement within the room, and the prerequisite of a profound understanding of the equipment as well as adequate training before its operational utilization. [101][70].

Ultrasound imaging is another method for evaluating spinal deformities. Research has shown that a radiation-free 3D ultrasound system can assess spinal curvature. This method generates a 3D visualization of the spinal anatomy through the utilization of ultrasound imagery and corresponding spatial data in three dimensions. While the volume projection imaging method using ultrasound shows potential for evaluating spinal deformities, it also has certain limitations. For instance, the ultrasound system and its associated data are prone to electromagnetic field interference, which can

introduce inaccuracies in spatial and directional measurements, manifesting as offsets or jitters. Moreover, the volume projection imaging-related methodologies possess additional limitations, including their cumbersome and heavy nature, a relatively high reliance on skilled operators, and the time-consuming process of evaluating the entire spine. Consequently, the application of the ultrasound volume projection imaging technique in clinical settings may be deemed unsuitable due to its limitations [18][94].

In conclusion, the primary limitations of the tactile posture measurement system are errors caused by electromagnetic and patient interference during data collection. The requirement for patients to sustain a stationary standing posture for prolonged durations poses a significant challenge, thereby heightening the risk of errors occurring. Furthermore, while the ultrasonic volumetric imaging technique shows potential for evaluating spinal deformities, it is affected by electromagnetic interference and other technical limitations. Thus, these limitations and constraints must be considered when selecting posture assessment tools.

Measurement of Spinal Curvature Using Non-tactile Tool

The utilization of 3D computed tomography (CT) scanning serves as a traditional imaging modality for assessing posture and spinal deformation.3D computed tomography (CT) scanning represents a traditional imaging technique that employs specialized X-ray devices to generate cross-sectional views of bodily tissues and organs across varying angles and planes, ultimately culminating in high-resolution three-dimensional data. This imaging modality enables visualization of the superior and transitional pelvic regions, facilitating the examination of the spine's rotational and deforming components. In clinical settings, CT scans are frequently employed to assess the efficacy of spinal implants and are instrumental in initial diagnostic processes or when symptoms indicate the need for further investigation of potential abnormalities. However, the main limitations of CT scanning are the high risk of patient

exposure to ionizing radiation and the longer time required to acquire cross-sectional images, which may result in motion artifacts [77].

The skin surface measurement system is another method for assessing posture and back shape. *Morie* topography and structured light photogrammetry are the most commonly used non-radiographic tools. These systems project structured light onto the back and generate *Morie* topography images through the reflection of this structured light. The contour lines in Moiré images help visualize the asymmetry of the back, and furthermore, they document spatial details pertaining to the subject's 3D back configuration and posture. A significant limitation of *Morie* topography lies in its reliance on the precise order of *Morie* fringes, which can be influenced by patient positioning and slight variations in movement. Therefore, direct examination of *Morie* fringes can be misleading, and data analysis is a complex process [103][73].

An improved skin surface measurement system is the $ISIS2$ system, which utilizes a digital camera and projector to accurately capture and measure the 3D back shape. The $ISIS2$ system gathers data through palpation and the identification of anatomic landmarks, subsequently utilizing *Fourier* transform contour measurement to translate distortions in reference grid lines into a three-dimensional representation of the back's surface topography. Compared to the traditional $ISIS$ system, the $ISIS2$ system offers higher measurement speed, accuracy, reliability, and ease of use. It can be used for screening and monitoring the development of spinal deformities and shows no statistically significant difference compared to measurements from X-ray images. However, the $ISIS2$ system is heavier, less mobile, and requires skilled clinicians. Additionally, identifying bony landmarks like spinous processes can be more challenging for extremely obese or heavily muscled patients [7][8][54].

Another surface measurement system is the Microsoft $Kinect^{TM}$ system, which uses a depth sensor to measure the 3D back shape. Previous research has shown that the $Kinect^{TM}$ system effectively measures the back surface of both scoliosis patients and healthy volunteers, demonstrating comparable intertrial reliability and correlation

with a reference standard. However, its accuracy in measuring the three-dimensional spine and body posture has not been fully validated [15].

In summary, three-dimensional computed tomography (CT) scanning and skin surface measurement systems are commonly used for evaluating posture and back shape. CT scanning provides high-quality three-dimensional data but has limitations regarding radiation risk and motion artifacts. Skin surface measurement systems collect three-dimensional shape data of the back using methods like $Morie$ topography or the $ISIS2$ system. Still, they have limitations regarding data analysis complexity and operational constraints. Additionally, the Microsoft $Kinect^{TM}$ system has been used to measure the 3D back surface but has not been fully validated for measuring the spine and body posture.

2.4 Preliminary for Scoliosis Screening

Adolescents suffering from scoliosis experience significant physical and psychological implications that affect their overall well-being, particularly during the critical growth phase between 8 to 12 years of age, where the progression of scoliosis deformity is notably rapid. Without timely intervention, the severity of the deformity may escalate, leading to diminished labor capacity, cardiovascular complications, lower back pain, and potentially paralysis, which may further contribute to social and psychological issues. In clinical practice, it is observed that a majority of scoliosis patients seek medical attention at advanced stages of the condition, thereby complicating the treatment process, escalating costs, and adversely affecting outcomes. Consequently, early detection, diagnosis, and intervention hold paramount importance for the well-being of scoliosis patients and the broader societal context [10].

Advancements in imaging technology and a deeper comprehension of three-dimensional space theory have progressively revealed that spinal deformities encompass more than

just imbalances or abnormal curvatures within a specific body plane. They also involve complex deformations across three-dimensional spaces, including the coronal, sagittal, and transverse planes. Characterized as a three-dimensional distortion involving spinal and trunk torsion, scoliosis manifests through lateral curvature in the coronal plane, vertebral rotation in the horizontal plane, and deviations from the spine's normal physiological curvature within the sagittal plane. The Scoliosis Research Society (SRS) categorizes scoliosis based on the *Cobb* method, which measures spinal curvature on upright X-rays at angles exceeding 10° [5]. Scoliosis is classified into congenital, acquired, and idiopathic forms, with acquired scoliosis further subdivided into postural, neuropathic, pathological thoracic, and malnutrition-related scoliosis according to its origins. Idiopathic scoliosis, particularly adolescent idiopathic scoliosis (AIS), is the most prevalent form, with an incidence rate of approximately 1%-3% [117], predominantly affecting girls. The typical onset age for scoliosis is around 10 years, and its etiology remains largely unknown. Nonetheless, current studies suggest a correlation with genetic factors, hormone levels, and endocrine anomalies, such as melatonin deficiencies [131].

The screening method for scoliosis in foreign countries: In the 1980s, scoliosis screening was carried out among school-age children, usually including physical examination, which visually observes whether there is an asymmetry in the shoulders, shoulder bones, and buttocks of the examinee. The *Adam*'s Forward Bending Test, commonly known as the *Adam* test, involves an examination of the back unbalance while the subject leans forward with their torso. During the *Adam* test, scoliometer is employed to quantify the torso's rotation angle. Conversely, the *Moire* measurement technique is adopted to delineate the 3D back contours. In the year 1979, an innovative approach utilizing Moire images was employed to investigate scoliosis and establish a correlation between the asymmetry of these images and the Cobb angle, which is a metric that serves as a standard for assessing the severity of spinal curvature disorders. Notably, *Moire* stripes exhibited pronounced deformation in concave areas

while appearing clearer in convex areas. This finding provided valuable insights into the structural characteristics of scoliosis and contributed to the understanding of the condition [120].

In 1981, a comprehensive screening method was introduced for scoliosis: *Adam* test + spinal X-ray imaging. This method is accurate but requires a large amount of X-ray imaging. *Adam* test + *Moire* measurement + X-ray imaging, *Adam* test is recognized as the primary examination method, and positive cases are measured using *Moire*. Combining the two can reduce false positives in the *Adam* test, save resources, and is suitable for the urban census. *Adam* test+spinal inclination angle measurement+spinal X-ray film, using a spinal measuring ruler to measure spinal inclination angle, convenient to carry, suitable for school and rural census [6]. In 1982, a formula was proposed for calculating the *Cobb* angle using a pair of asymmetric point information on *Morie* fringes in *Morie* images for determining the degree of scoliosis [50]. In 2006, some researchers used the $MinoltaVIVID700$ laser scanner to obtain three-dimensional accurate data on the human back. Based on its symmetry features and support vector machine method, they determined scoliosis with a discrimination rate of 85% [85]. Meanwhile, other researchers reconstructed the human back using rectangular structured light and extracted its three-dimensional symmetry features to determine scoliosis [7].

Scoliosis screening programs for children and adolescents are prevalent across various nations. Initiated in the 1960s in Delaware, USA, the screening for Adolescent Idiopathic Scoliosis (AIS) was subsequently adopted across the United States and extended to other countries and regions, including Canada and Europe. Despite this, the implementation of compulsory screening remains a subject of debate [3]. A systematic review in the United States, encompassing 14 studies with a total of 448,276 participants, concluded that such screenings are effective in identifying AIS and that early interventions, such as the utilization of braces and exercise therapy, to arrest or reduce the progression of this condition [41][29]. Similarly, evidence from Australia

advocates for the execution of scoliosis screenings within school settings to promote timely treatment for affected students [3]. A study in Denmark found that health-care systems that did not conduct school scoliosis screening had a greater angle of scoliosis when patients were detected compared to those that conducted school scoliosis screening [78]. The study in Singapore believes that screening for scoliosis has important clinical significance and will continue to be a routine health service project [31].

In 1995, the Hong Kong Department of Health included scoliosis screening in routine health services. In 2021, China governments and education departments at all levels have included scoliosis screening in physical examinations for primary and secondary schools. In 1985, the *Moire* measurement method and visual method were used to conduct a scoliosis survey on 2500 primary and secondary school students aged 7-16 in Shanghai, with a prevalence rate of 12.05%. In 1988, 20418 students aged 7-15 in Beijing were screened using a combination of prodromal testing, *Moire* measurement, and X-ray photography, and the incidence of scoliosis was found to be 1.04% [63]. From this, it can be seen that using different screening schemes and standards for scoliosis can lead to significant differences in screening results. A device-based screening standard strategy is needed globally.

Chapter 3

Back Shape Measurement and Three-dimensional Reconstruction of Spinal Shape Using RGB-D Sensor

Spinal screening relies mainly on direct clinical diagnosis or X-ray examination (which generates harmful radioactive exposure to the human body). In general, the lack of knowledge in this area will prevent parents to discover adolescents' spinal deformation problems at children's early age. Therefore, we propose a low-cost, easy to use, radiation free and high-accuracy method to quickly reconstruct the three-dimensional(3D) shape of the spine, which can be used to evaluate spinal deformation. Firstly, the depth images collected by *Kinect* sensor are transformed into 3D point clouds. Then, the features of anatomic landmark points and spinous processes line are classified and extracted. Finally, the correlation model of spinous processes line and spine midline is established to reconstruct the spine. The results show that the proposed method can extract anatomic landmark points and evaluate scoliosis accurately, which is fea-

sible and promising. In this chapter, we validated the high correlation between the 3D back point cloud and 3D spine curve, and we proposed a *Kinect* based low cost, easy to use, non radiation, and high accuracy method to quickly reconstruct the three dimensional shape of the spine, which can be used to evaluate spinal deformation

3.1 Introduction

It is important to monitor the spine trunk deviation when a person is standing straight because it can indicate whether or not the subject has orthopathology [125]. At present, the most serious spine problem is scoliosis caused by 3D deformation of the spine, which can be diagnosed based on the deviation of the spine from the vertical plane and the *Cobb* angle measured between the inflection points and the spine curve [27][87]. In the assessment of scoliosis, the computation of the Cobb angle proceeds through distinct stages: Firstly, the identification of the terminal vertebrae, characterized by the utmost tilt towards the concavity of the curvature, is crucial. Secondly, the delineation of horizontal lines on the superior margin of the uppermost vertebra and the inferior margin of the lowermost vertebra is performed. The angle that emerges from the intersection of these lines serves as the metric known as the Cobb angle, as illustrated in Figure 3.1 [130].In the context of scoliosis management, the Cobb angle serves as an important indicator for determining the appropriate course of treatment. Typically, patients presenting with a Cobb angle below 25° require close monitoring. However, if annual progression surpasses 5° and the Cobb angle exceeds 25°, brace therapy is recommended. For scoliosis cases with Cobb angles ranging from 25° to 40°, rthopedic braces are considered the primary treatment modality. In cases where progression exceeds 5° annually and the Cobb angle surpasses , surgical intervention is typically advised. Furthermore, scoliosis with a Cobb angle between 40° and 50° is prone to further progression due to the significant curvature, necessitating surgical treatment for immature patients. Mature patients with scoliosis exceeding 50° in

curvature and demonstrating significant progression during follow-up also require surgical intervention. Ultimately, a Cobb angle greater than 50° unequivocally indicates the need for surgical management. The quantification of the Cobb angle may exhibit variability due to factors such as patient positioning, radiographic technique, and delineation methodology, with a standard error value typically ranging from $3 - 5°$. Factors such as patient age, curve type (single or double), and curve apex location (thoracic, thoracolumbar, or lumbar spine) also influence these measurements [52].

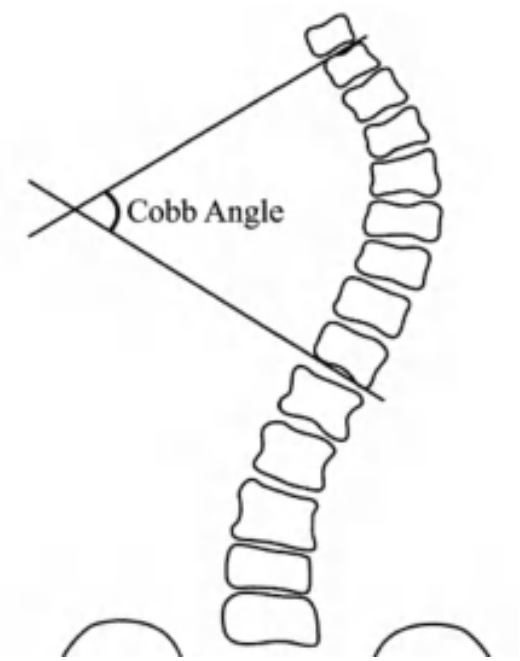

Figure 3.1: Illustration of *Cobb* angle.

Scoliosis is a chronic disease that can be found in children and adolescents at early ages. It is believed that prevention of such disease is far more important than later treatment [38]. At present, the main detection method for scoliosis is X-ray examination. Despite the popularity and authority in diagnose accuracy, it still has the following limitations. First, X-ray devices expose patients to radiation, especially adolescents and patients with scoliosis who need long-term rehabilitation and monitoring [23]. Secondly, the information obtained from the X-ray machine is a two-dimensional(2D) image, which is not sufficient to fully evaluate 3D spine deformity.

In addition, X-ray examinations are expensive, and they have strict requirements on the site and require a technician to operate.

These shortcomings have restricted the usage of the X-ray system, such as at home. Since it has not been widely used in the field of screening, patients generally are not able to know if they have scoliosis in time, thus missing the best chance of effective therapy. In addition, the main method for current screening is to use palpation, whose accuracy is highly related to the clinician's experience, and the clinicians often need to touch the back of the patient's body, which brings ethical issues. To solve these problems, many teams have proposed portable and non-invasive methods for the evaluation of scoliosis [82][98]. One team proposed a new ultrasound-based approach to image the spine shape [19]. Other teams have proposed 3D reconstruction of the back or the whole trunk using an optical non-invasive surface measurement system [80]. They mainly model the anatomical features of the back, represented in Fig.1, and then use the physical model to represent the spine's shape in three dimensions. Their systems are based on highly accurate surface measuring devices, which are generally expensive. Thus, the main challenge is to develop a non-invasive, non-contact, and low-cost method to achieve initial screening analysis of scoliosis and subsequent spinal rehabilitation follow-up. A group proposed using the low-cost RGB-D camera to locate the anatomical landmarks on the back of the human body [13]. Still, their methods have low back anatomical landmarks positioning accuracy and thus lack robustness. To estimate the anatomical landmarks and reconstruct the 3D shape of the spine automatically and accurately, this chapter proposes a systematic method based on the analysis of the back surface using a low-resolution *Kinect* sensor.

3.2 Challenges and Contribution

Through the analysis of non radiative spine 3D reconstruction methods mentioned above, the key challenges can be outlined as follows: 1. How to use low resolution

RGB-D cameras to achieve recognition of human back feature points; 2. How to reconstruct the midline of the spine based on three-dimensional back feature points; 3. Lack of three-dimensional point clouds on the human back and corresponding spinal X-ray databases for relevant experimental research. In response to the above challenges, the following significant contributions have been made in the present study:

1. We use depth images captured by RGB-D cameras to represent the concavity and convexity of the human back and find corresponding anatomic landmark points by calculating surface curvature;

2.We established a correlation model between the spinal midline and the symmetrical midline of the human back, which was derived by calculating the symmetrical midline based on the curvature of the human back. This integration incorporated the biomechanical characteristics of the spine and the relationship between the spinous process points and the spinal center. By identifying the 3D back landmark points, we reconstruct the 3D spinal midline curve;

3. We have established a dataset that includes 3D point cloud of the human back and corresponding spinal X-ray image and We developed a 3D spine and posture analysis system based on this algorithm using RGB-D, and have validated the results accordingly.

3.3 Materials and Methods

3.3.1 Data Acquisition

Six healthy people and two scoliosis patients have participated in the experiment. The subjects were asked to stand in the upright position naturally. As described in Figure 3.2, a *Kinect* 2 ($Microsoft^R$) sensor was located at 1m behind the subject and the height of the *Kinect* sensor was set to 1.3m. The *Kinect*'s sensing plane

remains relatively parallel to the wall. After the acquisition process, which lasted approximately 2 seconds, a back depth map was acquired. A global system of reference (XYZ) was defined corresponding to the wall position in Figure 3.2. According to the global reference system, a 3D back shape point cloud was created. The resolution of the 3D back shape reconstruction is proved to be below 2mm over a human's back [125]. Before data acquisition, an experienced clinician locates the anatomic landmarks and spinous processes line on the back of the subjects by palpation and marks them in Figure 3.3 in order to evaluate the accuracy of the proposed method. These anatomic landmarks include the 7th cervical($C7$), the sacrum, the posterior left and right iliacs spines(PSIS). In order to reduce the comparison error between different reconstructions of the subjects and that of the same subject with different angles relative to the main plane (XY plane) of the $Kinect$ sensor. It is essential to rotate the trunk 3D point cloud into a body-fixed coordinates reference [27].

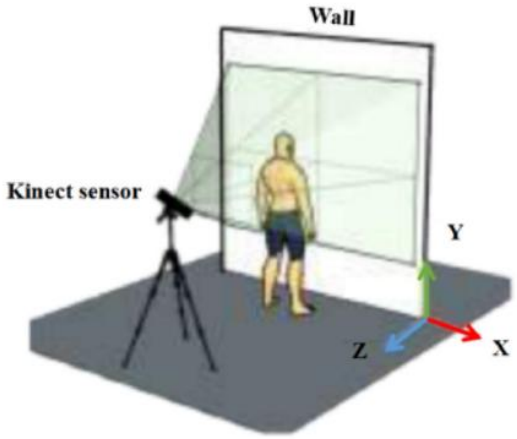

Figure 3.2: The global coordinates reference.

3.3.2 Human Back Extraction

Initially, the regions of interest, spanning from the neck to the hip, are automatically localized employing the $Faster - RCNN$ [87]. Subsequently, a $Resnet$ architecture

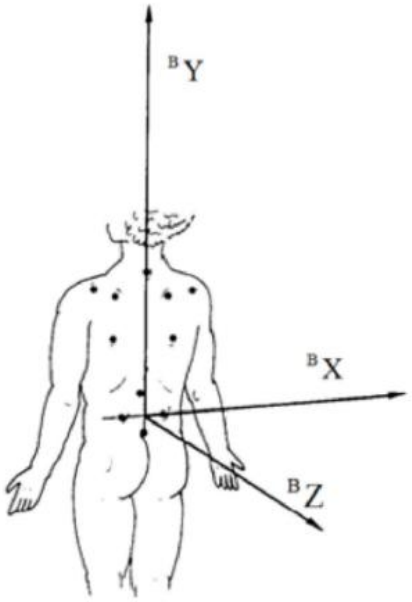

Figure 3.3: The body-fixed coordinates.

with 101 layers is employed to recognize the distinctive characteristics of each group [42]. Preprocessed images are then fed into the *Resnet* model to extract high-level features for both binary and multiclass classification tasks based on the groups mentioned above. Following this, the segmented 2D image is projected onto the 3D point cloud, leveraging an alignment function. Ultimately, this process leads to the segmentation of the 3D back point cloud. The results are represented in Fig. Figure 3.4(b).

3.3.3 Automatic Features Extraction

Anatomical Landmarks

To locate the anatomical landmarks automatically, the Gaussian curvature and Mean curvature are calculated from the 3D trunk point cloud [35]. These curvature maps help to represent the convexity and concavity of the 3D point cloud. Firstly, the 3D point cloud data is meshed. In the experiment, the data is about 500*700 points, which depends on the size of the human body. Secondly, Gaussian Blur is used to pre-

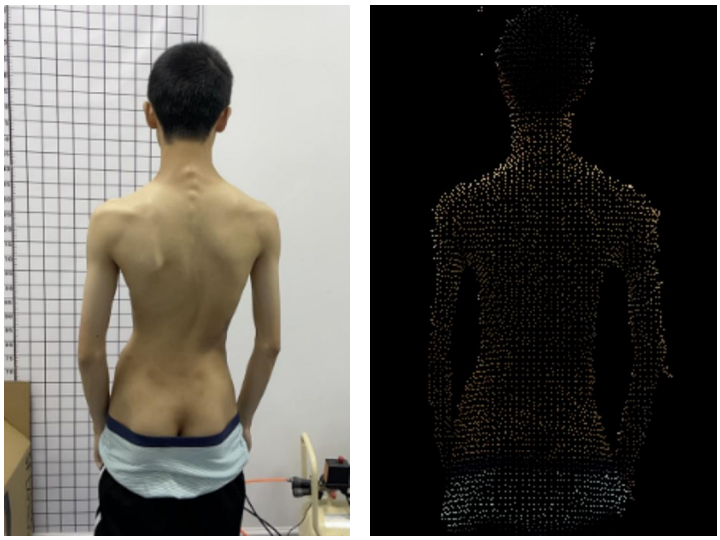

(a) Original point data (b) Human back point cloud

Figure 3.4: Illustration for human back extraction.

smoothing the grid plane to avoid the interference of the global curvature calculation caused by enlarging the local curvature properties of raw data. Finally, the Gaussian and Mean curvature maps are calculated based on the body reference:

$$H = \frac{1}{2}(k_1 + k_2) \tag{3.1}$$

$$K = k_1 \cdot k_2. \tag{3.2}$$

Where k_1 and k_2 are two directions of the principal curvature, and they are perpendicular to each other. H and K are the Mean curvature map and Gaussian curvature map, as depicted in Figure 3.5(a) and Figure 3.5(b).

According to [24][26], the anatomical landmarks are characterized by specific trunk surface curvature. The curvature criteria are as follows: Parabolic, Convex, Concave, and Saddle-shaped, which are listed in Table 3.1. We assume that $k2$ is the maximum and $k1$ is the minimum in the two principal curvatures. The Gaussian curvature map can be described as Figure 3.6.

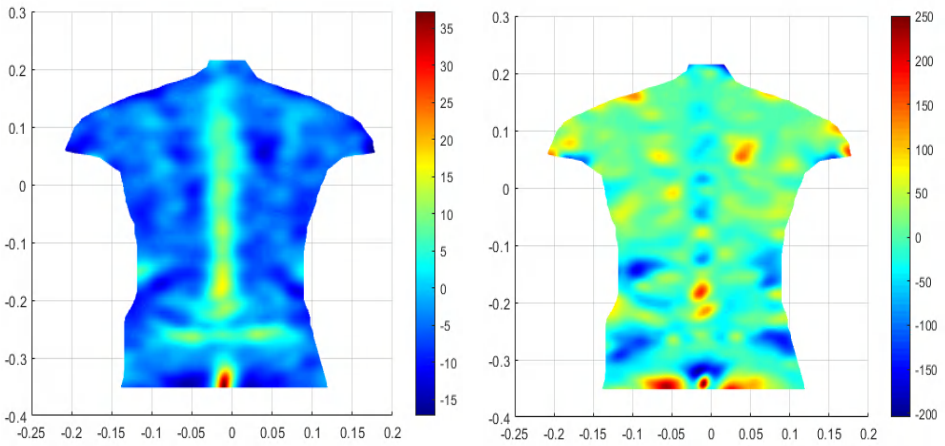

(a) Back Mean curvature map (b) Back Gaussian curvature map

Figure 3.5: Human back curvature.

Table 3.1: Surface curvature criteria.

Parabolic	$k_1 = 0$ or $k_2 = 0$
Convex	$k_2 < 0$
Concave	$k_1 > 0$
Saddle-shaped	$k_2 > 0 > k_1$

Back Spinous Processes Line

Before the location of the spinous processes line, we assume that the spinous processes line of a human's body is at the symmetrical midline of the human back, which divides the back into a left and right side with minimum asymmetry [99][127][44], as show in Figure 3.7.

However, some points in the midline are not consistent and cannot represent the accurate position of the spinous processes as the spinal deformation is continuously changing. To solve this problem, some criteria were obtained based on the midline:
(a)Depth of the minima in the transversal surface of human back point cloud;
(b)Smoothness of the spinous processes line;

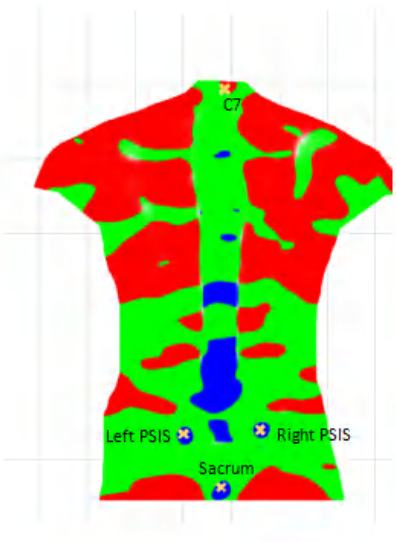

Figure 3.6: In the Gaussian curvature map, convex, parabolic, saddle-shaped, and concave regions are represented as red, white, green and blue respectively. All the anatomic landmarks are pointed out by the yellow cross.

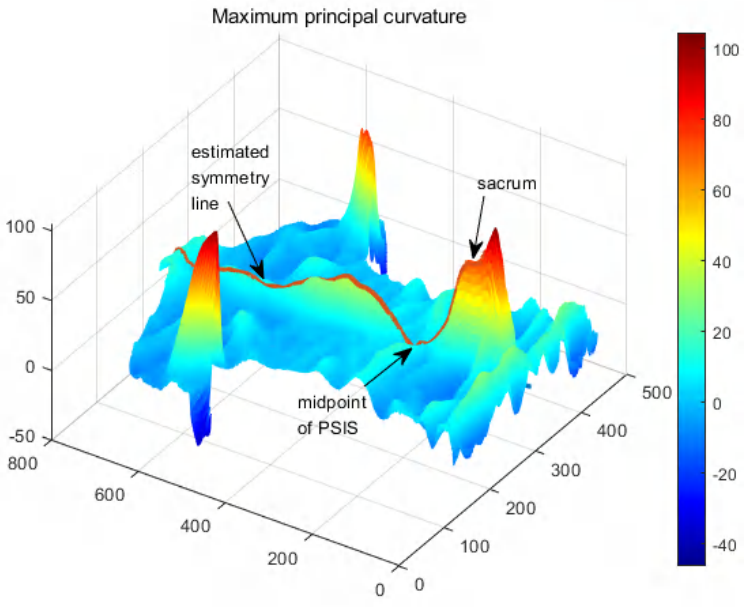

Figure 3.7: The symmetry line often passes through the midpoint of PSIS and sacrum.

For solving this problem, some criteria were obtained based on the midline: (a) depth of the minima, (b) smoothness of the resulting line. First, 16 points between $C7$ and

the mid-point of the PSIS on the midline were acquired at equal intervals, as shown in Figure 5.12(a). Second, we calculate the normal of 16 points on the midline and extract the cross-section that passes through these 16 points and is perpendicular to the midline, as shown in Figure 5.12(b). Third, We extract the profile of the cross-section and calculate its local minimum value, then compare whether the midpoint estimated through symmetry and the points of the local minimum value coincide. If they do not coincide, we select the local minimum value to replace the original value, as shown in Figure 5.12(c). Last, after the 18 points were determined, a two-dimensional second order polynomial was used to fit the spinous processes line to keep its smoothness, as shown in Figure 5.12(d)

3.3.4 Three-dimensional Construction of The Spinal Midline

The procedure of 3D spinal midline reconstruction is based on the spinous processes line based on the following assumptions:

1) The horizontal component of the normal angle is equal to vertebral rotation.

2) The direction of surface normals along the symmetry line represents the degree of vertebral rotation.

3) The distance between the center of a vertebra and the back surface is infinitely small, which can be ignored and is considered a function that varies with the order of different vertebrae in the spine and the length of the main body of the spine.

The spinal midline (x_m, y_m, z_m) was calculated based on the spinous processes line (x_s, y_s, z_s) using the following (Equation 3.3) proposed by [25]:

$$\begin{cases} x_m = x_s + L \cdot sin\theta \\ \quad y_m = y_s \\ z_m = z_s + L \cdot cos\theta \end{cases} \tag{3.3}$$

Among them, L represents the length of a single vertebrae, representing the distance from the skin surface of the back to the center of the vertebrae. θ is vertebral rotation,

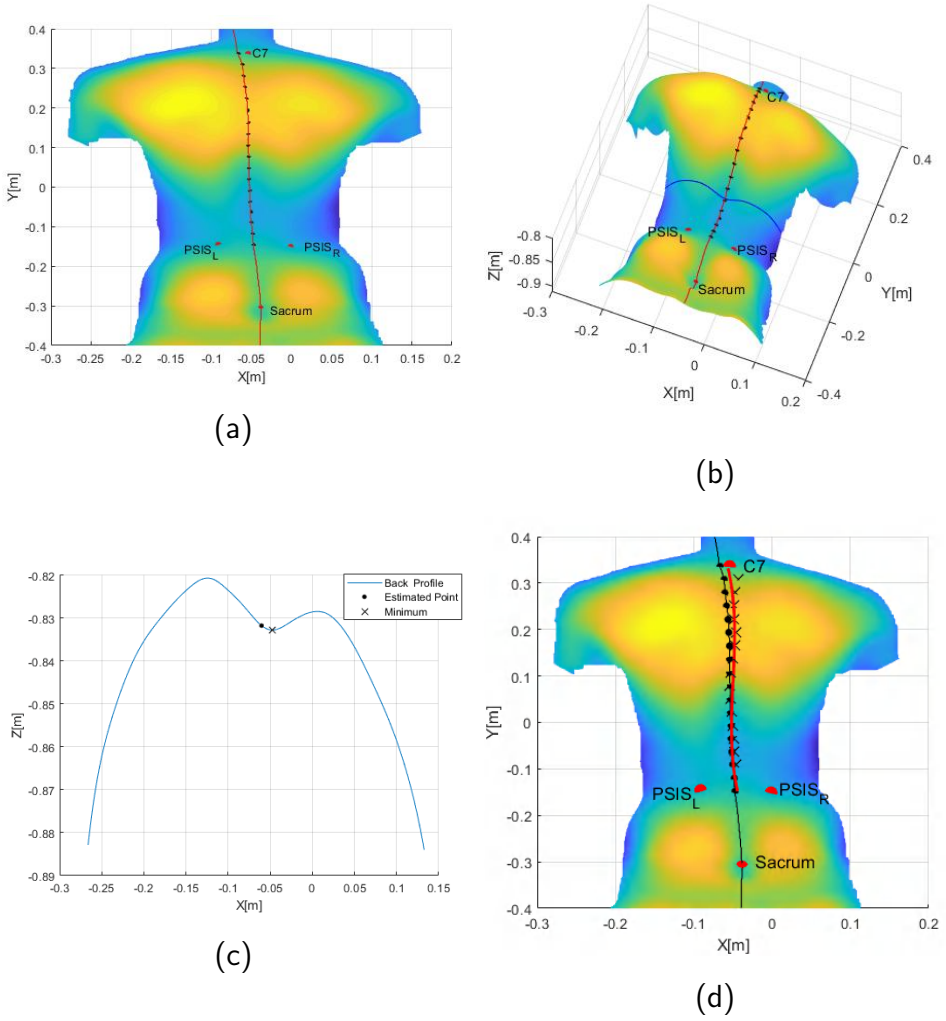

Figure 3.8: The schematic diagram for finding a more reasonable spinous processes line.

which represents the angular deviation between the normal vector of the spinous process point within the $x-z$ direction and the z-axis of the cross-section, as shown in Figure 3.9. By testing the samples, the main length of a single vertebra can be calculated by the scale factor, the length of the trunk of the spine, and the longitudinal coordinates of the spine. It is expressed as Equation 3.4:

$$L(y_s) = 0.132 \cdot T - 0.035 \cdot y_s \tag{3.4}$$

L is also a function of the longitudinal coordinates of the spine y_s. T is the main

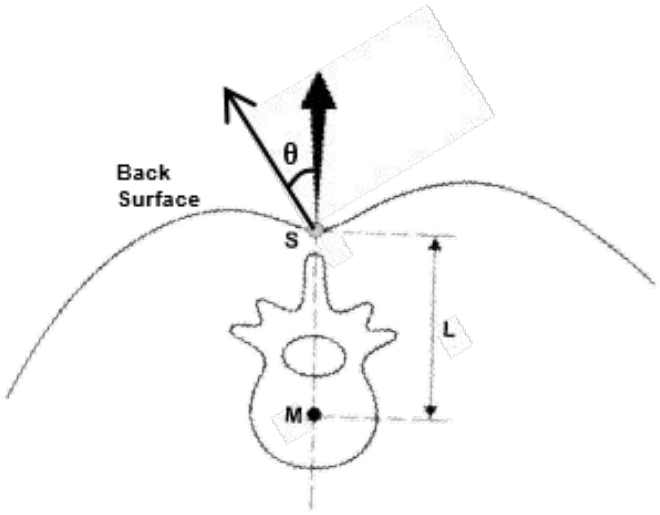

Figure 3.9: Establishment of the spinal midline in a transverse trunk section utilizing back surface data. Specifically, the vertebral midpoint M is constructed by traversing from the surface point S located on the spinous processes line, in a direction opposite to the normal, by a distance of L.

length of the spine(the projection distance from the $C7$ point to the midpoint of the PSIS). For a specific sample, it is equivalent to a constant.

Through (Equation 3.3) and (Equation 3.4), we are able to calculate the midline of scoliosis, but the results showed that due to only relying on the normal rotation angle of the spinous process points, some angles may have significant errors due to local unevenness on the body surface. To correct the overall body rotation, We attempt to use a new method for estimating the curvature of the spinal midline in the XY plane, leveraging biomechanical principles of the spine and relying on the spinous processes line as a reference. By calculating the rotation angle that conforms to spine biomechanics and inferring the 3D curve of the Spine midline.

In order to maintain body balance, there are usually 2-3 bends in the back of each

scoliosis patient, including one big bend and two small bends in the opposite direction, as shown in Figure 3.10(a). Vertical deviation of spinous processes line in scoliosis is closely related to spine rotation angle. Vertical deviation of the spinous processes line can reflect spine rotation angle positively. A single side bend is shown in Figure 3.10(b). C_a is the spinous processes line, C_b is the spine midline and d_max denotes the max vertical offset of the point on the spinous processes line to the line connecting $C7$ point and the midpoint of the right and left PSIS. Assuming that the endpoints of the spinous processes line coincide with those of the Spine spinous processes line midline, the coordinates of the C_b line can be predicted by the C_a line. The calculating model of the severity of scoliosis is expressed as (Equation 3.5):

$$V = \frac{l_{en\_chord}}{T} \tag{3.5}$$

Among them, V represents the severity of scoliosis, and l_{en_chord} represents the center chord length of each bend, as shown in Figure 3.10(a) and Figure 3.10(b). Further, the calculation model of the degree of deviation between the spinous processes line and the spine midline is expressed as (Equation 3.6):

$$r = \frac{d_1}{d_{max}} = 1 + \frac{w_{check}}{d_{max}} \tag{3.6}$$

r denotes the degree of deviation between the spine midline and spinous processes line in each curve; d_1 denotes the maximum distance between the spine midline point and the central chord; d_{max} denotes the maximum distance between the spinous processes line point and the central chord; w_{check} is the difference in the vertical distance between d_1 and d_{max}, their relationship can be expressed by (Equation 3.7):

$$d_1 = d_{max} + w_{check} \tag{3.7}$$

Further, the formula for calculating w_check can be interpreted as Equation 3.8:

$$w_{check} = p_1 \cdot 0.5 \cdot w_{y\_max} \cdot min(1, p_2) \tag{3.8}$$

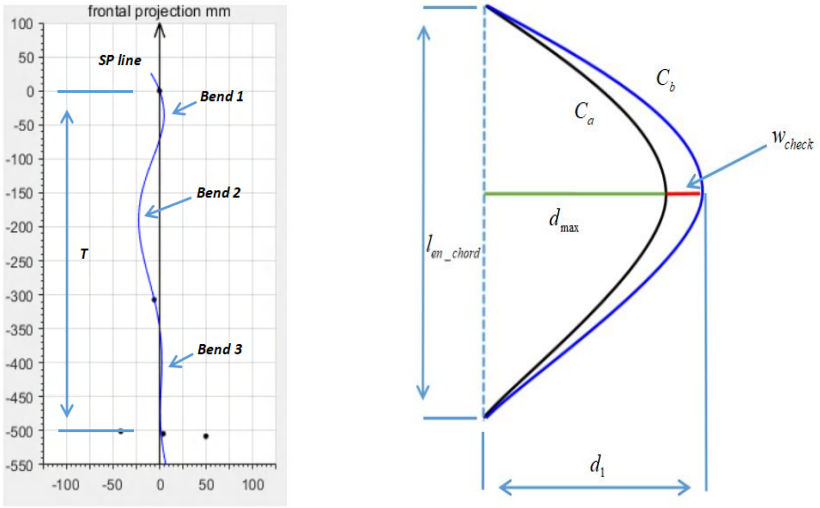

(a) Example of spinous processes line with three band

(b) Spine midline and spinous processes line in one band

Figure 3.10: Illustration for an spinous processes line with three bends in the XY plane and relationship between the Spine midline and spinous processes line on one bend.

p_1 represents an empirical value of the deviation strength parameter between the spine midline and the spinous processes line estimated from parameter V. According to experience, when $V < 0.1$, p_1 is 0.5; when $0.1 < V < 0.2$, p_1 is 0.8; when $0.2 < V < 0.4$, p_1 is 0.9; otherwise, p_1 is 1. p_2 represents the severity of single bend, which can be calculated by (Equation 3.9):

$$p_2 = \frac{d_{max}}{l_{en\_chord}} \tag{3.9}$$

w_{y_max}indicates the width between the spinous processes line and the center chord in the y-axis direction. $min(1, p_2)$ represents the minimum values of 1 and p_2.

We set the ratio r of the distance from each point on the spine midline to the central chord and the distance from the corresponding point on the spinous processes line to the central chord to be equal in each bend, according to the $r_i (i = 1, 2, 3)$ and spinous processes line coordinates of each bend, the coordinates of the corresponding spine

midline points can be calculated.

According to (Equation 3.3), the calculation equation of vertebral rotation angle can be expressed as follows (Equation 3.10):

$$\theta = arcsin\frac{x_m - x_s}{L} \tag{3.10}$$

After calculating the vertebral rotation angle of the spine, they are brought back into (Equation 3.3) to calculate the final 3D spine midline.

Body-fixed Coordinates

The camera plane needs to be relatively parallel to the back plane of the human body when collecting the original point cloud. However, due to the inability to fix the upper body of the human body, unnecessary left and right rotations can occur, resulting in incorrect point clouds obtained and affecting subsequent calculations. Due to the relative stability of the left and right PSIS and the fixed position of the keel within the human anatomy, it is expected that there will be no significant changes. Therefore, we established the body-fixed coordinates system using $C7$, left and right PSIS in the coordinate form of Figure 3.3 in subsection 3.3.1. Within this body-fixed coordinate system, the origin is designated as the midpoint between the left and right posterior superior PSIS. The Y-axis is defined by the line connecting point $C7$ to the origin, with positive direction being upward. In the plane encompassing $C7$ and the left and right PSIS, the X-axis is a straight line passing through the origin and perpendicular to the Y-axis, with positive direction towards the right. The Z-axis is perpendicular to the XY plane. To facilitate subsequent calculations, once the coordinate axes are established, the origin is shifted to point $C7$.

Single Vertebra Position Simulation

In order to better simulate the correlation between each vertebra, we annotated about 1000 X-ray images and statistically analyzed the length, width, and spacing of each vertebra from $C7$ to $L5$, and obtained their statistical correlation. After obtaining the 3D spine midline, we obtained the specific positions of each vertebra from $C7$ to $L5$ based on the correlation between cone size and spacing, which is used for subsequent calculation of parameters such as *Cobb* angle.

3.4 Accuracy Analysis Results

Figure 3.11 shows a representative result of one patient with moderate scoliosis. We can find out that the black spots are the anatomical landmark points marked by experienced clinical, and the red spots represent the point automatically found by the proposed algorithm.

Table 3.2: RMS error of the anatomical landmarks and *Cobb* angle.

	Proposed method	Bonnet method [13]
$C7$	$6 \pm 4(mm)$	$10 \pm 6(mm)$
Right PSIS	$4 \pm 3(mm)$	$5 \pm 4(mm)$
Left PSIS	$4 \pm 2(mm)$	$8 \pm 6(mm)$
Sacrum	$2 \pm 2(mm)$	$6 \pm 2(mm)$
Cobb	$3 \pm 2(^\circ)$	NAN

Figure 3.13 shows the results of 3D imaging of one subject spine, and Figure 3.12 shows the frontal and lateral views of the spinous processes line and spine midline by the proposed algorithm. Table 3.2 shows the accuracy of the anatomical markers location and the spine midline reconstruction based on the proposed system, which shows the excellent performance of this method. As can be seen from the table,

the average Root Mean Square(RMS) error of anatomical markers is less than 5 mm. There is the biggest error in the positioning of $C7$. Because of the accuracy of imaging equipment, it is not sensitive to the calculation of the back surface curvature of $C7$ area, which leads to a higher final positioning error. For the accurate analysis of 3D spine imaging results, the traditional *Cobb* angle parameters are used to compare the results calculated in this method with those calculated after X-ray detection and the final RMS error is around 3°.

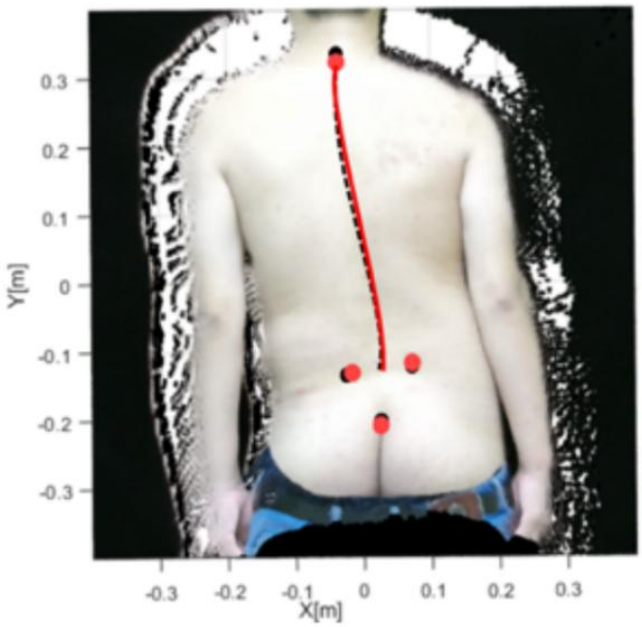

Figure 3.11: Representative result showing the estimate of anatomic landmarks positions and spinous processes line for a subject in the global coordinates $[m]$.

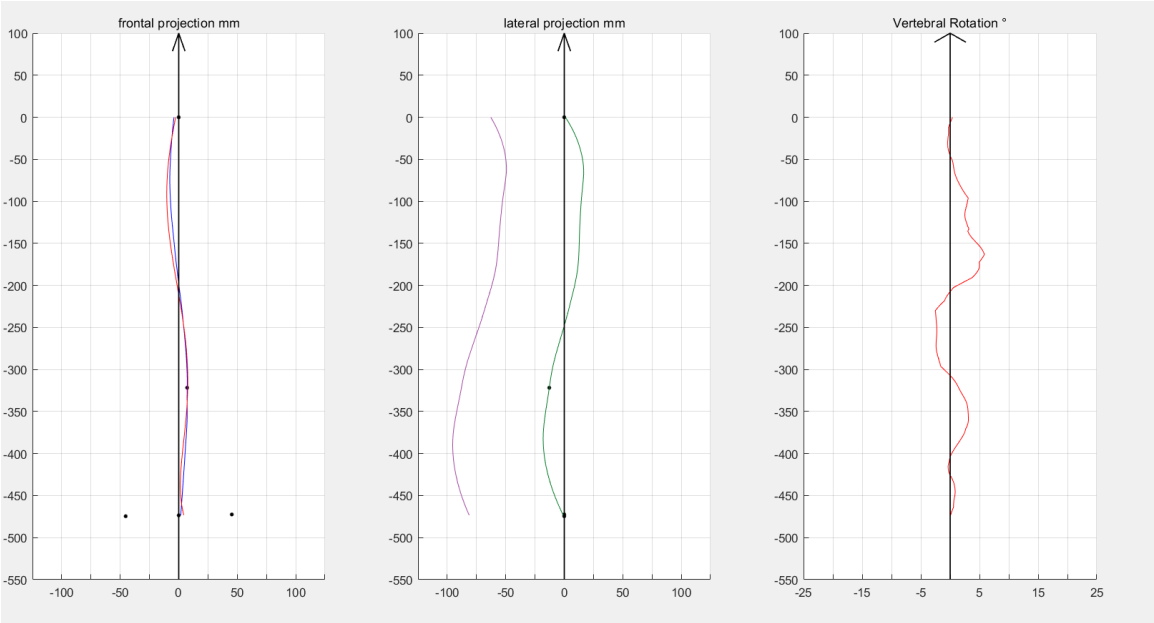

Figure 3.12: The frontal and lateral views of the spinous processes line and spine midline and the vertebral rotation of the spine calculated by the proposed method, the results are represented in the body-fixed coordinates[mm].

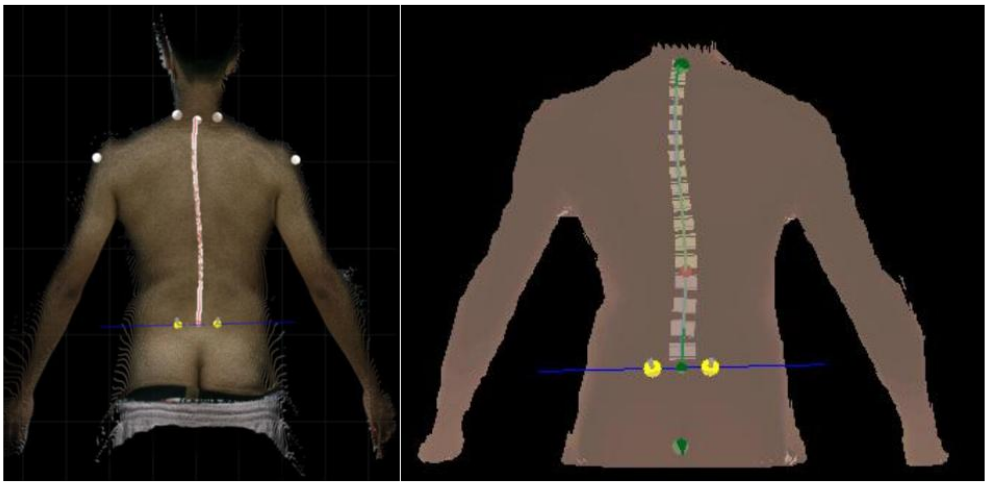

Figure 3.13: The 3D imaging of the spine($C7$-$L5$) with anatomic landmarks for a subject.

3.5 System Development and Comprehensive Validation

3.5.1 Equipment

Our device mainly consists of *Kinect* Sensor Version 2, a Windows laptop, and a retractable tripod, as shown in Figure 3.14.

Figure 3.14: Hardware composition of system.

The second-generation *Kinect*, known as *Kinect* v2, represents Microsoft's advanced iteration, integrated into the next-generation gaming console, *Xbox One*, for capturing 3D imagery and audio. The Time of Flight(ToF) processing unit within *Kinect* v2 utilizes the *TSMC* 0.13 chip [81][97]. As depicted in Figure 3.15, *Kinect* v2 comprises a color camera, a depth sensor, and an infrared emitter, enabling the acquisition of depth, color, and infrared data from the environment.

The Kinect v2 uses Time of Flight (ToF) technology, utilizing a square wave-modulated

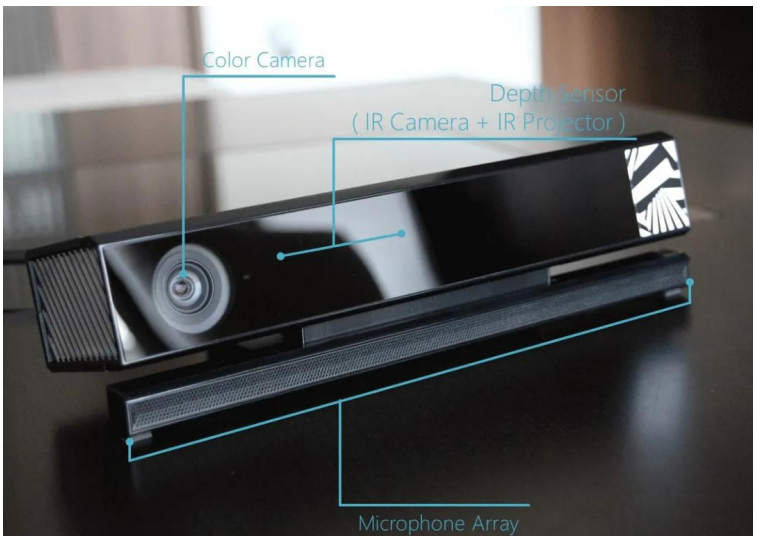

Figure 3.15: Structure of *Kinect*2.

illumination source originating from its camera and operating at an average frequency of 80MHz. Utilizing phase detection methods, the phase shift and attenuation of light is determined as it traverses from the emitter, reflects from the object, and returns to the sensor. This process enables the estimation of the light's round-trip transit time. Consequently, the distance between the object and the sensor can be derived based on the round-trip flight time of the light. The depth measurement is computed by applying the following (Equation 3.11):

$$2d = \frac{phase}{2\pi} \cdot \frac{c}{f} \tag{3.11}$$

d represents the depth, $phase$ denotes the modulation signal phase shift, c signifies the light speed, which is approximately $c = 3 \times 10^8 m/s$ when propagating through air, and f corresponds to the modulation frequency of the sensor.

The color camera resolution of *Kinect* v2 is 1920x1080, coupled with a horizontal field of view of 70° and a vertical field of view of 60°. Additionally, it offers a remarkable data transfer speed, capable of acquiring depth data at a maximum rate of 60 frames per second. In executing a 3D reconstruction of the human back utilizing the *Kinect* v2, the overarching 3D reconstruction algorithm of this system adheres to the

algorithmic framework of *Kinect* Fusion [72]. On this basis, the main contributions of this system are:

1. Firstly, using the basic Application Programming Interface(API) driver provided by *Kinect* v2 SDK, the depth data acquisition module of the reconstruction system is constructed;

2. Secondly, a depth data noise processing and depth camera calibration module are added;

3. Thirdly, a complete, low-cost, real-time, accurate 3D scanning solution is implemented.

In order to obtain a complete and relatively low noise image of the human back, we placed the *Kinect* device at a distance of about 1 meter behind the plane of the human back and adjusted the height of the device to the position between the third to seventh thoracic vertebrae of each person. A specific usage scenario is shown in Figure 3.16.

3.5.2 System Procedure

Data Acquirement

According to Figure 3.2 in subsection 3.3.1, we collect images of the human back. During the data collection process, we find that a significant deviation angle between the camera plane and the plane of the human back can introduce substantial errors in the 3D reconstruction, even after attempting to correct these errors using the human coordinate system. The original data inaccuracies resulting from this misalignment persist and are not adequately compensated. So before collecting, we need to find a wall and adjust the equipment plane to be relatively horizontal with the wall. During the testing process, the subject needs to have their feet together and lean vertically against the wall. To optimize the parallelism between the equipment and the wall,

Figure 3.16: Detection display.

we integrated a mesh structure into the data collection interface. This allows for precise adjustments in the left-right rotation of the equipment by identifying distinct horizontal and vertical line patterns on the wall. As depicted in Figure 3.17.

After obtaining the raw data, the algorithm automatically extracts a 3D point cloud map of the human back using the human back extraction model trained in subsection 3.3.2, as shown in Figure 3.18.

Calculation

Utilizing the method outlined in subsection 3.3.3, we determine the curvature of the human back and the 3D spinous processes line. Additionally, we identify and mark the midpoint of the spinal vertebrae ranging from $C1$ to $L4$, both the left and right PSIS, and their respective midpoints (representing $L5$'s center here). Furthermore, we locate and label the sacrum points, as shown in Figure 3.19.

Figure 3.17: Optimized data collection interface.

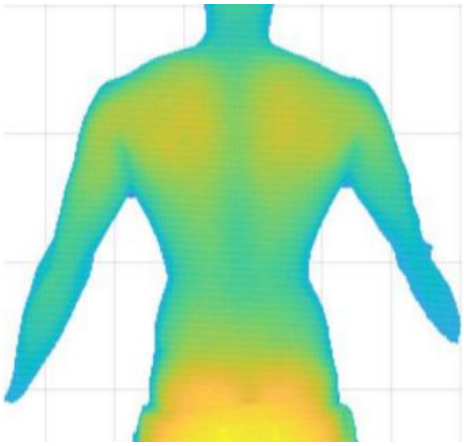

Figure 3.18: Human back 3D point cloud.

Finally, based on the content of subsection 3.3.4, we calculate the 3D spine midline in the human coordinate system based on the found feature points and spinous processes line, as shown in Figure 3.20.

Given that the assessment of the 3D spinal morphology relies heavily on X-ray imaging from coronal and sagittal views encompassing the entire spine, we conducted a com-

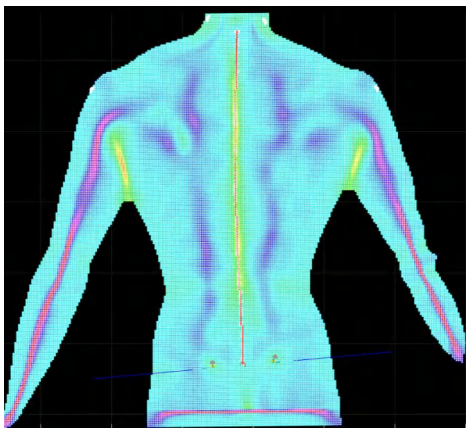

Figure 3.19: Human back curvature and landmarks.

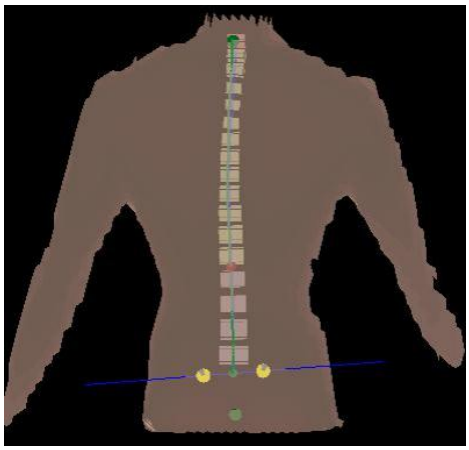

Figure 3.20: 3D human back and spine.

parative analysis of the 3D spine and body posture measurements obtained through our system against the corresponding X-ray findings. The comparison is shown in Figure 3.21 and Figure 3.22

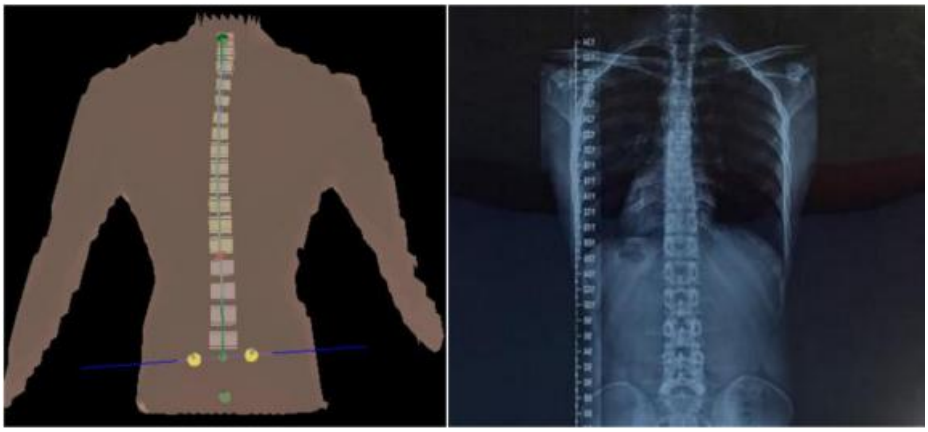

Figure 3.21: Comparative analysis of system outcomes and X-ray imaging in coronal view.

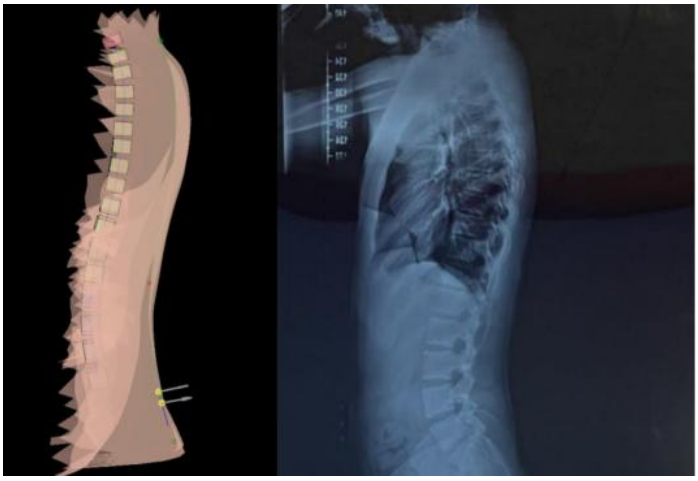

Figure 3.22: Comparative analysis of system outcomes and X-ray imaging in sagittal view.

3.5.3 Clinical Experiment

Experimental Motivation

Exploring the reliability and validity of our system infrared 3D spinal and posture evaluation systems(ITSPES) for measuring *Cobb* angle in AIS patients, guiding the further application of the research results in clinical diagnosis in the future.

Experimental Design

1) Experimental design: This experiment adopts a multicenter, single-blind diagnostic test;
2) Basic methods of clinical trials: Adhering to the Guidelines for Reporting Reliability and Agreement Studies (GRRAS), the current clinical investigation employed X-ray plain film outcomes as the benchmark control for evaluating the reliability and validity of the ITSPES system in quantifying the *Cobb* angle among patients;
3) Research subjects: 57 suspected adolescent idiopathic scoliosis patients were recruited from the Rehabilitation Medicine Center of West China Hospital of Sichuan University and the Traditional Chinese Medicine Hospital of Guangling District, Yangzhou City. All examination subjects are first-time patients who have not undergone any treatment related to scoliosis. They are between 6 and 16 years old and have a scoliosis degree between 5 and 50°;
4) Diagnosis and measurement methods: To reduce imaging and measurement errors, X-rays and ITSPES need to be performed at the same time. Three independent evaluators, blinded to the measurement process, assessed the *Cobb* angles of the thoracic and lumbar vertebrae for the subjects, utilizing both the X-ray results and the outcomes generated by our system. After measurement, a researcher who was unclear about the experimental content conducted statistical analysis on the results of the two groups.

Evaluation Methods

Utilize X-ray plain films and the ITSPES system to diagnose and calculate the *Cobb* angles pertaining to the thoracic and lumbar spinal segments. The measurement method for *Cobb* angles is shown in subsection 3.3.4.

3.5.4 Experimental Result

Table 3.3 shows the reconstructed spine model's *Cobb* angle errors. The overall average *Cobb* angle error is 4.67° in thoracic region, and 2.51° in lumbar region. The average error is about 3.59°.

Table 3.3: *Cobb* angle error of the reconstructed spine.

	$Error^{\circ}\ mean \pm std(max)$
Thoracic	$4.67 \pm 4.31(14.75)$
Lumbar	$2.51 \pm 3.22(10.25)$

Besides the *Cobb* angle in the coronal position of the spine, we also conducted morphological analysis on the morphology of the sagittal position and the concavity and convexity of the human back surface and found a high correlation between the 3D back surface and the range of scoliosis angle. Comparative cases of different *Cobb* angles of scoliosis are illustrated in Figure 3.23.

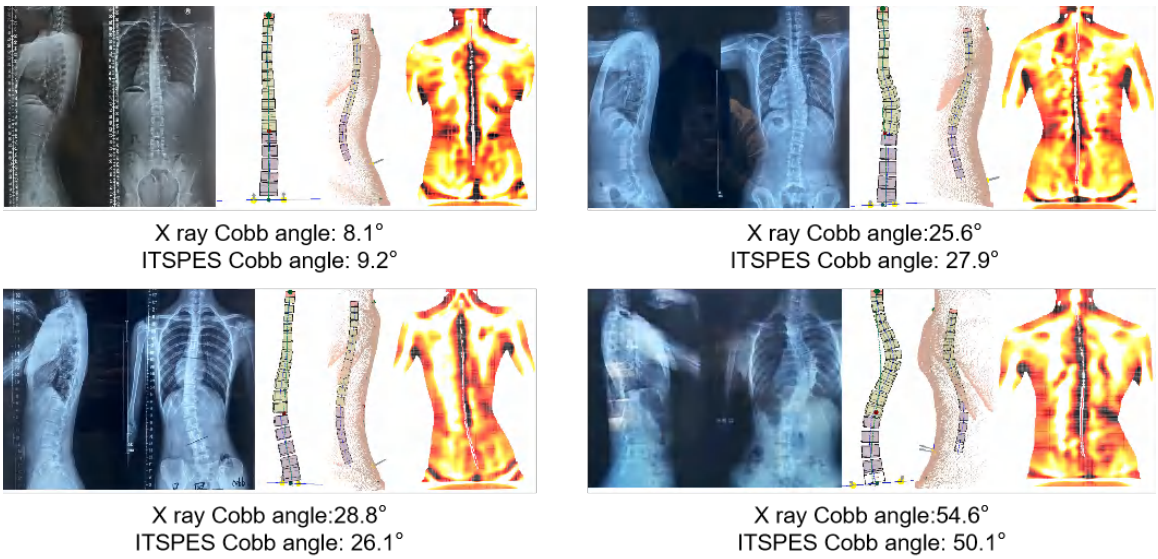

Figure 3.23: Comparison of sagittal, coronal, and back surface imbalances between our system(ITSPES) and X-rays at different *Cobb* angles.

3.6 Conclusion

In this work, we use a low-cost 3D camera (*Kinect*) to recognize the anatomical markers on the back of the human body and establish an accurate model to reconstruct the 3D spine. The performance of the proposed method is verified via experiments on practical investigation. Compared with the method proposed by Bonnet [8], our algorithm has higher accuracy. The average RMS difference calculated is around $5mm$. It is worth mentioning that when the patient's scoliosis is less than $50°$, the difference between the *Cobb* angle calculated by our method and that calculated by X-ray examination is around $3°$. Before putting the product into use, we use more data to verify the system's accuracy, and we collaborate with multiple hospital institutions to conduct clinical trials on the results. Through clinical validation with 57 people, our system has an average error of $3.6°$ in *Cobb* angle accuracy and X-ray. Due to the absence of a shared dataset and the lack of radiation-free equipment, such as ultrasound-based spinal analysis devices and grating 3D spinal analysis devices, we are currently unable to conduct an accurate precision comparison. However, based on the results from existing literature, our method, while slightly less accurate than ultrasound-based spinal analysis devices, offers higher stability and is non-contact. Compared to grating 3D spinal analysis devices, we cannot analyze the accuracy from the Cobb angle dimension as there are no articles on their Cobb angle accuracy analysis. Nevertheless, from a cost and convenience perspective, our method is more cost-effective and, utilizing far-infrared imaging, is not sensitive to visible light, thus eliminating the need for use in a darkroom. The significant error in the thoracic vertebrae may be due to the connection between the thoracic vertebrae, ribs, and scapula, which can easily lead to substantial morphological changes in the back, resulting in inaccurate results. This has also become a direction for improvement in the future.

Chapter 4

Inferring Back 3D Point Cloud Feature From 2D Back Images

Adolescent idiopathic scoliosis (AIS) is a high incidence disease in adolescents, with a long treatment time and difficult to cure. As a consensus, the preliminary AIS screening is of crucial importance to detect the disease at an early stage and allows proactive interventions to prevent the disease from becoming worse and reduce future treatment. Currently, the conventional palpation or Adam forward leaning is the most widely used preliminary screening method considering the Axial Trunk Rotation (ATR) value calculated by scoliosis assessment equipment. However, this method relies heavily on the subject's standing posture and the doctor's experience.

Through the content of chapter 3, we have learned that there is a high correlation between the 3D human back and scoliosis. In this chapter, we explore the correlation between important features (ATR) between 2D back images and corresponding 3D back point cloud images. We develop an efficient deep learning-based framework to enable a large-scale scoliosis screening by using only one unclothed two-dimensional(2D) human back image, without any X-radiation equipment. We classify the normal and abnormal scoliosis using ATR value as classification label which calculated from the

human back three-dimensional(3D) point cloud. Our accuracy in the task of AIS classification reaches 81.3%, far exceeding the accuracy of visual observation by the experienced doctor (65%), which can be used as a remote preliminary scoliosis screening method. This chapter verifies that 2D and 3D images of the human back on concave convex features (such as ATR) have strong correlation, which can lay the foundation for inferring the features of 3D point cloud images based on 2D images of the back in the future and it also validates the feasibility of screening for scoliosis using an unclothed back image

4.1 Introduction

AIS is the most common spinal disease in adolescents, with a global prevalence of $0.5 - 5.2\%$ [124]. Without intervention, AIS will continue to develop before the adolescent bone matures, affecting the body appearance, cardiopulmonary function, and even paralysis [118]. However, as a chronic disease, it can usually be found early in the disease, such as judging by abnormal posture and back muscle imbalance. Through timely regular review and health education, it can be effectively controlled and corrected. Therefore, it is considered that the prevention of such diseases is far more important than later treatment [122]. AIS is generally diagnosed by ATR angle or *Cobb* angle. Although *Cobb* angle is more authoritative in AIS diagnosis, it cannot be accurately calculated from human back shape, and additional invasive radiography is required to expose the characteristics of the whole spine. In the field of large-scale scoliosis screening, some research teams found through a large number of samples that judging whether adolescents have scoliosis by whether the ATR value exceeds 5° has achieved the highest sensitivity of 87% in the AIS classification task. Research shows a good correlation with the radiographic measurements, which become a more popular and universal AIS screening standard in the world [20].

The routine AIS screening process includes preliminary screening, outpatient screen-

ing and instrument screening. As the first step of AIS diagnosis, preliminary screening is an important basis for disease awareness and treatment. In the initial screening, patients judged to be at risk of spinal abnormalities will receive follow-up outpatient screening and instrument screening according to the recommendations to further diagnose posture abnormalities or scoliosis.

At present, the common means of preliminary screening include general examination, Adam forward leaning test [1] and scoliosis meter examination [14]. General examination and forward leaning test require the subject to expose his back, stand naturally or make a standard flexion posture, and the examiner shall make a diagnosis through visual observation. Their accuracy is highly dependent on the clinician's diagnostic experience, leading to the subjectivity of screening. Scoliosis measurement instrument detects ATR value through scoliosis measurement instrument on the basis of forward bending posture or standing posture. ATR value is highly correlated with back information, and the current mainstream screening method is to calculate ATR value. Previously, a research team estimated the rotation angle of vertebrae by calculating the 3D back surface ATR data of human body in standing position, and found that they had a high correlation [108].Although it is cheap, easy to obtain and harmless, complex processes and screening instruments with different quality levels are difficult to ensure the standardization of the screening process.

The well-known diagnostic method X-ray examination, although it is professional and authoritative in diagnostic accuracy, the radiation injury of X-ray, high cost and environmental requirements limit its large-scale application in primary screening. In order to solve the problems of large-scale AIS preliminary screening. Many noninvasive AIS evaluation methods have been proposed [82], such as Moire topographic map or parallel light to display the back surface shape, but strict equipment use conditions hinder their popularization and universal application. Another non-radiation injury evaluation method [19] through ultrasound is introduced to image the shape of the spine, but it needs to apply media on the back of the human body, professional

doctors to operate, and contact the back of the human body. This method has low efficiency and weak stability. In addition, the optical non-invasive surface measurement system [80] developed based on high-precision surface measurement equipment can realize 3D reconstruction of the back or the whole torso, but it is usually very expensive.

4.2 Challenges and Contribution

Based on the above preliminary screening work for scoliosis, the main challenges are as follows: 1. The current mainstream non-radiation scoliosis assessment equipment is relatively large and not portable enough; 2. The screening equipment costs are high; 3. The screening equipment detection efficiency is low. Since there is a high correlation between the 2D human back image of AIS patients and ATR, and ATR is also the standard for the primary screening of scoliosis, we use deep learning technology to predict scoliosis based on the unclothed human back 2D image and ATR value. This system takes one single 2D image of the unclothed human back and uses ATR value as an indicator to classify whether adolescents have scoliosis. First, we collect the 2D back image of the same sample and its corresponding 3D back point cloud data, and based on the point cloud data, we calculate the ATR value of the back of the human body and mark whether there is scoliosis according to the size of the ATR value. At the same time, an experienced doctor will judge whether the sample has scoliosis through the naked eye. Then, we use the $UNET$ model [89] and the $Yolo$ mode [86] l to train the human back segmentation model to segment the human back region on the 2D image to achieve preprocessing. After that, we train the $EFFICIENTNET - B4$ network [106] to classify images by using the 2D image of the human back and corresponding label calculated by using ATR values and 3D human back. The experimental results reveal that there is a high correlation between 2D human back image and ATR values. Using the result of classifying scoliosis by

ATR value as a label can well realize the classification of scoliosis based on one singe 2D human back image. In summary, the contributions of this paper are outlined below:

1. We are the first to establish a 2D human back image and the corresponding 3D point cloud database to analyze the correlation between 2D and 3D point cloud images of the human back on ATR features. All data contain the 2D human back image of the same sample and the corresponding labeled 3D back point cloud.

2. We propose a fast, accurate, and low-cost scoliosis screening algorithm. This method creatively uses ATR-based classification results as labels. This system learns the correlation between the 2D human back image and the ATR-related information calculated from the 3D point cloud of the unclothed human back. Finally, the system can classify scoliosis based on a single 2D image of the back and the screening effect is better than that observed by experienced doctors with the naked eye.

3. This method realizes the user's family's independent screening without professional doctors and radiation.

4.3 Related Works

4.3.1 AIS Screening Using 3D Image

A research group proposed to use low-cost RGB-D camera to locate the anatomical landmarks on the back of the human body [122]. This method has high accuracy and stability, but the subjects need to take off their clothes in public, which is still limited to large-scale screening. Some other teams use the support vector machine model to classify the severity of scoliosis based on the 3D human back surface. However, the main classification ranges are the *Cobb* angle less than 60° and greater than 30°, which can not be used for preliminary screening [85].

4.3.2 AIS Screening Using 2D Image

With the the image processing technology and deep learning technology rapidly developing, some researchers have applied image processing and deep learning algorithm to AIS screening by using one single 2D human unclothed back image. A research group proposed an edge-based contour model to reconstruct the contour of the back of the human body and the center of the spine. Although this method is very simple and has a certain degree of accuracy, the results are unstable and inaccurate due to the complex background and the uneven light on the back of the human body [79]. Another research team uses one single RGB image of the human back, the *Cobb* angle interval is predicted based on $RESNET$ model to realize classification. The classification accuracy is only about 60%, which is similar to that of experienced doctors' visual diagnosis [124]. Deep learning methods are popular in many screening fields. However, there are less studies are proposed for AIS screening.

4.4 Data Acquisition

1935 subjects participate in the experiment. They are healthy or have different degrees of scoliosis, and their ages are concentrated between 5 and 14 years old with ATR ranges from $1 - 15°$. All the images used in the experiment are taken when the subjects stood naturally facing the wall without upper clothes (above the sacrum and completely exposed the anatomical landmarks on the back). $Kinect2$ (Microsoft) sensor is located 1 meter behind the subject, and the height of $Kinect$ sensor is about the position of the fifth thoracic vertebra of the subject. The sensing plane of $Kinect$ is still relatively parallel to the wall [122]. After the acquisition process lasting about 2 seconds, a group of RGB-D images of the back of the same person at the same time are obtained, which includes 2D human back image and depth map. The ATR value and classification label are obtained by 3D point cloud data, which calculated by

depth map. We use 2D human back image as input and its corresponding ATR value as label for training and testing. In order to compare with the artificial naked eye diagnosis, an experienced doctor uses the naked eye to judge whether the sample has scoliosis. The doctor marks 1 for the samples with scoliosis, and 0 for those without scoliosis. We count the data observed by doctors with the naked eye for comparison. Our collection method and collected data example are shown in Figure 4.1.

(a) (b) (c)

Figure 4.1: The data acquisition method, 2D back image and depth map data are shown in (a), (b) and (c) respectively.

4.5 Scoliosis Risk Assessment Model

Figure 4.2 shows the framework of our model. Our scoliosis risk assessment model includes three modules: 2D image data processing, 3D human back ATR calculation and label classification, and scoliosis risk classification. The data processing module helps to remove interference features and retain the necessary image features for scoliosis risk assessment. The scoliosis risk classification module classifies the spinal abnormalities based on the label calculated by ATR value under international AIS criteria.

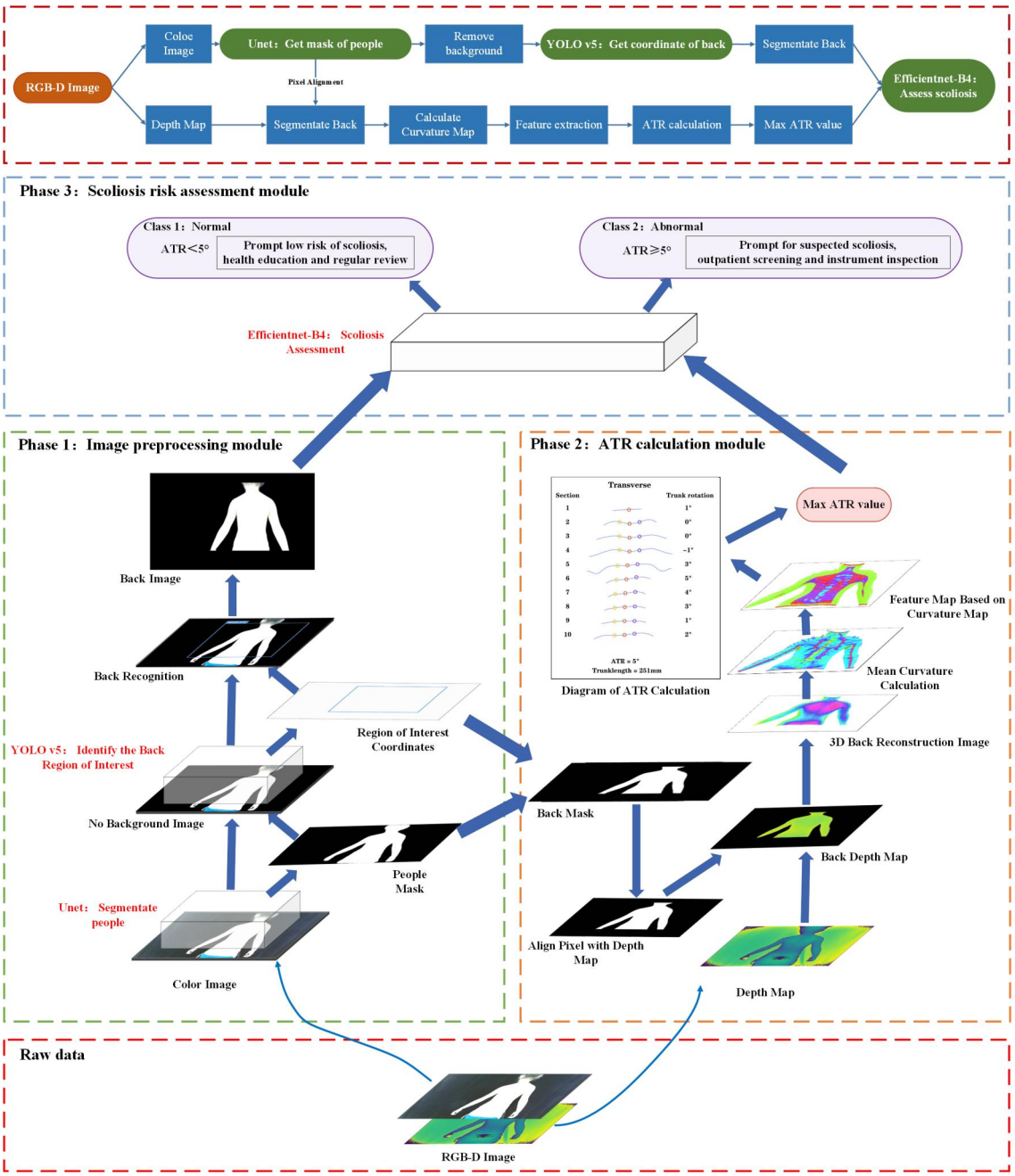

Figure 4.2: The framework of proposal model.

4.5.1 Image Pre-processing Module

Before assessing the risk of scoliosis, we process the original 2D images to obtain back images. As shown in Figure 4.2, we first segment the people in the 2D image

with $UNET$ model. Using the model information our data pre-trained on the human matching dataset [16], we obtain an image mask in which the background area is black and the human back is white. Mask the image mask on the 2D image, and fill the background with black according to formula (1) to eliminate the interference caused by background information.

$$a_{ij} = min(c_{ij}, m_{ij}) \tag{4.1}$$

where a_{ij}, c_{ij} and m_{ij} respectively represent the pixel values with coordinates (i, j) in the segmented 2D image, original 2D image and human mask. Further, in order to extract the region of interest in the human back, we train a $Yolo$ algorithm to identify the back region of interest from $C7$ to the sacrum. We use $Yolo$ V5 released in June 2020 as the back region recognition model, which is faster, more flexible and lighter than the previously released version [12]. So as to obtain our training data.

4.5.2 ATR Calculation Module

We extract feature points from the 3D human back, as shown in Figure 4.3(a). The following anatomical landmarks need to be located: Carinal point ($C7$), posterior superior iliac spine (PSIS), spinous process line (a series of lines from carinal bone to the midpoint of left and right PSIS).

In order to reduce the comparison error between different the reconstructions of the subjects and that of the same subject with different angle relative to the main plane(XY plane)of the $Kinect$ sensor. It is essential to rotate the trunk 3D point cloud into a body-fixed coordinates reference [122].

According to the method in [122], based on the Mean curvature and Gaussian curvature calculated by the 3D point cloud, we obtain the curvature map of the human back according to a certain curvature criterion, as shown in Figure 4.3(b); and calculate the line of the spinous processes, as shown in the red line in Figure 4.3(c). As shown

in Figure 4.3(d), 10 transverse sections (y = 0, plane, near horizontal) are divided by equal distance from $C7$ to the midpoint of left and right PSIS. In each section, the paramedian lines are 10% of the length of the back body to the left and right of the spinous process point, the red point represents the spinous process point, and the right and left paramedian line are represented by yellow and purple respectively. The trunk rotation angle is a positive number when the right side is higher; Then, we do polynomial fitting on the rotation angle calculated by 10 transverse sections, and calculate the value with the largest absolute value as the final ATR value in the results [108]. Finally, according to the international scoliosis classification standard, we label the data as 0 or 1 based on the ATR value as training and testing labels. 0 means that the sample has no scoliosis, and 1 means that the sample has scoliosis [123].

4.5.3 Scoliosis Risk Assessment Module

At present, the standard of medical treatment is to refer the subjects with ATR$\geq 5^\circ$ to the hospital for X-ray evaluation, while the subjects with ATR $<5^\circ$ should not be re-screened [123]. The screening classification criteria based on ATR value are as follows:

1. If ATR $<5^\circ$, it indicates that the sample is normal with low scoliosis risk.
2. If ATR$\geq 5^\circ$, It means that the sample is abnormal and is suspected of scoliosis.

We train $EFFICIENTNET-B4$ network to classify images and minimize the loss function (2) to obtain the best classifier f:

$$f = argmin \sum_{i=1}^{N} [y_i log(p_i) + (1 - y_i) log(1 - p_i)] \tag{4.2}$$

where n is the number of samples, y is the real label, and p is the prediction probability.

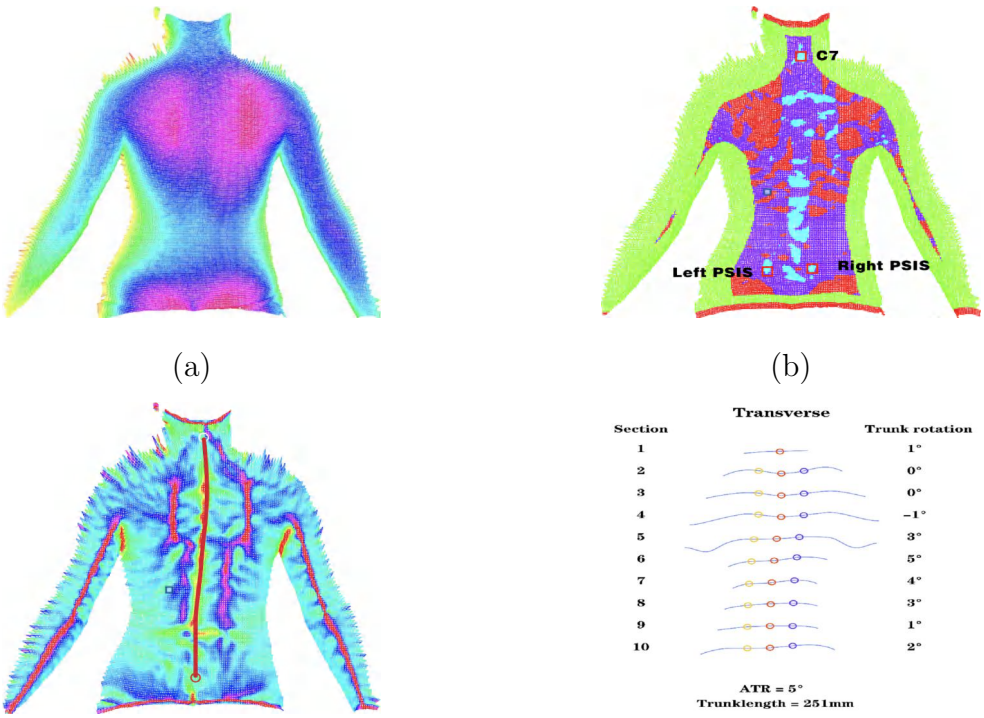

(a) (b)

(c) (c)

Figure 4.3: Point cloud map of human back; Curvature anatomical feature point map; The spinous process line diagram and ATR value calculation diagram are represented by (a), (b), (c) and (d) respectively

4.6 Experiment Results

4.6.1 Evaluation Metrics

Five evaluation indicators are used to evaluate our model, which are defined as follows:

$$Accuracy = \frac{TP + FN}{TP + FN + TN + FP} \tag{4.3}$$

$$F_1 = \frac{2 \times Precision \times Recall}{Precision + Recall} \tag{4.4}$$

$$Precision = \frac{TP}{TP + FP} \tag{4.5}$$

$$Recall/Sensitivity = \frac{TP}{TP + FN} \tag{4.6}$$

$$Specificity = \frac{TN}{TN + FP} \tag{4.7}$$

where TP and TN represent true positive and true negative respectively, which means that people with normal and suspected scoliosis are predicted to be in the correct category; FP indicates false negative, indicating that subjects with suspected scoliosis are predicted to be normal; FN indicates false negative, indicating that the model wrongly judges normal people as suspected scoliosis. Their meaning is shown in Figure 4.4.

True / Predicate	Positive	Negative
Positive	True Positive (TP)	Fales Positive (FP)
Negative	Fales Negative (FN)	True Negative (TN)

Figure 4.4: The meaning of TP,TN,FP,FN.

In addition, the $false\ positive\ rate$ represents the misdiagnosis rate, that is, the percentage of actual normal samples judged as suspected scoliosis(Equation 4.8); The $false\ negative\ rate$ represents the missed diagnosis rate, that is, the percentage of samples actually suspected of scoliosis but mistakenly recognized as normal(Equation 4.9). It is an important index to judge whether the model is available.

$$false\ positive\ rate = 1 - Specificity \tag{4.8}$$

$$false\ negative\ rate = 1 - Sensitivity \tag{4.9}$$

4.6.2 Model Training and Testing

The training and testing of all our deep learning models are performed on a *Linux* server with four $NVIDIA\ Tesla\ V100$.

Firstly, the $Yolo$ V5 algorithm is trained on a private dataset containing 1935 images without background. They are labeled using *Labelimg* software [109], a rectangular

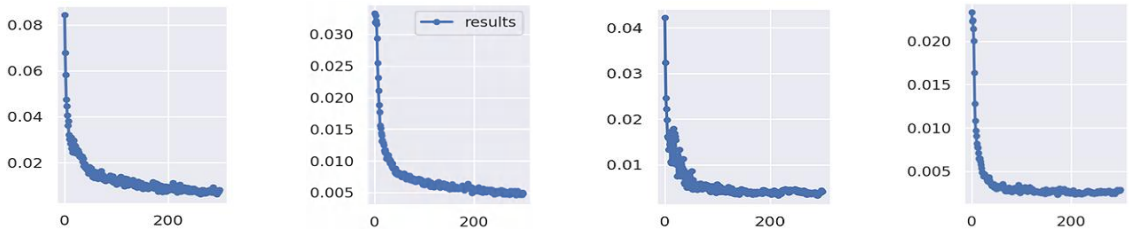

(a) (b) (c) (c)

Figure 4.5: The loss change of human back segmentation model in training and verification dataset : (a) is the generalized intersection over union(GIoU) loss function on the training dataset; (b) is the loss of target detection during training; (c) is the bounding box loss on the verification dataset; (d) is the loss of verification dataset target detection.

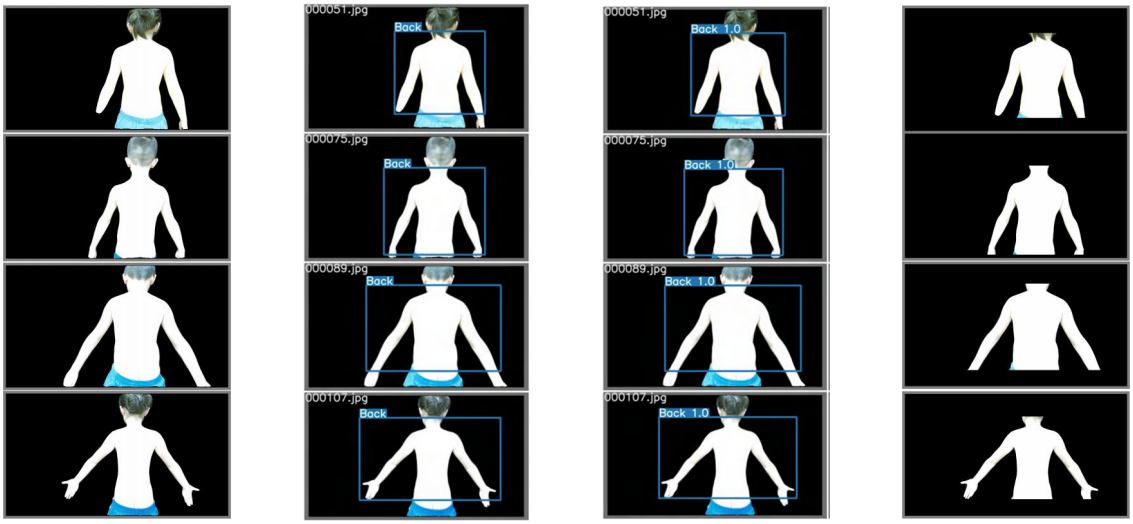

(a) (b) (c) (d)

Figure 4.6: Partial results of human segmentation, target detection label, human back recognition, and human back segmentation on test data. (a) is original 2D image; (b) is ground truth of human back detection; (c) is the segmentation result predicted by *Yolo* V5 model; (d) is segmented human back.

frame is used to surround the back area, which is slightly larger than the area from the $C7$ to the sacrum. An experienced doctor helps us to correct the labeling results.

80% of the data is divided into the training dataset and the remaining 20% is used in the testing process. The maximum number of iterations is 300 epochs and the batch size is 16. Other parameters are set using default.

The final model for human back recognition has an average map value of 0.999 when the Intersection Over Union(IOU) threshold is 0.5. When the step size is 0.05, the average map value is 0.945. Figure 4.5 shows the changes in loss, precision, and recall on the training and verification dataset. Figure 4.6 shows part of the results of the human body segmentation and back segmentation process.

Subsequently, we train and test the scoliosis evaluation model. After ATR value calculation and labeling, 948 available images are marked as normal and the other 987 are marked as abnormal. We arbitrarily split the images for training and the rest for testing(75% of the images are used as training dataset and the rest as test dataset). When training the scoliosis risk assessment model, the dataset was enhanced by rotation and turnover, and it is expanded by 8 times. The input image size is adjusted to 380×380 to adapt to the network.

Table 4.1: Performance of our model scoliosis assessment task.

Metric	Normal	Abnormal
f1-score	0.832	0.788
precision	0.754	0.907
Recall/Sensitivity	0.929	0.696
Specificity	0.696	0.929

The final scoliosis risk classification model accuracy is 0.813.The observation accuracy of experienced doctors is 65.1%, which is much higher than the naked eye observation of experienced doctors. Therefore, it can be concluded that there is a high correlation between 2D back images and 3D back point cloud images in terms of ATR feature. Its Receiver Operating Characteristic(ROC) curve is shown in Figure 4.7(a), and the

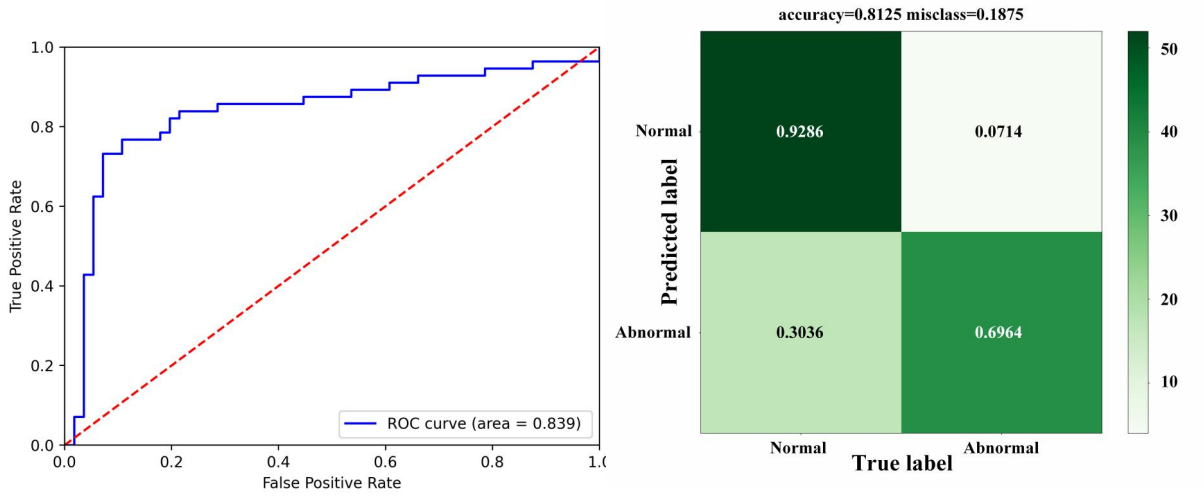

(a) (t)

Figure 4.7: Performance of the model on test dataset.(a)The ROC curve and AUC value of proposal method for discerning whether the ATR >5°.(b)Confusion matrix on the test dataset

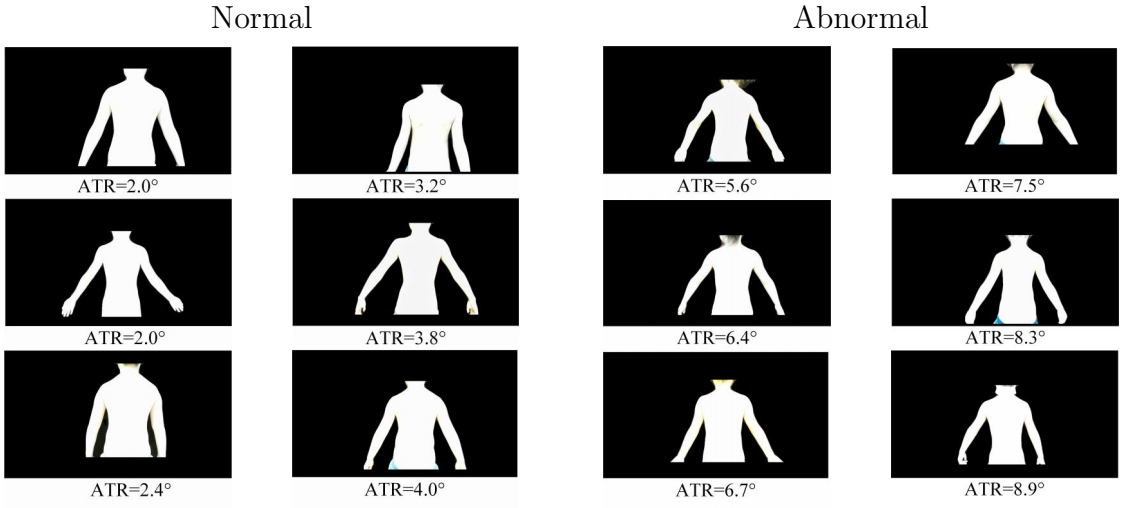

(a) (b) (c) (d)

Figure 4.8: Correctly classified samples. (a) For normal samples correctly classified, ATR <5°(label=0); (b) For abnormal samples correctly classified, ATR≥ 5°(label=1)

Area Under the Curve(AUC) of the algorithm is 0.839. The confusion matrix on the test dataset is shown in Figure 4.7(b). The results recorded in Table 4.1 show

that the system has the precision and specificity of 0.907 and 0.929 to detect suspect scoliosis, indicating that this system can well detect the occurrence of abnormalities despite the possibility of missed detection. Most of the normal samples with the wrong classification have ATR values close to 5° because these samples have slight differences in 2D characteristics. However, for abnormal samples, our model has a high $false\ negative\ rate$ (0.304), which means that it will predict some abnormal samples as normal. Most of the incorrectly classified abnormal samples have large ATR values, which means that they have severe scoliosis. The failure of this model is due to the lack of enough samples of severe scoliosis. In fact, these samples can be easily identified by the naked eye. An example of correctly classified samples is shown in Figure 4.8.

4.7 Conclusion

In this chapter, We have verified the high correlation between 2D back images of the human body and 3D back point clouds on the key feature of ATR, and by verifying this correlation, we have developed a new preliminary AIS screening method, which puts the scoliosis screening power into the user's hand. This method uses 2D human back image to classify scoliosis normal and abnormal based on deep learning algorithm, so as to realize the large-scale preliminary scoliosis screening. No need for professional doctors, high precision and no radiation are the main contributions of this paper. In addition, ATR is creatively classified as a classification label and screening ground truth, based on the high correlation between ATR value and scoliosis risk. Experimental results verify the effectiveness of the proposed model with state-of-the-art accuracy(81.3%) over naked eye tests by professional doctors(65.1%).

Chapter 5

Novel Back Topology and Deep Learning Algorithms for Automated Scoliosis and Abnormal Posture Evaluation Using 2D Back Images

Adolescent idiopathic scoliosis is becoming a common spinal disorder among adolescents. The traditional methods of scoliosis diagnosis are labor-intensive and can result in unnecessary referrals and radiological exposure for adolescents due to their low positive predictive value. In order to enable early screening, diagnosis and sustained monitoring of scoliosis patients, a new low-cost, convenient, and accurate method needed to be proposed.

In chapter 4, we have verified the high correlation between 2D and 3D human back images on certain important features. To better describe the correlation between 2D body features and scoliosis, we propose a novel set of 2D human back feature

points and topological structures based on deep learning algorithms. We establish a database with labeled 2D unclothed back images and corresponding whole-spine standing posterior-anterior X-ray images, and innovatively propose a new network topology of the 2D back images to localize the back landmarks. With three unclothed back images, this system can automatically classify normal, abnormal posture and scoliosis with an overall classification accuracy of 88.1%. This system has the potential to overcome the time and space limitations of conventional screening for scoliosis and abnormal posture. In addition, we have developed a mobile based, cost free, accurate, and radiation free scoring screening and monitoring system for early screening and monitoring of scoring and abnormal posture based on this structure.

5.1 Introduction

Adolescent idiopathic scoliosis (AIS) is medically defined as a curvature of the spine [55] with more than 10° of deformity and the cause of scoliosis is unclear. The *Cobb* angle is generally used to measure the presence of scoliosis in adolescents. Scoliosis is defined when the *Cobb* angle exceeds a threshold of 10° [69]. Scoliosis is highly insidious and usually occurs in adolescents between the ages of 10 and 18 years. If not intervened in time before the adolescent's skeletal maturity, scoliosis has a high probability of becoming severe, which not only affects the appearance of the body and cardiopulmonary function, but also may cause musculoskeletal and neurological pain [116] [117][118]. Therefore, in order to achieve early screening and early intervention for scoliosis and reduce the risk of scoliosis becoming severe in the future, the school scoliosis screening (SSS) program has been advocated [40].

SSS includes a variety of assessment methods, except for radiation-based X-rays, the majority of screening is based on radiation-free methods, including appearance inspection, *Adam* forward bending tests, scoliometer measurement, Moire/Infrared topography and ultrasound [30, 65, 110]. The main screening method is the forward

bending tests combined with scoliometer measurement, which can improve the accuracy [60]. Moire/Infrared topography related screening method based on the high correlation between the back surface and the center of the spine, is used to predict scoliosis by analyzing the three-dimensional topographic asymmetry of the back, which is efficient and accurate, and does not require specialized physician, but the overall screening cost is still high and some studies have shown that this method has a high false positive rate [26, 122]. Screening using ultrasound is highly accurate, but screening is inefficient due to the need to apply media and contact with the human back, and is difficult to use in large-scale school scoliosis screening scenarios because the equipment is expensive and cannot replace X-rays for definitive diagnosis [18].

Due to the current imbalance in medical resources and high labor costs in many regions, SSS is difficult to spread on a large scale. In addition, because the government often organizes scoliosis screening, the screening process can cause conflicts between parents and the government or hospitals due to various reasons such as missed diagnoses, misdiagnosis, and privacy leaks, so scoliosis screening in schools is prohibited in some developed countries due to a combination of cost and social conflicts [29, 93]. In order to make scoliosis screening widely available, some research teams have introduced the concept of home scoliosis screening, based on a single unclothed 2D back human back image, using image processing and AI algorithms to assist parents with home adolescent screening using mobile devices. This reduces the financial burden on society and gives parents the right to screen [124].

A research team has proposed the classification of scoliosis based on 2D unclothed back image, which classifies patients by traditional image processing techniques for Lenke type 1 and other types. However, this method has low detection accuracy and low robustness [91]. Another research team used unclothed 2D back images to determine the midline of the human back from the edge of the back and screen scoliosis on the basis of this midline. Although this method achieved reasonable accuracy, it requires a high level of background complexity and human back edge condition and

has low robustness [79]. Recently, a research team has used deep learning algorithm to train correlation models of unclothed back images and corresponding X-rays to classify scoliosis severity by inputting one single image. The method is effective for screening scoliosis greater than 20°, but it is poor in screening patients in the range of $10 - 20°$ and cannot determine abnormal posture. Also, this method does not allow for quantitative analysis and follow-up of people with postural abnormalities and scoliosis [124].

Recent developments reveal that deep convolutional neural networks have achieved state-of-the-art performance in human pose estimation [105]. Besides, there is a high correlation between abnormal back pose and spinal abnormality [108]. To better screen for scoliosis and classify postural abnormalities, we propose a mobile-based scoliosis screening system based on unclothed back image. The system automatically locates and calculates parameters of human back landmarks by deep learning algorithm and specific topological network based on human biomechanics, and finally classifies the results by correlation analysis with corresponding X-ray calculated labels. In addition to accurately screening for mild scoliosis, the system also classifies problems with only postural abnormalities (Only postural abnormalities, such as high and low shoulders, but without scoliosis).

5.2 Challenges and Contribution

Through the analysis of the above research works it can be found that currently, most of the work on using 2D images for scoliosis analysis mainly focuses on direct classification and does not describe scoliosis and body abnormalities through more features. In order to better describe the correlation between 2D human body posture features and scoliosis, there are some challenges: 1. Lack of corresponding 2D human back image and corresponding spine X-ray databases; 2. The feature points contained in traditional motion tracking algorithms [66] cannot accurately describe the posture

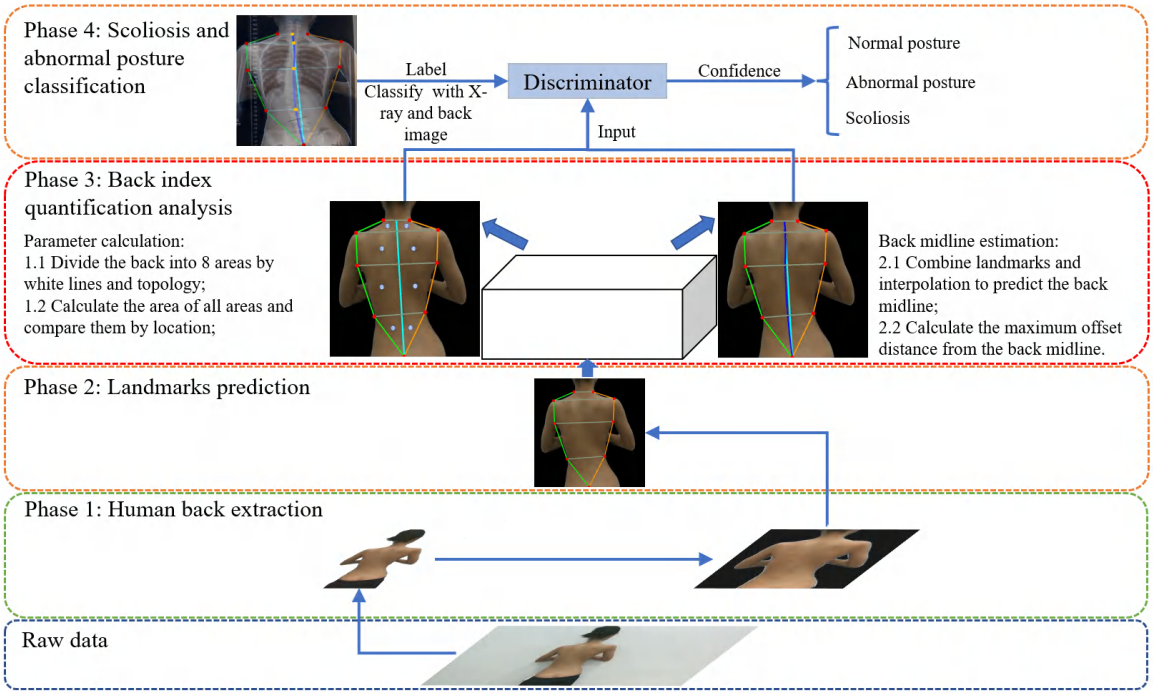

Figure 5.1: Details of the methods

and scoliosis of the human body; 3. Due to the need for the subject to take off their shirt for measurement if put into large-scale use, it may cause privacy leakage issues. In response to the above challenges, the following contributions have been made in this chapter:

1. We have established a database of 2D human back photos and corresponding spinal X-ray images;

2. We have established a new set of human back feature points and verified their high correlation with scoliosis;

3. Based on a novel human back network topology and training on small models, we have achieved feature point localization on the smallest possible model. This model can be installed on mobile phones to achieve edge computing and solve the problem of privacy leakage.

4. We have developed a scoliosis and abnormal posture assessment system based on

two-dimensional human back photos using this proposed method.

5.3 Materials and Methods

The system is capable of screening adolescents for scoliosis using only a 2D unclothed back image, and the results are classified as normal posture, abnormal posture, and scoliosis. Abnormal posture means the subject has abnormal posture(including high and low shoulder, and back asymmetry) but has no scoliosis; scoliosis means abnormal posture with a *Cobb* angle over 10°. The details of the methods are shown in Figure 5.1: first, extract the human back region from the image; then calculate the landmarks of the back and the network topology; then, based on these landmarks and the network topology, the back midline and the area of the different back region are determined, and finally, the discriminator classifies the spine condition using the parameters calculated by the back midline and the contrast of different back areas.

5.3.1 Data Acquisition and Pre-Processing

A total of 1050 validated data are collected from Chinese subjects aged 6-24 years (including male and female), of whom 65 have different degrees of scoliosis (nontrue scoliosis and other spine diseases are excluded). We collected unclothed images of the human back of the subjects in different scenarios using a 1920×1080 resolution camera and whole-spine standing posterior-anterior X-ray images. The experienced physicians used the annotation software to annotate the unclothed images with landmarks and calculate the spinal curvature based on the X-ray images and finally classified the subjects by the calculated results. We used the classification results as ground truth and labels.

The image pre-processing effect is shown in Figure 5.2. The initial data is firstly removed from the background, and then the back segmentation is performed to obtain

the human back image. Since the background noise greatly reduces the accuracy of back recognition, we use a human body extraction model to process the image. In terms of model selection, we decided to use the Robust Video Matting (RVM) model [61] due to its suitability for mobile deployment. The architecture of this model is depicted in Figure 5.3. Also, given that the officially provided pre-trained RVM model is not applicable to human body extraction, we made a dataset containing 1050 sheets containing only human bodies and divided it into training and test dataset in a 4:1 ratio to enhance the model's proficiency in handling this task. To reduce the influence of other body parts on the later back landmarks recognition, we used the *Yolo* V5 model [107] to perform back segmentation on the human image without the background to get the human back image. Also, to make the model more suitable for the back segmentation task, we made a human back detection dataset containing 500 images to help the training. Finally, we obtain the human back image for subsequent detection of landmarks on the human back.

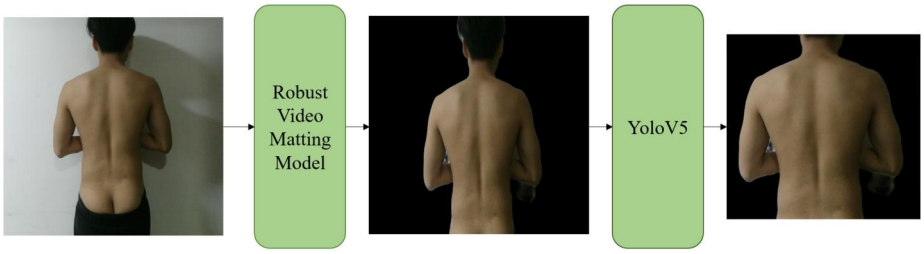

Figure 5.2: The workflow of human back extraction

5.3.2 Back Landmarks Estimation

Network Topology

We present a new topology using 9 points on the human body, as shown in Figure 5.4. Compared to predicting the human back landmarks individually, the introduction of network topology using the principles of human anatomy is beneficial to accurately

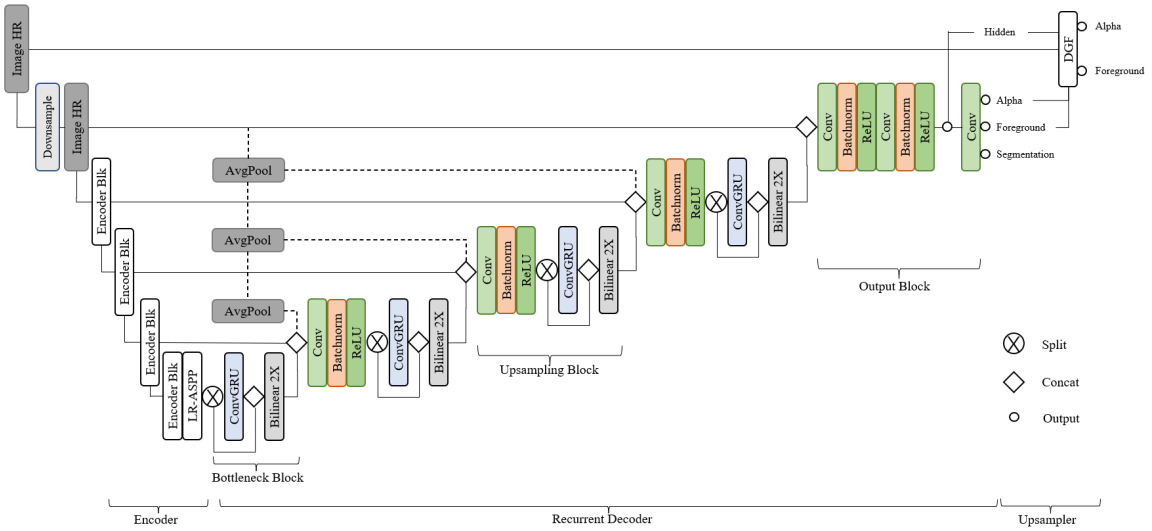

Figure 5.3: RVM model framework

predict the landmarks [67]. The definition of the back landmarks is explained in Table 5.1.

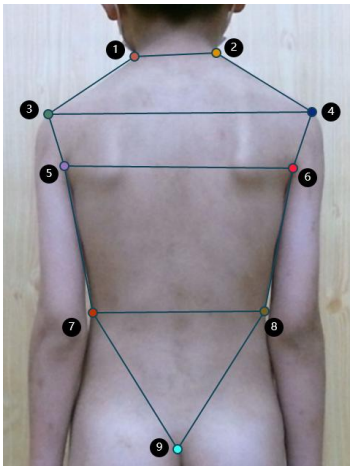

Figure 5.4: Back landmarks and topology

Model Selection

ResNet [43] is the most common backbone network for image feature extraction and it is proven for key points estimation. *MMPose* [21] framework suggests a methodology

Table 5.1: Definition of back anatomical landmarks

1	Left inner shoulder
2	Right inner shoulder
3	Left outer shoulder
4	Right outer shoulder
5	Left axilla
6	Right axilla
7	Most proximal points on left side of waist
8	Most proximal points on right side of waist
9	Top of the intergluteal furrow

characterized by the exclusive addition of several deconvolutional layers subsequent to the concluding convolutional stage within the *ResNet* [121] and introduces Squeeze-and-Excitation (SE) block [47] to improve the accuracy of landmarks detection. The whole model architecture is illustrated in Figure 5.5. We opted for this structure due to its arguable simplicity in generating heatmaps from deep, low-resolution features. Specifically, it incorporates three deconvolutional layers, each incorporating batch normalization [48] and ReLU activation [57]. Each layer consists of 256 filters with a 4×4 kernel. A stride of 2 is employed, and a 1×1 convolutional layer is appended at last to produce predicted heatmaps $H_1, H_2, H_3, ..., H_9$ for all 9 landmarks.

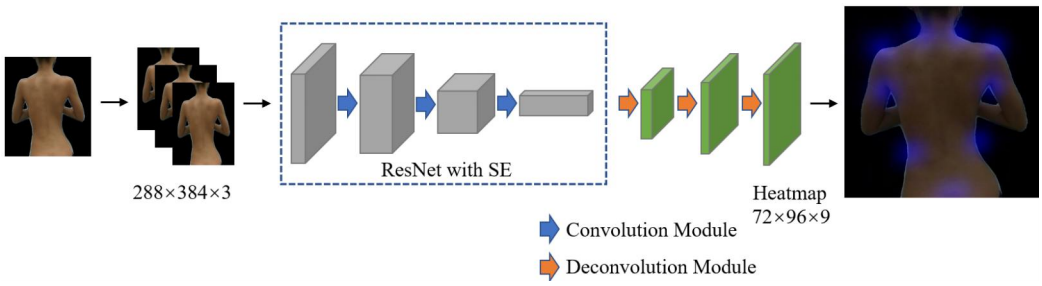

Figure 5.5: The architecture and workflow of *SENet*

Training Details

We first expanded the height or width of the human detection box to an aspect ratio (aspect ratio = height/width) and then cropped the box from the image to resize it to 288×384. Additionally, a number of data enhancement methods are employed, such as affine transformation, half-body data transformation, random scaling and rotation, and center-of-box randomization. By performing pre-training on the COCO dataset [62], our network is built up (including 57K images and 150K individual instances). The basal learning rate for the landmark estimation training task is 1e-4, and it decreases to 1e-5 and 1e-6 at the 35th and 70th epochs, respectively. The *Adam* optimizer [53] ends the training phase after 100 epochs.

Loss Function

Mean Squared Error (MSE) used in heatmap regression has two broad issues: (I) The insensitivity of Mean Squared Error (MSE) to minor errors has significant implications on the precision of identifying the mode of a Gaussian distribution. (II) During training, all landmarks having the same loss function and equal weights can impact the learning process. However, the difficulty of predicting critical points in different parts of the back will be inconsistent. Inspired by Adaptive Wing (AWing) loss [114], different landmark types may have different target weights. The loss function is defined as follows:

$$Loss\left(y,\hat{y}\right)=\begin{cases}\omega\ln\left(1+\left|\frac{y-\hat{y}}{\kappa}\right|^{\beta-y}\right), & if\ |(y-\hat{y})|<\theta\\ A\left|y-\hat{y}\right|-C, & otherwise\end{cases} \tag{5.1}$$

Where y and $\hat{y}$ are the pixel values on the ground truth heatmap and the predicted heatmap respectively. $A=\omega(1/(1+(\theta/\kappa)^{(\alpha-y)}))(\alpha-y)((\theta/\kappa)^{(\alpha-y-1)})(1/\kappa)$ and $C=(\theta A-\omega\ln(1+(\theta/\kappa)^{\alpha-y}))$ are used to make loss function continuous and smooth at $|y-\hat{y}|=\theta$. ω, θ, κ and β are hyperparameters. We empirically used $\omega=14$, $\theta=0.5$, $\kappa=1$ and $\beta=2.1$ in our model. Equation 5.1 is the loss between the predicted and

targeted heatmaps.

5.3.3 Back Midline Estimation

The back midline is defined to divide the human back into left and right symmetrical sides. We calculated four midpoints on the back based on the symmetrical landmarks on both sides of the human body(such as the midpoint of point 1 and point 2 in Figure 5.4) and the top of the intergluteal furrow(point 9 in Figure 5.4), and then used the quadratic Newton interpolation method (Equation 5.2, Equation 5.3) to fit the pairs[37], where $x_i, i = 1, 2, ..., 5$ are the identified 5 points, $f(x)$ is the corresponding y-coordinate, $N(x)$ is the Newton fitting function, and finally stitched to obtain the human back midline.

As shown in Figure 5.6, the dark blue line is the interpolated back midline, and the light blue line(back baseline) connects the midpoint of the two inner shoulder points and the top location of the intergluteal furrow used to analyze the maximum offset distance of back midline. In addition, the topography and the back baseline divide the human back into 8 areas (as shown in Figure 5.1 Phase 3 left), after which we will use the area contrast between these 8 areas as one of the features to distinguish scoliosis from the abnormal posture. In order to visualize the high correlation between the predicted back midline and the trend of the spinal midline of the X-ray, we selected the corresponding landmarks of the RGB map and the X-ray in order and used the affine transformation to make the latter image transparent and align the two images according to the corresponding landmarks.

$$\begin{aligned} N_3(x) =& f(x_0) + f[x_0, x_1](x - x_0) + \\ & f[x_0, x_1, x_2](x - x_0)(x - x_1) \end{aligned} \tag{5.2}$$

$$f[x_0, \cdots, x_m] = \sum_{k=0}^{m} \frac{f(x_k)}{\prod_{i=0, i \neq k}^{m} (x_k - x_i)} \tag{5.3}$$

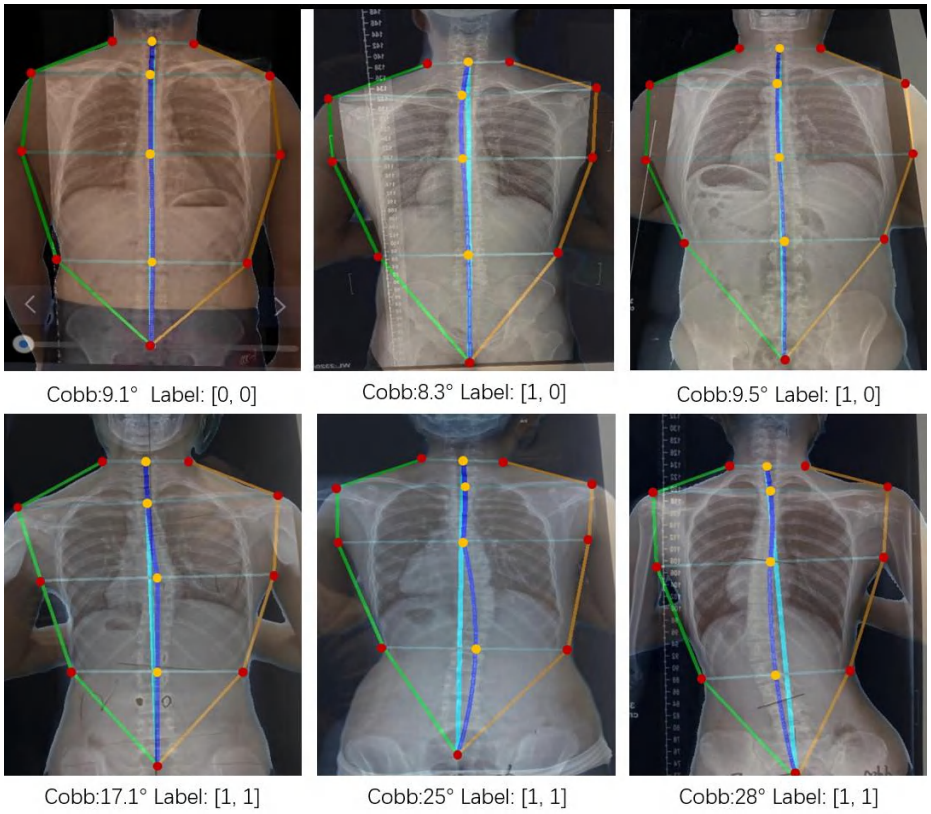

Figure 5.6: Alignment of spine midline and X-ray: the dark blue line is the back midline obtained by interpolation, the black dotted line represents the ground truth(Spline midline) marked by X-ray and the light blue line is the back baseline. Label: [0, 0] represents normal; [1, 0] represents abnormal posture; [1, 1] represents scoliosis, and [0, 1] represents classification error.

5.3.4 Scoliosis and Abnormal Posture Classification

A discriminator is designed using the contrast of the region area and the maximum offset distance of the back midline as input. The contrast of the area is calculated according to Equation 5.4, where S_i represents the area of the i area and S_{2i} represents

the area of the $2*i$ area. The maximum offset distance of the top of the back midline is calculated according to Equation 5.5, where l_{gt} is the back baseline, and l_{pred} is the interpolated back midline. After computing these parameters, we will use a BN layer to normalize them to reconstruct the inconstancy of the different modals. We randomly divided the samples of normal, abnormal posture, and scoliosis into training and test sets respectively in the ratio of about 4:1. The discriminator is trained using 840 samples, and 210 samples are used for testing and accuracy analysis. As shown in Figure 5.1 Phase 4, in which the discriminator consists of a BN layer with a Multi-Layer Perceptron(MLP) network to be labeled based on the X-ray and the physician's judgment of the subject. The final output is the confidence level for the three cases of normal, abnormal posture, and scoliosis.

$$Contrast = \begin{cases} \frac{|S_{2i}-S_{2i+1}|}{S_{2i}+S_{2i+1}}, i = 0,1,2,3 \\ \frac{|S_{2i}+S_{2i+2}-S_{2i+1}-S_{2i+3}|}{S_{2i}+S_{2i+2}+S_{2i+1}+S_{2i+3}}, i = 0,1,2 \\ \frac{|S_{2i}+S_{2i+2}+S_{2i+4}-S_{2i+1}-S_{2i+3}-S_{2i+5}|}{S_{2i}+S_{2i+2}+S_{2i+4}+S_{2i+1}+S_{2i+3}+S_{2i+5}}, i = 0 \end{cases} \tag{5.4}$$

$$Offset = \max(l_{gt} - l_{pred}) \tag{5.5}$$

5.4 Results

5.4.1 Effectiveness of Back Extraction

We use two metrics in the model evaluation. (1) The mean Intersection-Over-Union (mIOU) is utilized to measure the cross-merge ratio between the prediction and the groundtruth of the segmentation target, which is shown in Equation 5.6, where the p_{ij} means that the model categorizes a pixel into j-th category but the pixel truly is i-th category. In this task, we simply categorize the pixel into the human with background category and the human without background category. As shown in Figure 5.7, our

RIM model and the RVM model perform similarly. (2) The binary cross entropy loss shown in Equation 5.7 is utilized to let our model learn the segmentation probability by the prediction mask S_t and the ground-truth binary label S_t^*. Figure 5.8 shows that RIM has less loss than RVM and performs better.

$$mIOU = \frac{1}{2}\sum_{i=0}^{1}\frac{p_{ii}}{\sum_{j=0}^{1}p_{ij} + \sum_{j=0}^{1}p_{ji} - p_{ii}} \tag{5.6}$$

$$L^S = S_t^*(-\log(S_t)) + (1 - S_t^*)(-\log(1 - S_t)) \tag{5.7}$$

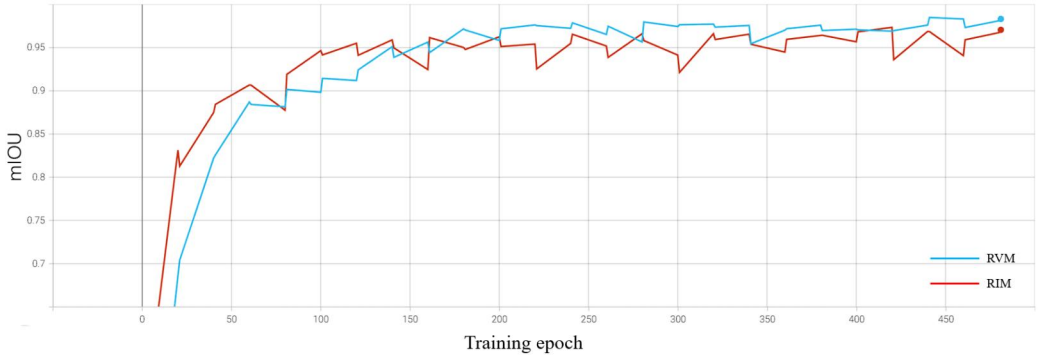

Figure 5.7: The mIOU curve in training epoch

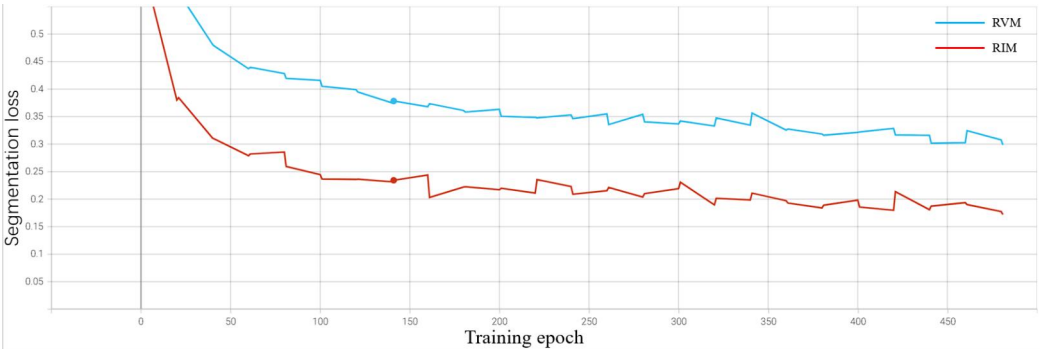

Figure 5.8: The binary cross entropy loss curve in training epoch

5.4.2 Effectiveness of Landmarks Estimation

In the evaluation index of landmarks estimation, the PCK (torso-normalized probability of correct key point) score is used [92]. Considering that this model needs to be deployed to edge devices, this model needs to be small with guaranteed accuracy. Different baselines are used on our data. As shown in Table 5.2, the results of the original dataset contain the PCK@0.03 results and the model parameters. The SEResNet is the most suitable model baseline.

As shown in Table 5.3, the results of cross dataset contain three methods, "Baseline" and "Ours" have the same model structure, hyperparameter settings, and runtime environment, but landmarks in the dataset label of "Ours" have topology. The "Noise" and "Ours" method is the same but the former dataset label retains the background noise. The PCK@0.1 and PCK@0.05 scores are reported. Figure 5.9 shows that our method can predict each landmark consistently by connecting specific points. More importantly, the score of "Ours" is 7.9 higher than the score of "Baseline" as shown in Table 5.3, which verifies the topology, and the RIM model is beneficial for the landmarks estimation model.

Table 5.2: Comparison of different baselines on the original dataset. Inn. represents the inner shoulder, Out. represents the outer shoulder, Axi. represents the Aixlla, Wai. represents the Waist, and Fur. represents the intergluteal furrow.

Method	Inn.	Out.	Axi.	Wai.	Fur.	Total	Param
SwinT[64]	**90.8**	79.0	**85.2**	61.4	**72.6**	**78.4**	203.39M
PVTV2[113]	88.1	82.2	82.6	62.9	60.4	76.2	29.05M
SEResNet[47]	90.1	**84.7**	82.0	**63.2**	62.8	78.1	57.77M

Table 5.3: Comparison of same method and settings on the cross dataset.

	Method	Inn.	Out.	Axi.	Wai.	Fur.	Total
PCK@0.1	Baseline	97.3	85.3	97.5	88.1	95.2	91.7
	Noise	99.7	97.9	100	97	100	98.9
	Ours	**100**	**99.5**	100	**98.6**	100	**99.6**
PCK@0.05	Baseline	97	**95.6**	97.3	76.2	65.2	86.4
	Noise	**99.1**	83.8	98.5	**86.9**	72.3	89.8
	Ours	97.5	82.1	**99.7**	82.1	**97.3**	**91.1**

5.4.3 Effectiveness of Classification

As shown in Table 5.4, our discriminator achieves an overall classification accuracy of 88.1% on our test set.

Table 5.4: Accuracy analysis

Situation	Number of images	Correct Results	Accuracy
Normal	159	143	89.9%
Abnormal Posture	36	28	77.8%
Scoliosis	15	14	93.3%
Total	210	185	88.1%

5.4.4 Ablation Study

To assess the efficacy of each component in our proposed methodology, we conducted an extensive evaluation on our self-made dataset. Notably, all results were consistently generated under identical hardware and software conditions.

Topological landmarks on the back. We empirically analyzed the effect of our

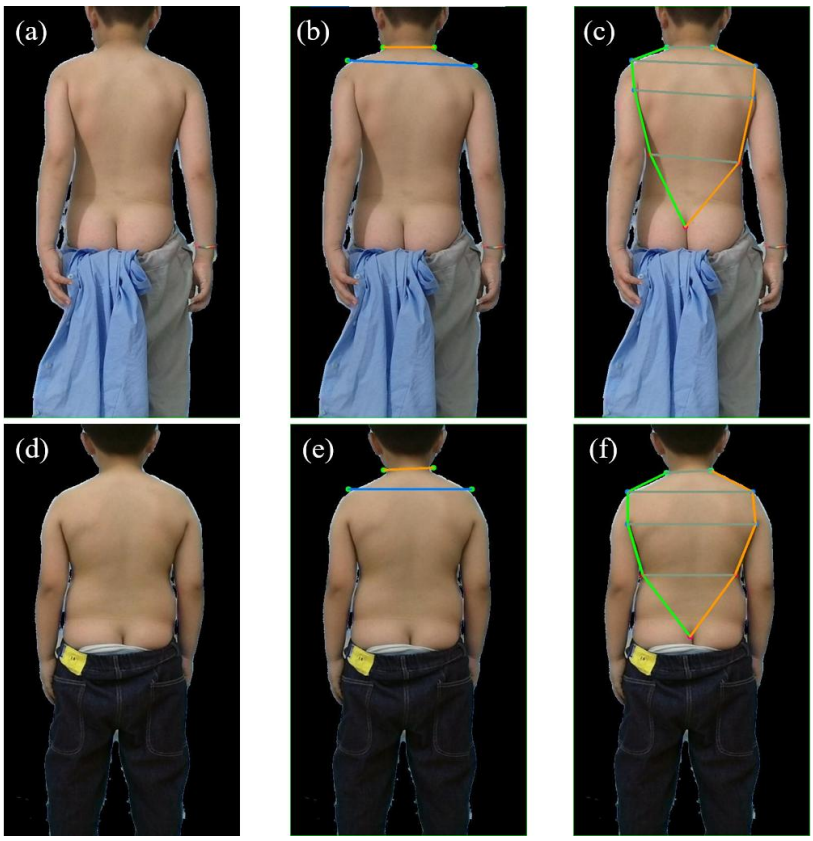

Figure 5.9: Comparisons of "Ours" and "Baseline". (a)(d) input image; (b)(e) "Baseline"; (c)(f) "Ours"

method of making back landmarks in a topological way. If they are asymmetric, each landmark is a separate point. Figure 5.9 shows that our method is able to predict each landmark consistently by the connection of specific points. More importantly, the score of "Ours" is 7.9 higher than the score of Baseline.

5.5 Discussion

In this chapter, We propose a new set of 2D human back feature points and topological structure, and verify the correlation between 2D human back images and the degree of scoliosis. Also, we propose a system that enables AIS and abnormal pos-

ture screening on mobile edge devices using different deep learning algorithms. This system breaks the time and space limitations of AIS and abnormal posture screening and is cost-free, fast, accurate, and radiation-free. Only one 2D unclothed back image is needed to classify scoliosis, abnormal or normal posture. By establishing color images of the human back, X-ray data, and the corresponding calibration database, we innovatively define a new network topology of the human back and combine deep learning algorithms to achieve an accurate normal posture, abnormal posture, and scoliosis classification accuracy(88.1%).

5.6 System Development

To promote this technology better, we have developed a mini-program called *DrBody* on the *WeChat* platform. After logging in, users only need to upload a photo of their back for early screening. To reduce the errors caused by non-standard image acquisition, we have asked users to supplement the anterior bending back images of the thoracic and lumbar vertebrae according to the requirements of the *Adam*'s forward bending test. This approach aids in the screening and analysis of scoliosis and abnormal posture, as the *Adam*'s test is currently recognized as an international benchmark for initial scoliosis screening and monitoring. The comprehensive usage procedure is outlined in Figure 5.10.

During the system's development process, we encountered two noteworthy challenges:

1. It is difficult to determine whether the *Adam* forward bending test is correct, and incorrect movements can lead to errors in the evaluation results;

2. Lack of sufficient dataset to annotate feature points in images of *Adam* forward bending test to achieve ATR calculation;

To address the aforementioned issues, we have designed a real-time pose-tracking algorithm based on a human pose-tracking system to ensure that the subject's move-

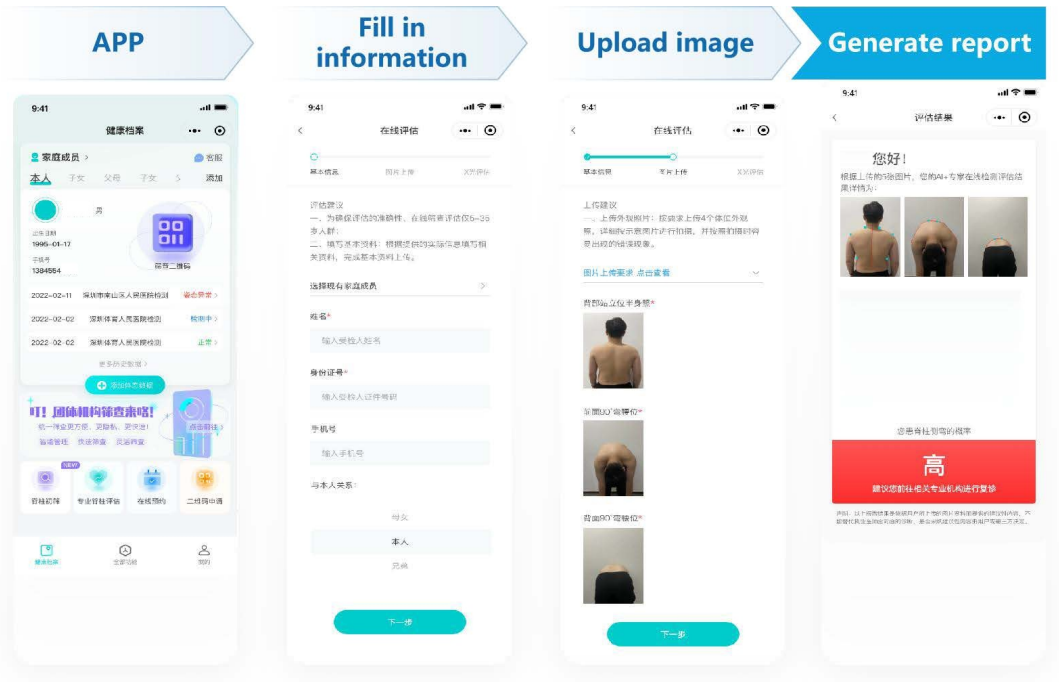

Figure 5.10: User operation process.

ments are correct during the *Adam* forward bending test. Finally, we built a database and network topology of over 10000 annotated images of *Adam* forward bending test to annotate feature points, achieving automatic ATR angle calculation. We also classified scoliosis and posture abnormalities based on single back photos and ATR quantification results.

5.6.1 Posture Recognition

The positioning protocol for subjects undergoing the *Adam*'s Forward Bending Test necessitates the following: 1. bowing their heads; 2. Legs straight and at around 90° to the ground; 3. Place their hands in front of their knees; 4. Fold their hands in front of their knees; 5. Keep their feet together. When measuring the ATR angle of the thoracic spinal segment, the palm position should be slightly above the knee cap. When measuring the lumbar spine segment, the palm should be slightly below the

kneecap.

Firstly, we established correct and incorrect datasets for different *Adam* bending positions, annotated key points, and used *MMPose* to customize human key point data and identify key points. Based on the relationship between the positions and angles of each key point, we set thresholds and detected the results. Illustrative examples of both accurate and inaccurate results are presented in Figure 5.11(a) and Figure 5.11(b).

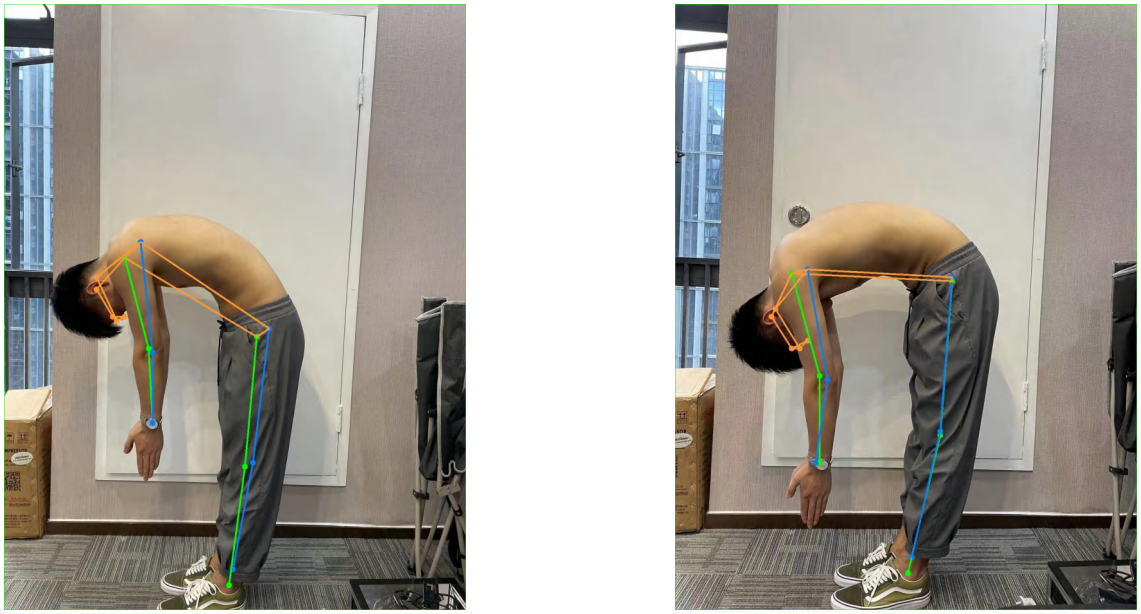

(a) *Adam* test position(front) (b) *Adam* test position(back)

Figure 5.11: Correct *Adam* forward bending position.

5.6.2 ATR Calculation

After collecting 12030 photos of the standard *Adam* test, we established the topological structure and annotated it using the same method as section 5.3 and used the same model for training. Since the form is the same, we will not repeat it here. The results are depicted in Figure 5.13(a) and Figure 5.13(b).

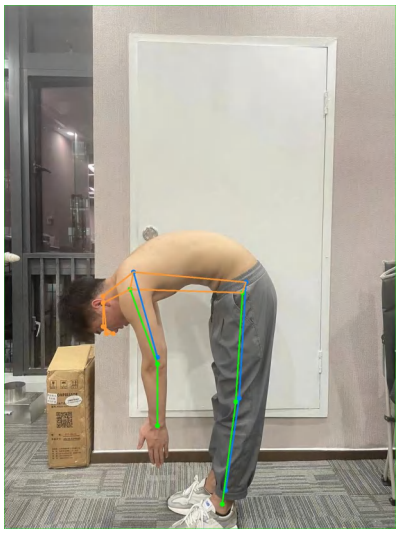

(a) Feet not aligned

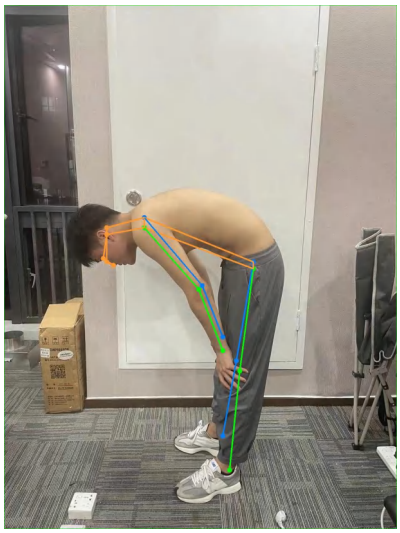

(b) Wrong palm position and feet not aligned

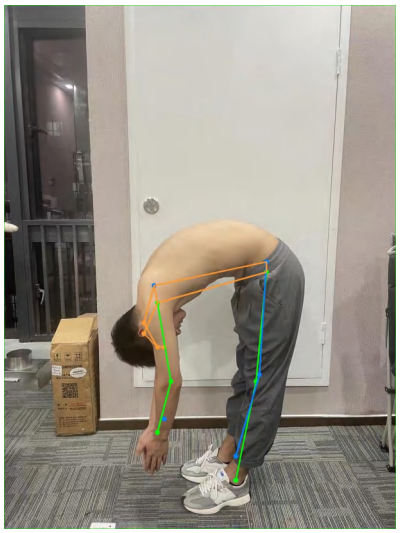

(c) Legs not straightened

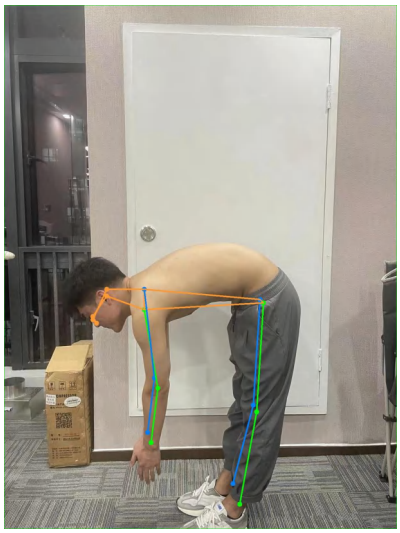

(d) Legs not straightened and head not lowered

Figure 5.12: Wrong *Adam* forward bending position.

By determining the positions of two specific points on the subject's back profile, the system is capable of estimating the angle between them. Among the angles derived from the two images, the system selects the maximum ATR angle and designates it

(a) Label in *Adam* test(front) (b) Label in *Adam* test(back)

Figure 5.13: Label in *Adam* forward bending position.

as the subject's overall maximum ATR angle.

5.6.3 Result Judgment Criteria

The system evaluates the final result based on a single back photo and the maximum ATR value of the *Adam* test.

If the result of a single back photo is scoliosis and the ATR degree exceeds 5°, the algorithm system's judgment result is scoliosis; If the result of a single back photo is scoliosis and the ATR angle is less than 5°, the algorithm system's judgment is abnormal posture. If the judgment result of a single back photo is abnormal posture, but the ATR angle exceeds 5°, then the judgment result of the algorithm system is scoliosis; If the judgment result of a single back photo is abnormal posture, but the ATR angle is below 5°, then the judgment result of the algorithm system is abnormal posture; If the result of a single back photo is normal and the ATR angle exceeds 5°, the algorithm system's judgment result is abnormal posture; If the result of a single

back photo is normal and the ATR angle is less than 5°, then the algorithm system's judgment is normal.

5.6.4 Clinical Experiment

Experimental Motivation

This study aims to investigate and evaluate the sensitivity and specificity of utilizing artificial intelligence algorithms for diagnosing scoliosis through mobile phone-based applications.

Experimental Design

1) Experimental design: This experiment adopts a multicenter, single-blind diagnostic test

2) Basic methods of clinical trials: Pursuant to the Guidelines for Reporting Reliability and Agreement Studies (GRRAS), the present clinical investigation employed X-ray plain film findings as the benchmark for assessing the diagnostic sensitivity and specificity of the mobile phone-based artificial intelligence diagnose algorithms in AIS patients.

3) Research subjects: From September 2023 to December 2023, 80 suspected adolescent idiopathic scoliosis patients underwent treatment at the Rehabilitation Medicine Center of West China Hospital of Sichuan University and the Traditional Chinese Medicine Hospital of Guangling District, Yangzhou City. All examination subjects are the first diagnosis and have not undergone any treatment related to scoliosis.

4) Diagnostic method: a) X-ray plain film examination: After understanding the patient's medical history and basic information, the same senior imaging physician uses the same measuring instrument to examine the patient's standing position in the front, side, and left and right functional positions through X-ray examination. At

the initial diagnosis, radiographic imaging in both anteroposterior and lateral orientations of the patient's spine must be acquired, alongside functional images capturing the left and right positions, to ensure a comprehensive evaluation;

b)Palpation: A senior rehabilitation therapist uses the palpation method to label situations of scoliosis and abnormal posture;

c) Mobile Scoliosis Diagnosing Algorithm: Operated by a seasoned rehabilitation therapist. Firstly, open the online testing program and fill in patient information. Then, ask the patient to take off their coat, put their feet together, straighten their knees, and stand upright. The therapist takes photos of the patient's back standing position, front 90° bending position, and back 90° bending position. During the process of taking detection images, a detection pose frame and immersive visual interaction in this system can be added to reduce the uploading of incorrect detection images, eensuring the precision of the patient's posture prior to advancing to the subsequent imaging step. After uploading the images, the algorithm calculates the early screening and judgment of scoliosis and generates an evaluation report. It should be noted that the mobile spinal scoliosis screening algorithm method is only performed at the initial diagnosis. The therapist needs to repeat the above operation once.

Evaluation Methods

Calculate the ATR results and corresponding report results based on the AI scoliosis screening algorithm of the mobile phone, as well as the doctor's palpation results. A senior orthopedic doctor annotated and statistically analyzed the X-ray results of the same subjects, while a researcher who was not familiar with the experimental content conducted statistical analysis on the three groups of results.

5.6.5 Experimental Result

Our mobile AI screening system has been compared with X-ray experiments and found that our optimized system has a sensitivity of 96% and a specificity of 89% for screening scoliosis. The probability of misjudging abnormal posture as scoliosis is 8%; The probability of misjudging scoliosis as abnormal posture is 5%; The sensitivity of manual palpation for scoliosis is 81%, and the specificity is 86%. Our system has achieved state of art results, far exceeding offline manual screening and scoliosis screening. Additionally, by calculating the maximum offset distance from the back midline and the ATR angle from the *Adam* forward bending test, we can analyze the progression trend of the subject, serving the purpose of progress monitoring. We present the practical use case results of the mini program in Figure 5.14 and corresponding image results Figure 5.15.

Figure 5.14: Report of evaluation result.

In the experiment, we found that there is still room for improvement in distinguishing between mild scoliosis and abnormal posture. We found a few cases of adolescents with obvious abnormal posture on their body surface and ATR angles exceeding 5°

Figure 5.15: Evaluation result and ground truth for scoliosis.

bending position and back 90° bending position. During the process of taking (the empirical threshold used to distinguish scoliosis in the *Adam* forward bending test). Still, their X-ray *Cobb* degree deficiency was only close to 10° bending position and back 90° bending position. This type of case can lead to misjudgment of abnormal posture as scoliosis, thereby reducing the specificity of screening for scoliosis. The case results are depicted in Figure 5.16 and Figure 5.17. This is also the direction we can explore and solve in the future.

5.7 Conclusion

In this chapter, We propose a system that enables AIS and abnormal posture screening on mobile edge devices. This method breaks the time and space limitations of AIS screening and is cost-free, fast, accurate, and radiation-free. Only a single unclothed back image is needed to classify scoliosis and abnormal or normal posture. By creating color images of the human back, X-ray data, and the corresponding calibration database, we innovatively define a new topological network of the human back and combine image processing algorithms and deep learning to achieve accurate scoliosis screening classification (88.1%).In order to better promote this technology to the public, we have developed an online mini program where users only need to

Figure 5.16: Report of abnormal posture evaluation result.

Figure 5.17: Evaluation result and ground truth for abnormal posture

upload three photos to achieve precise screening of scoliosis and abnormal posture at home. The optimized system has a sensitivity of 96% and a specificity of 89% for scoliosis, far exceeding the accuracy of experienced screening doctors (sensitivity of 81% and specificity of approximately 86%). Owing to the absence of publicly accessible datasets and open-source algorithms, we are currently precluded from employing identical datasets to replicate the findings of other investigators. Nonetheless, when examining the prevailing results from mainstream studies based on single back

photographs for the classification of scoliosis, these studies report an accuracy of 85.6%, with sensitivity and specificity of 87% and 83%, respectively. Our method has achieved significantly higher accuracy, sensitivity, and specificity compared to these results. However, a limitation of our system is the requirement for capturing three photographs, which inevitably leads to increased time and computational resource consumption.

Chapter 6

Conclusions and Suggestions for Future Research

6.1 Conclusion

The screening and evaluation of adolescent scoliosis has been widely spread worldwide, from radiation-based X-ray screening and evaluation to non-radiation-based manual palpation to using scoliosis rulers, moiré imaging equipment, and subsequent ultrasound scoliosis screening and evaluation. Technology has constantly improved, but each technology has significant limitations. The current mainstream non-radiative scoliosis evaluation method is ultrasonic scoliosis screening evaluation. Still, it is difficult to popularize on a large scale due to excessive reliance on manual operation, complex operation processes, and high costs. At present, the screening of scoliosis still mainly relies on manual screening in schools. Still, the low accuracy and high cost of manual screening have become the most significant limitations of this government public welfare project. To address the pain points in screening and evaluation mentioned above, We first explored and validated the correlation between the 3D back point cloud captured using an economical RGB-D camera and the X-ray of the

entire spine segment, and developed a 3D spine and posture analysis system; Afterwards, we explored and verified the correlation between 2D back images and 3D back point clouds on the key parameter of ATR, and achieved the accurate classification of scoliosis and normal based on 2D image of the human back; Finally, we established a new set of feature points and topology structures for the human back, which better explained the correlation between 2D human back image and X-ray image of scoliosis. Based on model improvements, we developed a precise evaluation system for scoliosis and body abnormalities on edge devices such as smartphones.

In summary, We have explored and validated the correlation between 2D back images of the human body, 3D point cloud images of the human back, and spinal X-ray images, and innovatively proposed a non-radiative and accurate solution for screening and evaluating scoliosis and body abnormalities based on edge devices such as RGB-D cameras and RGB cameras and have achieved large-scale engineering implementation. The entire report also revolves around the above solutions' research, development, and validation.

- we validate the high correlation between the 3D back point cloud and 3D spine curve, and we proposed a Kinect based low cost, easy to use, non radiation, and high accuracy method to quickly reconstruct the 3D shape of the spine, which can be used to evaluate spinal deformation. We use ultra-low-cost RGB-D cameras for non-radiative 3D spine and posture screening and evaluation. ITSPES has the characteristics of non-radiation, non-contact, low cost, and high accuracy. By reconstructing the human back in 3D, medical anatomical feature points are found, and a correlation model between the back feature points and the center of the spine is established to infer the 3D curve of the spine. Finally, relevant clinical demand parameters are calculated based on the parameters of the spine and posture. Through multi-center scientific clinical comparison verification, our system has an average error of 3.6° in *Cobb* angle accuracy and X-ray, and the imbalance of the human back surface can be seen,

which is also valuable clinical information that cannot be obtained by X-ray but is valuable for rehabilitation therapists The entire measurement process has low requirements for the testing environment and does not require professional personnel to touch the back for operation. The overall sample cost is less than 600 U.S. dollars. Our products can be used in school screening for scoliosis, scoliosis re-examination, exercise rehabilitation centers, women's postpartum centers, traditional Chinese medicine clinics, gyms, and other scenarios.

- We verify that that 2D and 3D images of the human back on concave convex features (such as ATR) have strong correlation, which can lay the foundation for inferring the features of 3D point cloud images based on 2D images of the back in the future and it also validates the feasibility of screening for scoliosis using an unclothed back image. We have developed a classification system for scoliosis and normal posture based on a single photo of the human back. We innovatively use the international scoliosis screening standard ATR angle as a label to achieve binary classification of individual images of the human back. We are the first to establish a 2D human back image and the corresponding 3D point cloud database for scoliosis screening to achieve this goal. All data contain 2D human back image of the same sample and the corresponding 3D back point cloud. This system learns the correlation between the 2D human back image and the ATR-related information calculated from the 3D point cloud of the unclothed human back. Finally, the system can classify scoliosis based on a single 2D image of the back and the screening accuracy(81.3%) over naked eye test by professional doctors(65.1%)

- we verify that a new set of feature points and network topology based on deep learning algorithms can effectively describe the correlation between 2D body features and scoliosis. Also we have developed a system for screening scoliosis and abnormal body posture based on color photos of the human back. Firstly, we used a single photo of the human back and X-ray results as labels. Based on

deep learning algorithms and novel topological structures, we found the relationship between color feature points of the human back and X-rays. Finally, we achieved the classification of scoliosis, abnormal body posture, and normal body posture based on a single photo of the back. To better quantify scoliosis and abnormal posture, we introduced the Adam forward bending test and obtained more quantitative parameters, which will significantly improve the screening of scoliosis and abnormal posture and achieve progressive monitoring. At the same time, we have developed a home-based online scoliosis and body posture assessment system based on the above principles, which can help teenagers achieve home-based screening and monitoring of scoliosis and body posture abnormalities. It can reduce the screening cost of about 2 U.S. dollars per person to below 0.07 U.S. dollars, and solve pain points such as inaccurate on-site school screening and inability to continue monitoring in the future. While the third part of the work can potentially replace the second part, the model in the third part is more complex and has higher demands on computational power and real-time performance. Additionally, the work in the second part actually lays the foundation for subsequent efforts to infer 3D back images from single 2D back images.

6.2 Future Work

Although we have proposed new solutions for screening and evaluating scoliosis in adolescents, they can effectively address the pain points currently encountered. In practice and industry implementation, we have also discovered many areas that need improvement and are worth exploring.

- The ITSPES we have developed, even though we can simulate the 3D shape of the spine very well, in the thoracic segment, it is still difficult to simulate and infer the true shape due to the complexity of the human body surface,

which is greatly influenced by other bones; In addition, the positioning of the SP line on the back is a decisive factor in the 3D reconstruction of the spine. In our practical process, we found that some obese subjects ($BMI > 28kg/m^2$), due to their obesity, have unclear or absent medical anatomical landmarks on their backs, which can cause the system to be unable to calculate. This is also a major drawback of our system. In the future, for subjects whose back anatomical landmarks disappear or are not obvious due to obesity, we still need to manually find the position of the anatomic landmark points on the human back and attach reflective markers, thereby facilitating the system's assessment capabilities. In addition, during the practical implementation process, we found that the unevenness of the back surface can effectively reflect the progression of scoliosis. In the future, we can analyze the imbalance of the back surface by defining parameters that can assist rehabilitation therapists in evaluating other musculoskeletal problems, including scoliosis.

- In the process of industrial implementation, we have also encountered some challenging issues regarding the mobile side scoliosis and abnormal posture screening system. The most obvious one is that the user did not tie up their hair according to the shooting requirements or did not take off their clothes, which resulted in the algorithm being unable to automatically recognize back feature points, as shown in Figure 6.1. On this issue, we are also developing and researching anti-occlusion algorithms for human posture, achieving automatic recognition of feature points when some features of the human body are occluded. In the future, it can be achieved that there is no need to remove clothing altogether, and underwear with less occlusion can be worn for analysis, better protecting user privacy. In addition, since we already have image data and corresponding X-ray data of different postures of the human back, we can use deep learning to learn the correlation between them. Not only can we use ATR single parameters as classification criteria, but we can also achieve end-to-end training

by inputting only three photos of the human back and directly outputting the classification results of scoliosis. In addition, we will continue to expand our dataset in the future, based on photos of the human back, to achieve more analysis of body shape problem parameters and have a greater impact on the fields of sports rehabilitation and clothing customization.

Figure 6.1: Some cases of back landmarks localization failure due to different degrees of occlusion caused by underwear, pants, and hair.

6.3 Social Impact

Our developed ITSPES and mobile spine and posture evaluation system have been used in the market after self-development and clinical research. The ITSPES can complete radiation-free and high-precision detection within 3 seconds through Time of flight(TOF) imaging technology analysis and image algorithms. At the same time, the instrument is lightweight and portable, making it easy to operate. After uploading

data to the cloud, it will integrate health records, making it convenient for patients and physicians to follow up on treatment situations in a timely manner, enormously meeting the current needs of large-scale spine screening, daily rehabilitation, and body training follow-up, The usage scenarios are shown in Figure 6.2 and Figure 6.3. At the same time, the mobile spine and posture evaluation system, with the support of self-developed AI image algorithms, allows users to quickly and accurately self-check their physical health status and contact experts at home using artificial intelligence. The usage scenario is shown in Figure 6.4.

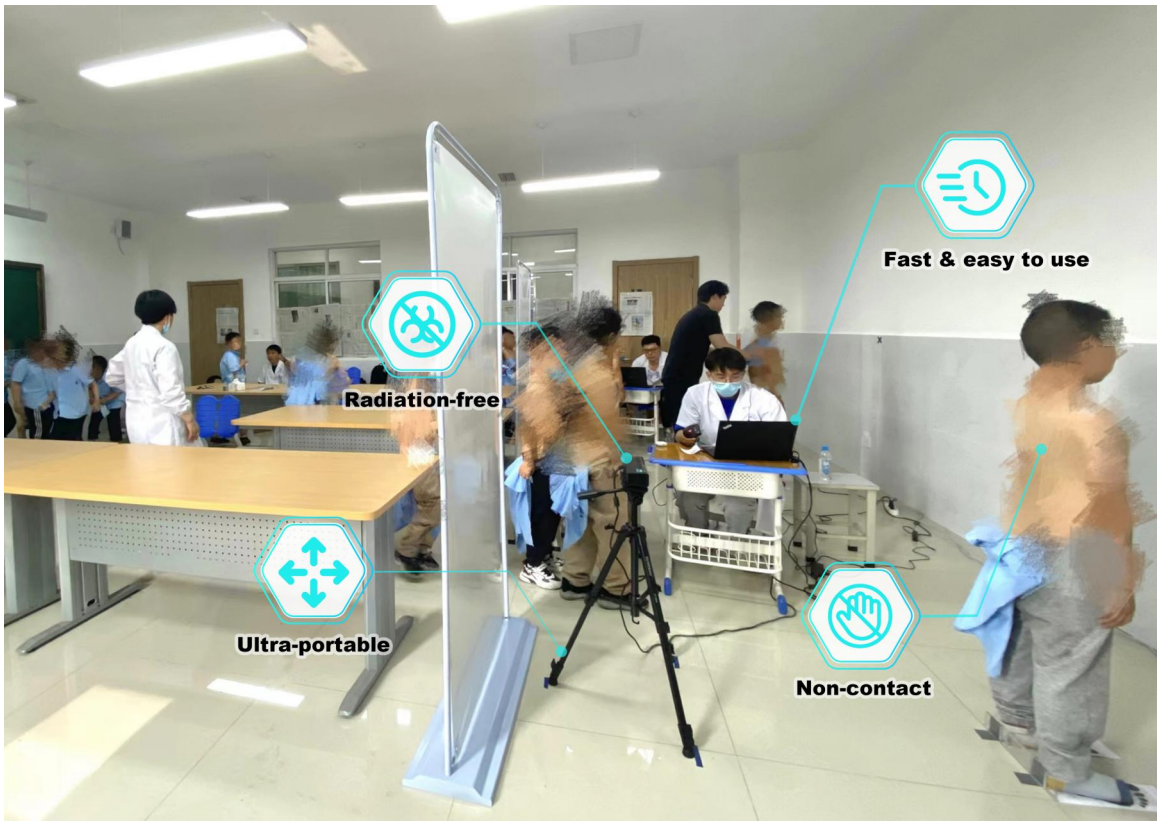

Figure 6.2: School scoliosis screening.

So far, we have provided our system services to more than 20 hospitals, insurance institutions, and rehabilitation institutions, providing screening and evaluation services for more than 300000 adolescents with scoliosis. We have detected more than 1300 adolescents with scoliosis early, helping them and their parents to become aware of the

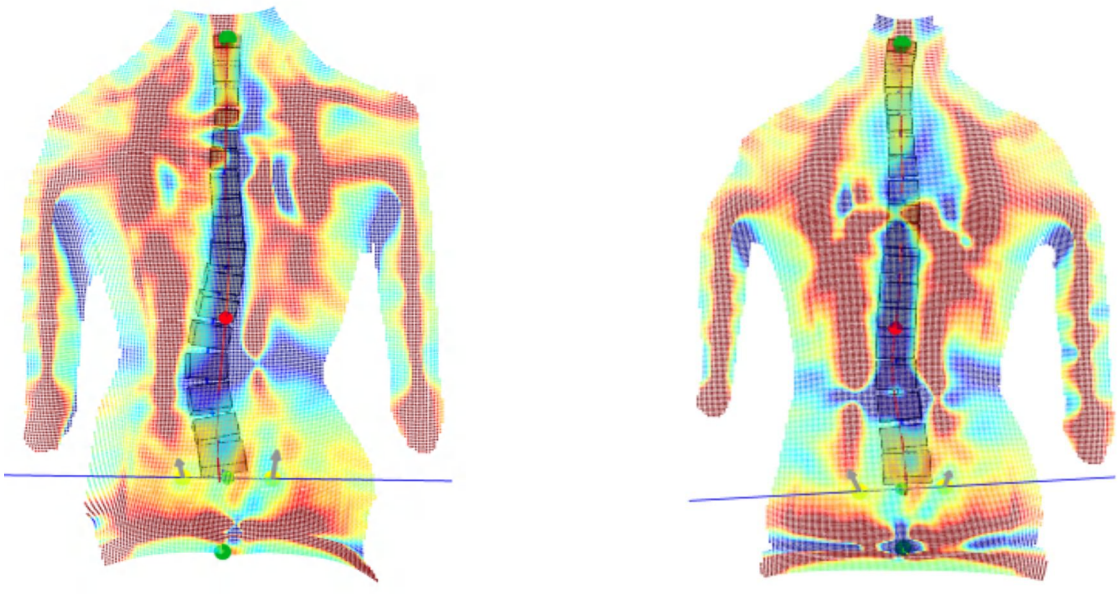

(a) Before exercise rehabilitation

(b) After six months of exercise rehabilitation

Figure 6.3: Spinal curve and body surface imbalance before and after six months exercise rehabilitation. The blue region indicates the concavity of the body surface, the red region indicates the convexity of the body surface, and the darker the color, the greater the degree of concavity and convexity

problem and take relevant intervention measures. The service areas are distributed in Jiangsu Province, Guangdong Province, Yunnan Province, Sichuan Province, and Hong Kong in China. According to the screening summary data, abnormal posture accounts for 27.69%; Scoliosis accounts for 3.09%. Notably, the incidence rate of scoliosis in adolescents aged 10-14 can reach up to 8.42%. Therefore, in the future, screening can focus on the high-risk scoliosis population aged 10-14. Since its launch, the system has won multiple international and Hong Kong invention awards, like Geneva International Invention Award - Gold award, Hong Kong ICT Gold Awards and Grand of the year 2021(Student Innovation Award), China International College Students' "Internet+" Innovation and Entrepreneurship Competition - Silver Award

and First prize in the Hong Kong College Student Innovation and Entrepreneurship Competition, as shown inFigure 6.5,Figure 6.6, Figure 6.7 and Figure 6.8.

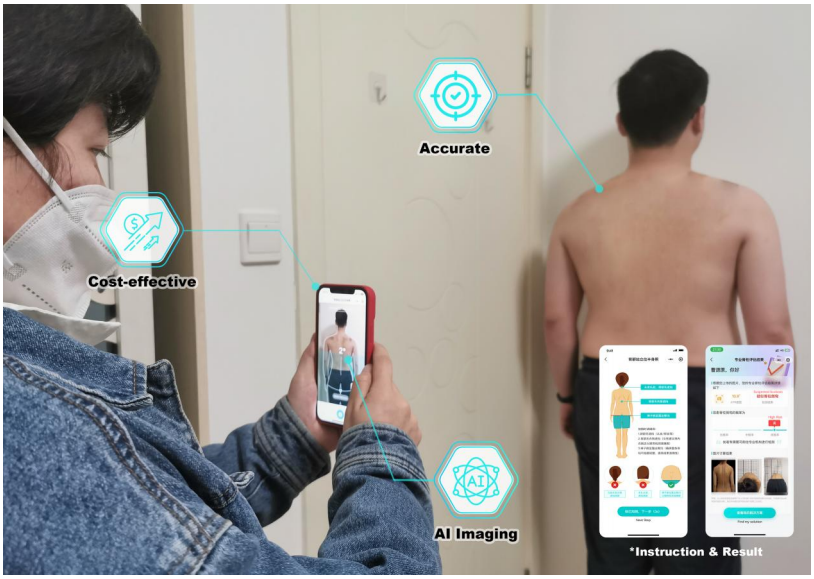

Figure 6.4: Home-based scoliosis and abnormal posture screening and monitoring.

Figure 6.5: Geneva International Invention Award - Gold award.

Figure 6.6: Hong Kong ICT Gold Awards and Grand of the year 2021(Student Innovation Award).

Figure 6.7: China International College Students' "Internet+" Innovation and Entrepreneurship Competition - Silver Award.

Figure 6.8: Hong Kong College Student Innovation and Entrepreneurship Competition - First prize.

References

[1] William Adams. *Lectures on the pathology and treatment of lateral and other forms of curvature of the spine*. J. & A. Churchill, 1882.

[2] Arbi Aghali. Craniofacial bone tissue engineering: current approaches and potential therapy. *Cells*, 10(11):2993, 2021.

[3] Farhaan Altaf, Jarryd Drinkwater, Kevin Phan, and Andrew K Cree. Systematic review of school scoliosis screening. *Spine deformity*, 5(5):303–309, 2017.

[4] Marília Fernandes Andrade, Érika de Cássia Lopes Chaves, Michele Rita Oliveira Miguel, Talita Prado Simão, Denismar Alves Nogueira, and Denise Hollanda Iunes. Evaluation of body posture in nursing students. *Revista da Escola de Enfermagem da USP*, 51:e03241, 2017.

[5] Marc A Asher and Douglas C Burton. Adolescent idiopathic scoliosis: natural history and long term treatment effects. *Scoliosis*, 1:1–10, 2006.

[6] MA Ashworth and AK Ersil. The management of rib hump inclination: a potential aid in scoliosis screening. *Orthop Trans*, 5:334, 1981.

[7] Fiona Berryman, Paul Pynsent, Jeremy Fairbank, and Simon Disney. A new system for measuring three-dimensional back shape in scoliosis. *European Spine Journal*, 17:663–672, 2008.

[8] J Bettany-Saltikov and L Cole. The effect of frontpacks, shoulder bags and handheld bags on 3d back shape and posture in young university students: an isis2 study. *Stud Health Technol Inform*, 176:117–121, 2012.

[9] Josette Bettany-Saltikov, Gokulakannan Kandasamy, S Schreiber, L Stolinski, D Czaprowski, and Julian Warren. Normative data of 3d back shape in asymptomatic subjects. In *SOSORT 2017*, 2017.

[10] Josette Bettany-Saltikov, Hans-Rudolf Weiss, Nachiappan Chockalingam, Razvan Taranu, Shreya Srinivas, Julie Hogg, Victoria Whittaker, Raman V Kalyan, and Tracey Arnell. Surgical versus non-surgical interventions in people with adolescent idiopathic scoliosis. *Cochrane Database of Systematic Reviews*, (4), 2015.

[11] Randal R Betz. Kyphosis of the thoracic and thoracolumbar spine in the pediatric patient: normal sagittal parameters and scope of the problem. *Instructional course lectures*, 53:479–484, 2004.

[12] Alexey Bochkovskiy, Chien-Yao Wang, and Hong-Yuan Mark Liao. Yolov4: Optimal speed and accuracy of object detection. *arXiv preprint arXiv:2004.10934*, 2020.

[13] Vincent Bonnet, Takazumi Yamaguchi, Arnaud Dupeyron, Sebastien Andary, Antoine Seilles, Philippe Fraisse, and Gentiane Venture. Automatic estimate of back anatomical landmarks and 3d spine curve from a kinect sensor. In *2016 6th IEEE International Conference on Biomedical Robotics and Biomechatronics (BioRob)*, pages 924–929. IEEE, 2016.

[14] WILLIAM P Bunnell. An objective criterion for scoliosis screening. *The Journal of bone and joint surgery. American volume*, 66(9):1381–1387, 1984.

[15] APG Castro, JD Pacheco, C Lourenço, S Queirós, AHJ Moreira, NF Rodrigues, and João L Vilaça. Evaluation of spinal posture using microsoft kinect™: A

preliminary case-study with 98 volunteers. *Porto biomedical journal*, 2(1):18–22, 2017.

[16] Quan Chen, Tiezheng Ge, Yanyu Xu, Zhiqiang Zhang, Xinxin Yang, and Kun Gai. Semantic human matting. In *Proceedings of the 26th ACM international conference on Multimedia*, pages 618–626, 2018.

[17] Farida Cheriet, Catherine Laporte, Samuel Kadoury, Hubert Labelle, and Jean Dansereau. A novel system for the 3-d reconstruction of the human spine and rib cage from biplanar x-ray images. *IEEE transactions on biomedical engineering*, 54(7):1356–1358, 2007.

[18] Chung-Wai James Cheung, Guang-Quan Zhou, Siu-Yin Law, Tak-Man Mak, Ka-Lee Lai, and Yong-Ping Zheng. Ultrasound volume projection imaging for assessment of scoliosis. *IEEE transactions on medical imaging*, 34(8):1760–1768, 2015.

[19] Ben Church, Andras Lasso, Christopher Schlenger, Daniel P Borschneck, Parvin Mousavi, Gabor Fichtinger, and Tamas Ungi. Visualization of scoliotic spine using ultrasound-accessible skeletal landmarks. In *Medical Imaging 2017: Image-Guided Procedures, Robotic Interventions, and Modeling*, volume 10135, pages 166–174. SPIE, 2017.

[20] Daniel M Coelho, Guilherme H Bonagamba, and Anamaria S Oliveira. Scoliometer measurements of patients with idiopathic scoliosis. *Brazilian journal of physical therapy*, 17:179–184, 2013.

[21] MMPose Contributors. Openmmlab pose estimation toolbox and benchmark. `https://github.com/open-mmlab/mmpose`, 2020.

[22] Aina J Danielsson, Ingela Wiklund, Kerstin Pehrsson, and Alf L Nachemson. Health-related quality of life in patients with adolescent idiopathic scoliosis:

a matched follow-up at least 20 years after treatment with brace or surgery. *European spine journal*, 10:278–288, 2001.

[23] Michele Morin Doody, John E Lonstein, Marilyn Stovall, David G Hacker, Nickolas Luckyanov, Charles E Land, US Scoliosis Cohort Study Collaborators, et al. Breast cancer mortality after diagnostic radiography: findings from the us scoliosis cohort study. *Spine*, 25(16):2052–2063, 2000.

[24] B Drerup and E Hierholzer. Objective determination of anatomical landmarks on the body surface: measurement of the vertebra prominens from surface curvature. *Journal of biomechanics*, 18(6):467–474, 1985.

[25] B Drerup and E Hierholzer. Back shape measurement using video rasterstereography and three-dimensional reconstruction of spinal shape. *Clinical Biomechanics*, 9(1):28–36, 1994.

[26] Burkhard Drerup. Rasterstereographic measurement of scoliotic deformity. *Scoliosis*, 9:1–14, 2014.

[27] Burkhard Drerup and Eberhard Hierholzer. Automatic localization of anatomical landmarks on the back surface and construction of a body-fixed coordinate system. *Journal of biomechanics*, 20(10):961–970, 1987.

[28] ES Duff and R Draper. Survey of normal adolescent back shape as measured by isis. *Stokes, Pekelsky IF, Moreland, MS Surf Topogr Spinal Deform IV. Stuttgart, New York: Gustav-Fisher*, pages 163–169, 1987.

[29] John Dunn, Nora B Henrikson, Caitlin C Morrison, Paula R Blasi, Matt Nguyen, and Jennifer S Lin. Screening for adolescent idiopathic scoliosis: evidence report and systematic review for the us preventive services task force. *Jama*, 319(2):173–187, 2018.

[30] Daniel Yee Tak Fong, Chun Fan Lee, Kenneth Man Chee Cheung, Jack Chun Yiu Cheng, Bobby Kin Wah Ng, Tsz Ping Lam, Kwok Hang Mak, Paul

Siu Fai Yip, and Keith Dip Kei Luk. A meta-analysis of the clinical effectiveness of school scoliosis screening. *Spine*, 35(10):1061–1071, 2010.

[31] Daniel YT Fong, Kenneth MC Cheung, Yat-Wa Wong, Yuen-Yin Wan, Chun-Fan Lee, Tsz-Ping Lam, Jack CY Cheng, Bobby KW Ng, and Keith DK Luk. A population-based cohort study of 394,401 children followed for 10 years exhibits sustained effectiveness of scoliosis screening. *The Spine Journal*, 15(5):825–833, 2015.

[32] US Preventive Services Task Force et al. Screening for idiopathic scoliosis in adolescents: recommendation statement. *http://www. preventiveservices. ahrq. gov*, 2004.

[33] Carole Fortin, Debbie Ehrmann Feldman, Farida Cheriet, and Hubert Labelle. Clinical methods for quantifying body segment posture: a literature review. *Disability and rehabilitation*, 33(5):367–383, 2011.

[34] Carole Fortin, Debbie Ehrmann Feldman, Farida Cheriet, Denis Gravel, Frédérique Gauthier, and Hubert Labelle. Reliability of a quantitative clinical posture assessment tool among persons with idiopathic scoliosis. *Physiotherapy*, 98(1):64–75, 2012.

[35] W Frobin and E Hierholzer. Analysis of human back shape using surface curvatures. *Journal of Biomechanics*, 15(5):379–390, 1982.

[36] Tássia Silveira Furlanetto, Juliana Adami Sedrez, Cláudia Tarragô Candotti, and Jefferson Fagundes Loss. Photogrammetry as a tool for the postural evaluation of the spine: a systematic review. *World journal of orthopedics*, 7(2):136, 2016.

[37] Aurel Galántai. The theory of newton's method. *Journal of Computational and Applied Mathematics*, 124(1-2):25–44, 2000.

[38] Mary Allen Grice. *A scoliotic line of chickens: the relationship of environmental factors and physiological and biochemical characteristics to the expression of scoliosis*. North Carolina State University, 1999.

[39] Theodoros B Grivas, Elias S Vasiliadis, Constantinos Mihas, Georgios Triantafyllopoulos, and Angelos Kaspiris. Trunk asymmetry in juveniles. *Scoliosis*, 3:1–11, 2008.

[40] Theodoros B Grivas, Marian H Wade, Stefano Negrini, Joseph P O'Brien, Toru Maruyama, Martha C Hawes, Manuel Rigo, Hans Rudolf Weiss, Tomasz Kotwicki, Elias S Vasiliadis, et al. Sosort consensus paper: school screening for scoliosis. where are we today? *Scoliosis*, 2:1–23, 2007.

[41] Alex S Ha and Eduardo C Beauchamp. Editorial on "screening for adolescent idiopathic scoliosis: Us preventive services task force recommendation statement". *Journal of Spine Surgery*, 4(4):812, 2018.

[42] Kaiming He, Xiangyu Zhang, Shaoqing Ren, and Jian Sun. Deep residual learning for image recognition. In *Proceedings of the IEEE conference on computer vision and pattern recognition*, pages 770–778, 2016.

[43] Kaiming He, Xiangyu Zhang, Shaoqing Ren, and Jian Sun. Deep residual learning for image recognition. In *Proceedings of the IEEE conference on computer vision and pattern recognition*, pages 770–778, 2016.

[44] Eberhard Hierholzer. Analysis of left-right asymmetry of the back shape of scoliotic patients. In *Biostereometrics' 85*, volume 602, pages 266–271. SPIE, 1986.

[45] Tabatha Hines, Sandy Roland, Dylan Nguyen, Beth Kennard, Heather Richard, Carroll W Hughes, Shawn M McClintock, Brandon Ramo, and Tony Herring. School scoliosis screenings: family experiences and potential anxiety after orthopaedic referral. *Spine*, 40(21):E1135–E1143, 2015.

[46] M Timothy Hresko, Vishwas Talwalkar, and Richard Schwend. Early detection of idiopathic scoliosis in adolescents. *JBJS*, 98(16):e67, 2016.

[47] Jie Hu, Li Shen, and Gang Sun. Squeeze-and-excitation networks. In *Proceedings of the IEEE conference on computer vision and pattern recognition*, pages 7132–7141, 2018.

[48] Sergey Ioffe and Christian Szegedy. Batch normalization: Accelerating deep network training by reducing internal covariate shift. In *International conference on machine learning*, pages 448–456. PMLR, 2015.

[49] DH Iunes, D Bevilaqua-Grossi, AS Oliveira, FA Castro, and HS Salgado. Comparative analysis between visual and computerized photogrammetry postural assessment. *Brazilian Journal of Physical Therapy*, 13:308–315, 2009.

[50] KENNETH JACKMAN. Moiré fringe topography and spinal deformity. *American Journal of Diseases of Children*, 136(6):565–566, 1982.

[51] Florence Peterson Kendall, Elizabeth Kendall McCreary, Patricia Geise Provance, Mary McIntyre Rodgers, William Anthony Romani, et al. *Muscles: testing and function with posture and pain*, volume 5. Lippincott Williams & Wilkins Baltimore, MD, 2005.

[52] N Khouri, R Vialle, P Mary, and B Biot. Scoliose idiopathique en période de croissance. indications et programmes thérapeutiques. *EMC-Rhumatologie-Orthopedie*, 1(1):45–63, 2004.

[53] Diederik P Kingma and Jimmy Ba. Adam: A method for stochastic optimization. *arXiv preprint arXiv:1412.6980*, 2014.

[54] Patrick Knott, Eden Pappo, Michelle Cameron, Jean Claude deMauroy, Charles Rivard, Tomasz Kotwicki, Fabio Zaina, James Wynne, Luke Stikeleather, Josette Bettany-Saltikov, et al. Sosort 2012 consensus paper: reducing x-ray exposure in pediatric patients with scoliosis. *Scoliosis*, 9(1):4, 2014.

[55] Markus Rafael Konieczny, Hüsseyin Senyurt, and Rüdiger Krauspe. Epidemiology of adolescent idiopathic scoliosis. *Journal of children's orthopaedics*, 7(1):3–9, 2013.

[56] Tomasz Kotwicki, Edyta Kinel, Wanda Stryla, and Andrzej Szulc. Discrepancy in clinical versus radiological parameters describing deformity due to brace treatment for moderate idiopathic scoliosis. *Scoliosis*, 2:1–8, 2007.

[57] Alex Krizhevsky, Ilya Sutskever, and Geoffrey E Hinton. Imagenet classification with deep convolutional neural networks. *Advances in neural information processing systems*, 25, 2012.

[58] Hubert Labelle, Stephens B Richards, Marinus De Kleuver, Theodoros B Grivas, Keith DK Luk, Hee Kit Wong, John Thometz, Marie Beauséjour, Isabelle Turgeon, and Daniel YT Fong. Screening for adolescent idiopathic scoliosis: an information statement by the scoliosis research society international task force. *Scoliosis*, 8:1–6, 2013.

[59] Renaud Lafage, Frank Schwab, Vincent Challier, Jensen K Henry, Jeffrey Gum, Justin Smith, Richard Hostin, Christopher Shaffrey, Han J Kim, Christopher Ames, et al. Defining spino-pelvic alignment thresholds: should operative goals in adult spinal deformity surgery account for age? *Spine*, 41(1):62–68, 2016.

[60] CF Lee, Daniel YT Fong, Kenneth MC Cheung, Jack CY Cheng, Bobby KW Ng, TP Lam, KH Mak, Paul SF Yip, and Keith DK Luk. Costs of school scoliosis screening: a large, population-based study. *Spine*, 35(26):2266–2272, 2010.

[61] Shanchuan Lin, Linjie Yang, Imran Saleemi, and Soumyadip Sengupta. Robust high-resolution video matting with temporal guidance. In *Proceedings of the IEEE/CVF Winter Conference on Applications of Computer Vision*, pages 238–247, 2022.

[62] Tsung-Yi Lin, Michael Maire, Serge Belongie, James Hays, Pietro Perona, Deva Ramanan, Piotr Dollár, and C Lawrence Zitnick. Microsoft coco: Common objects in context. In *European conference on computer vision*, pages 740–755. Springer, 2014.

[63] Shang-li Liu and Dong-sheng Huang. Scoliosis in china: A general review. *Clinical Orthopaedics and Related Research (1976-2007)*, 323:113–118, 1996.

[64] Ze Liu, Yutong Lin, Yue Cao, Han Hu, Yixuan Wei, Zheng Zhang, Stephen Lin, and Baining Guo. Swin transformer: Hierarchical vision transformer using shifted windows. In *Proceedings of the IEEE/CVF International Conference on Computer Vision*, pages 10012–10022, 2021.

[65] Keith DK Luk, Chun Fan Lee, Kenneth MC Cheung, Jack CY Cheng, Bobby KW Ng, Tsz Ping Lam, Kwok Hang Mak, Paul SF Yip, and Daniel YT Fong. Clinical effectiveness of school screening for adolescent idiopathic scoliosis: a large population-based retrospective cohort study. *Spine*, 35(17):1607–1614, 2010.

[66] Ginés Hidalgo Martınez. *Openpose: Whole-body pose estimation*. PhD thesis, Carnegie Mellon University Pittsburgh, PA, USA, 2019.

[67] Jakub Michonski, Marcin Witkowski, Robert Sitnik, and Wojciech M Glinkowski. Automatic recognition of surface landmarks of anatomical structures of back and posture. *Journal of biomedical optics*, 17(5):056015, 2012.

[68] Jovana M Milanesi, Graciele Borin, Eliane CR Corrêa, Ana MT da Silva, Daniel C Bortoluzzi, and Juliana A Souza. Impact of the mouth breathing occurred during childhood in the adult age: biophotogrammetric postural analysis. *International journal of pediatric otorhinolaryngology*, 75(8):999–1004, 2011.

[69] RAYMOND T Morrissy, GS Goldsmith, EC Hall, D Kehl, and GH Cowie. Measurement of the cobb angle on radiographs of patients who have scoliosis. evaluation of intrinsic error. *JBJS*, 72(3):320–327, 1990.

[70] Andrzej Mroczkowski. The effect of aikido exercises on shaping spinal curvatures in the sagittal plane. *Journal of Combat Sports & Martial Arts*, 4(2), 2013.

[71] Frank H Netter. *Atlas of human anatomy, Professional Edition E-Book: including NetterReference. com Access with full downloadable image Bank*. Elsevier health sciences, 2014.

[72] Richard A Newcombe, Shahram Izadi, Otmar Hilliges, David Molyneaux, David Kim, Andrew J Davison, Pushmeet Kohi, Jamie Shotton, Steve Hodges, and Andrew Fitzgibbon. Kinectfusion: Real-time dense surface mapping and tracking. In *2011 10th IEEE international symposium on mixed and augmented reality*, pages 127–136. Ieee, 2011.

[73] M Nissinen, M Heliövaara, K Tallroth, and M Poussa. Trunk asymmetry and scoliosis anthropometric measurements in prepuberal school children. *Acta Pædiatrica*, 78(5):747–753, 1989.

[74] No. The curvatures of spine. [Online]. `https://evolvedspine.com/wpcontent/uploads/2023/03/Curves_of_the_spine.jpg`.

[75] No. Posterior view of back surface anatomic landmarks. [Online]. `https://www.wikitomy.com/2021/04/surface-anatomy-of-back.html`.

[76] No. Sagittal, coronal, and transverse planes of human body. [Online]. `https://api.www.labxchange.org/api/v1/xblocks/lb:LabXchange:7de11c35:html:1/storage/35-anatomical_planes-en-copy-2_16x91677075466924-09409723d707f9f608fbbe37c5e86638.png`.

[77] Alan E Oestreich, Lionel W Young, and Tina Young Poussaint. Scoliosis circa 2000: radiologic imaging perspective: I. diagnosis and pretreatment evaluation. *Skeletal radiology*, 27:591–605, 1998.

[78] Søren Ohrt-Nissen, Dennis W Hallager, Jeppe L Henriksen, Martin Gehrchen, and Benny Dahl. Curve magnitude in patients referred for evaluation of adolescent idiopathic scoliosis: five years' experience from a system without school screening. *Spine deformity*, 4(2):120–124, 2016.

[79] Weishen Pan, Guangdong Hou, and Changshui Zhang. Automatic methods for screening and assessing scoliosis by 2-d digital images. In *International Conference on Intelligent Science and Big Data Engineering*, pages 392–400. Springer, 2015.

[80] Petros Patias, Theodoros B Grivas, Angelos Kaspiris, Costas Aggouris, and Evangelos Drakoutos. A review of the trunk surface metrics used as scoliosis and other deformities evaluation indices. *Scoliosis*, 5:1–20, 2010.

[81] Andrew Payne, Andy Daniel, Anik Mehta, Barry Thompson, Cyrus S Bamji, Dane Snow, Hideaki Oshima, Larry Prather, Mike Fenton, Lou Kordus, et al. 7.6 a 512× 424 cmos 3d time-of-flight image sensor with multi-frequency photo-demodulation up to 130mhz and 2gs/s adc. In *2014 IEEE International Solid-State Circuits Conference Digest of Technical Papers (ISSCC)*, pages 134–135. IEEE, 2014.

[82] Valérie Pazos, Farida Cheriet, Jean Danserau, Janet Ronsky, Ronald F Zernicke, and Hubert Labelle. Reliability of trunk shape measurements based on 3-d surface reconstructions. *European Spine Journal*, 16:1882–1891, 2007.

[83] PJ Penha, RA Casarotto, ICN Sacco, AP Marques, and SMA João. Qualitative postural analysis among boys and girls of seven to ten years of age. *Brazilian Journal of Physical Therapy*, 12:386–391, 2008.

[84] Rafael ZA Pinto, Thales R Souza, Renato G Trede, Renata N Kirkwood, Elyonara M Figueiredo, and Sergio T Fonseca. Bilateral and unilateral increases in calcaneal eversion affect pelvic alignment in standing position. *Manual therapy*, 13(6):513–519, 2008.

[85] Lino Ramirez, Nelson G Durdle, V James Raso, and Doug L Hill. A support vector machines classifier to assess the severity of idiopathic scoliosis from surface topography. *Ieee transactions on information technology in biomedicine*, 10(1):84–91, 2006.

[86] Joseph Redmon, Santosh Divvala, Ross Girshick, and Ali Farhadi. You only look once: Unified, real-time object detection. In *Proceedings of the IEEE conference on computer vision and pattern recognition*, pages 779–788, 2016.

[87] Shaoqing Ren, Kaiming He, Ross Girshick, and Jian Sun. Faster r-cnn: Towards real-time object detection with region proposal networks. *Advances in neural information processing systems*, 28, 2015.

[88] Paul Richardson. *Grays Atlas of Anatomy*. Elsevier-Health Sciences Division, 2014.

[89] Olaf Ronneberger, Philipp Fischer, and Thomas Brox. U-net: Convolutional networks for biomedical image segmentation. In *Medical image computing and computer-assisted intervention–MICCAI 2015: 18th international conference, Munich, Germany, October 5-9, 2015, proceedings, part III 18*, pages 234–241. Springer, 2015.

[90] Nurbaity Sabri, Haza Nuzly Abdull Hamed, Zaidah Ibrahim, and Kamalnizat Ibrahim. 2d photogrammetry image of scoliosis lenke type classification using deep learning. In *2019 IEEE 9th International Conference on System Engineering and Technology (ICSET)*, pages 437–440. IEEE, 2019.

[91] Nurbaity Sabri, Haza Nuzly Abdull Hamed, Zaidah Ibrahim, and Kamalnizat Ibrahim. 2d photogrammetry image of scoliosis lenke type classification using deep learning. In *2019 IEEE 9th International Conference on System Engineering and Technology (ICSET)*, pages 437–440. IEEE, 2019.

[92] Ben Sapp and Ben Taskar. Modec: Multimodal decomposable models for human pose estimation. In *Proceedings of the IEEE conference on computer vision and pattern recognition*, pages 3674–3681, 2013.

[93] John F Sarwark and Matthew M Davis. Evolving recommendations for scoliosis screening: a compelling need for further research. *Jama*, 319(2):127–129, 2018.

[94] Gwendolijne GM Scholten-Peeters, Nicole Franken, Annechien Beumer, and Arianne P Verhagen. The opinion and experiences of dutch orthopedic surgeons and radiologists about diagnostic musculoskeletal ultrasound imaging in primary care: a survey. *Manual therapy*, 19(2):109–113, 2014.

[95] Frank J Schwab, Benjamin Blondel, Shay Bess, Richard Hostin, Christopher I Shaffrey, Justin S Smith, Oheneba Boachie-Adjei, Douglas C Burton, Behrooz A Akbarnia, Gregory M Mundis, et al. Radiographical spinopelvic parameters and disability in the setting of adult spinal deformity: a prospective multicenter analysis. *Spine*, 38(13):E803–E812, 2013.

[96] Debora Soccal Schwertner, Raul Oliveira, Giovana Zarpellon Mazo, Fabiane Rosa Gioda, Christian Roberto Kelber, and Alessandra Swarowsky. Body surface posture evaluation: construction, validation and protocol of the spgap system (posture evaluation rotating platform system). *BMC musculoskeletal disorders*, 17:1–11, 2016.

[97] John Sell and Patrick O'Connor. The xbox one system on a chip and kinect sensor. *IEEE Micro*, 34(2):44–53, 2014.

[98] Lama Seoud, Mathias M Adankon, Hubert Labelle, Jean Dansereau, and Farida Cheriet. Prediction of scoliosis curve type based on the analysis of trunk surface topography. In *2010 IEEE International Symposium on Biomedical Imaging: From Nano to Macro*, pages 408–411. IEEE, 2010.

[99] Lama Seoud, Jean Dansereau, Hubert Labelle, and Farida Cheriet. Noninvasive clinical assessment of trunk deformities associated with scoliosis. *IEEE journal of biomedical and health informatics*, 17(2):392–401, 2013.

[100] Deepika Singla and Zubia Veqar. Methods of postural assessment used for sports persons. *Journal of clinical and diagnostic research: JCDR*, 8(4):LE01, 2014.

[101] Aleksandra Stachoń, Anna Burdukiewicz, Justyna Andrzejewska, and Jadwiga Pietraszewska. The imaging and evaluation of body posture defects in hearing impaired children. *Bio-Algorithms and Med-Systems*, 8(2):221–236, 2012.

[102] PEIRRE Stagnara, Jean Claude De Mauroy, Georges Dran, GEORGES P GONON, Giuseppe Costanzo, Joannes Dimnet, and Annick Pasquet. Reciprocal angulation of vertebral bodies in a sagittal plane: approach to references for the evaluation of kyphosis and lordosis. *Spine*, 7(4):335–342, 1982.

[103] Ian AF Stokes, JR Pekalsky, and Morey S Moreland. Surface topography and spinal deformity. In *Proceedings of the 4-th International Symposium. New York: Gustaw Verlag*, 1987.

[104] Ke Sun, Bin Xiao, Dong Liu, and Jingdong Wang. Deep high-resolution representation learning for human pose estimation. In *Proceedings of the IEEE/CVF conference on computer vision and pattern recognition*, pages 5693–5703, 2019.

[105] Ke Sun, Bin Xiao, Dong Liu, and Jingdong Wang. Deep high-resolution representation learning for human pose estimation. In *Proceedings of the IEEE/CVF conference on computer vision and pattern recognition*, pages 5693–5703, 2019.

[106] Mingxing Tan and Quoc Le. Efficientnet: Rethinking model scaling for convolutional neural networks. In *International conference on machine learning*, pages 6105–6114. PMLR, 2019.

[107] Do Thuan. Evolution of yolo algorithm and yolov5: The state-of-the-art object detention algorithm. 2021.

[108] Alan R Turner-Smith, J Derek Harris, Gregory R Houghton, and Rosalind J Jefferson. A method for analysis of back shape in scoliosis. *Journal of biomechanics*, 21(6):497–509, 1988.

[109] D Tzutalin. Labelimg. *GitHub Repository*, 6, 2015.

[110] Tamas Ungi, Hastings Greer, Kyle R Sunderland, Victoria Wu, Zachary MC Baum, Christopher Schlenger, Matthew Oetgen, Kevin Cleary, Stephen R Aylward, and Gabor Fichtinger. Automatic spine ultrasound segmentation for scoliosis visualization and measurement. *IEEE Transactions on Biomedical Engineering*, 67(11):3234–3241, 2020.

[111] Sjan-Mari Van Niekerk, Quinette Louw, Christopher Vaughan, Karen Grimmer-Somers, and Kristiaan Schreve. Photographic measurement of upper-body sitting posture of high school students: a reliability and validity study. *BMC musculoskeletal disorders*, 9:1–11, 2008.

[112] Stefano Viazzi, Claudia Bahr, Tom Van Hertem, Andres Schlageter-Tello, CEB Romanini, Ilan Halachmi, Cees Lokhorst, and Daniel Berckmans. Comparison of a three-dimensional and two-dimensional camera system for automated measurement of back posture in dairy cows. *Computers and Electronics in Agriculture*, 100:139–147, 2014.

[113] Wenhai Wang, Enze Xie, Xiang Li, Deng-Ping Fan, Kaitao Song, Ding Liang, Tong Lu, Ping Luo, and Ling Shao. Pvt v2: Improved baselines with pyramid vision transformer. *Computational Visual Media*, 8(3):415–424, 2022.

[114] Xinyao Wang, Liefeng Bo, and Li Fuxin. Adaptive wing loss for robust face alignment via heatmap regression. In *Proceedings of the IEEE/CVF international conference on computer vision*, pages 6971–6981, 2019.

[115] JG Warren, J Bettany-Saltikov, Paul Van Schaik, and SL Papastefanou. 3-d measurement of posture and back shape using a low cost, portable system-a reliability study. In *Research into Spinal Deformities 3*, pages 100–104. IOS Press, 2002.

[116] SL Weinstein and IV Ponseti. Curve progression in idiopathic scoliosis. *The Journal of bone and joint surgery. American volume*, 65(4):447–455, 1983.

[117] Stuart L Weinstein, Lori A Dolan, Jack CY Cheng, Aina Danielsson, and Jose A Morcuende. Adolescent idiopathic scoliosis. *The lancet*, 371(9623):1527–1537, 2008.

[118] Stuart L Weinstein, Lori A Dolan, Kevin F Spratt, Kirk K Peterson, Mark J Spoonamore, and Ignacio V Ponseti. Health and function of patients with untreated idiopathic scoliosis: a 50-year natural history study. *Jama*, 289(5):559–567, 2003.

[119] Stuart L Weinstein, Lori A Dolan, James G Wright, and Matthew B Dobbs. Effects of bracing in adolescents with idiopathic scoliosis. *New England Journal of Medicine*, 369(16):1512–1521, 2013.

[120] Stig Willner. Moiré topography—a method for school screening of scoliosis. *Archives of orthopaedic and traumatic surgery*, 95(3):181–185, 1979.

[121] Bin Xiao, Haiping Wu, and Yichen Wei. Simple baselines for human pose estimation and tracking. In *Proceedings of the European conference on computer vision (ECCV)*, pages 466–481, 2018.

[122] Zhenda Xu, Yong Zhang, Chunyang Fu, Limin Liu, Cong Chen, Wenchao Xu, and Song Guo. Back shape measurement and three-dimensional reconstruction of spinal shape using one kinect sensor. In *2020 IEEE 17th International Symposium on Biomedical Imaging (ISBI)*, pages 1–5. IEEE, 2020.

[123] Bin Yan, Xinhai Lu, Guohui Nie, and Yeen Huang. China urgently needs a nationwide scoliosis screening system. *Acta Paediatrica*, 109(11):2416–2417, 2020.

[124] Junlin Yang, Kai Zhang, Hengwei Fan, Zifang Huang, Yifan Xiang, Jingfan Yang, Lin He, Lei Zhang, Yahan Yang, Ruiyang Li, et al. Development and validation of deep learning algorithms for scoliosis screening using back images. *Communications biology*, 2(1):390, 2019.

[125] Lin Yang, Longyu Zhang, Haiwei Dong, Abdulhameed Alelaiwi, and Abdulmotaleb El Saddik. Evaluating and improving the depth accuracy of kinect for windows v2. *IEEE Sensors Journal*, 15(8):4275–4285, 2015.

[126] Barbara P Yawn and Roy A Yawn. The estimated cost of school scoliosis screening. *Spine*, 25(18):2387–2391, 2000.

[127] Chi Zhang, Xiaomin Liu, Wei Guo, Hanxiong Wang, and Zihao Li. An innocuous spine structure analysis method based on surface asymmetry evaluation. In *2015 8th International Conference on Biomedical Engineering and Informatics (BMEI)*, pages 158–162. IEEE, 2015.

[128] Rui Zheng, Michelle Young, Douglas Hill, LH Le, Douglas Hedden, Marc Moreau, James Mahood, Sarah Southon, and Edmond Lou. Improvement on the accuracy and reliability of ultrasound coronal curvature measurement on adolescent idiopathic scoliosis with the aid of previous radiographs. *Spine*, 41(5):404–411, 2016.

[129] Yong-Ping Zheng, Timothy Tin-Yan Lee, Kelly Ka-Lee Lai, Benjamin Hon-Kei Yip, Guang-Quan Zhou, Wei-Wei Jiang, James Chung-Wai Cheung, Man-Sang Wong, Bobby King-Wah Ng, Jack Chun-Yiu Cheng, et al. A reliability and validity study for scolioscan: a radiation-free scoliosis assessment system using 3d ultrasound imaging. *Scoliosis and spinal disorders*, 11:1–15, 2016.

[130] Zhifeng Zhou, Jia Zhu, and Chengxian Yao. Vertebral center points locating and cobb angle measurement based on deep learning. *Applied Sciences*, 13(6):3817, 2023.

[131] Zezhang Zhu, Nelson Leung-Sang Tang, Leilei Xu, Xiaodong Qin, Saihu Mao, Yueming Song, Limin Liu, Fangcai Li, Peng Liu, Long Yi, et al. Genome-wide association study identifies new susceptibility loci for adolescent idiopathic scoliosis in chinese girls. *Nature communications*, 6(1):8355, 2015.